



**HAL**  
open science

# Prestress and bearing capacity loss of pre-tensioned concrete beams due to corrosion cracks

Lizhao Dai

► **To cite this version:**

Lizhao Dai. Prestress and bearing capacity loss of pre-tensioned concrete beams due to corrosion cracks. Materials. Université de Lorraine; Changsha University of Science and Technology (Chine), 2019. English. NNT: 2019LORR0266 . tel-02558359

**HAL Id: tel-02558359**

**<https://hal.univ-lorraine.fr/tel-02558359>**

Submitted on 24 Nov 2020

**HAL** is a multi-disciplinary open access archive for the deposit and dissemination of scientific research documents, whether they are published or not. The documents may come from teaching and research institutions in France or abroad, or from public or private research centers.

L'archive ouverte pluridisciplinaire **HAL**, est destinée au dépôt et à la diffusion de documents scientifiques de niveau recherche, publiés ou non, émanant des établissements d'enseignement et de recherche français ou étrangers, des laboratoires publics ou privés.



## AVERTISSEMENT

Ce document est le fruit d'un long travail approuvé par le jury de soutenance et mis à disposition de l'ensemble de la communauté universitaire élargie.

Il est soumis à la propriété intellectuelle de l'auteur. Ceci implique une obligation de citation et de référencement lors de l'utilisation de ce document.

D'autre part, toute contrefaçon, plagiat, reproduction illicite encourt une poursuite pénale.

Contact : [ddoc-theses-contact@univ-lorraine.fr](mailto:ddoc-theses-contact@univ-lorraine.fr)

## LIENS

Code de la Propriété Intellectuelle. articles L 122. 4

Code de la Propriété Intellectuelle. articles L 335.2- L 335.10

[http://www.cfcopies.com/V2/leg/leg\\_droi.php](http://www.cfcopies.com/V2/leg/leg_droi.php)

<http://www.culture.gouv.fr/culture/infos-pratiques/droits/protection.htm>



**UNIVERSITÉ  
DE LORRAINE**



**LABORATOIRE D'ÉTUDE DES MICROSTRUCTURES  
ET DE MÉCANIQUE  
DES MATÉRIAUX**

**Université de Lorraine**

**Laboratoire d'Étude des Microstructures et de Mécanique des Matériaux (UMR CNRS 7239)**

**Thèse de doctorat**

**Discipline: Génie Civil**

**Présentée et soutenue publiquement par**

**Lizhao DAI**

**2019**

**Contribution à l'estimation de la résistance en flexion  
de poutres en béton précontraint avec prise en  
compte de la corrosion d'armature**

Devant le Jury Composé de:

<b>Prof. BALAYSSAC Jean-Paul, Université Paul Sabatier Toulouse, France</b>	<b>Rapporteur</b>
<b>Prof. BUYLE-DODIN François, Université de Lille, France</b>	<b>Rapporteur</b>
<b>Prof. BURLION Nicolas, Université de Lille, France</b>	<b>Examineur</b>
<b>MCF. CHEN Wen, Université de Lorraine, France</b>	<b>Examineur</b>
<b>Prof. ZHANG Jianren, Université des Sciences et Technologies de Changsha, Chine</b>	<b>Examineur</b>
<b>MCF-HDR. BIAN Hanbing, Université de Lille, France</b>	<b>Co-encadrant</b>
<b>Prof. POTIER-FERRY Michel, Université de Lorraine, France</b>	<b>Directeur de thèse</b>

PRESTRESS AND BEARING CAPACITY LOSS OF  
PRE-TENSIONED CONCRETE BEAMS DUE TO CORROSION  
CRACKS

by  
DAI Lizhao

A DISSERTATION

Submitted to  
UNIVERSITY OF LORRAINE  
in partial fulfillment of the requirements  
for the degree of  
DOCTOR OF PHILOSOPHY  
Civil Engineering

2019

# RESUME

Les ponts sont des structures destinées au franchissement des obstacles et ayant généralement une portée plus large que ces obstacles. Ils jouent un rôle clé dans le trafic terrestre. Le béton précontraint est largement utilisé dans la construction des ponts. Cependant, vu les échanges de masse avec l'environnement (eau, CO<sub>2</sub> et autres agents chimiques ...), les armatures de précontrainte ont tendance à se corroder. Comme le produit corrodé a un volume plus important que le matériau sain, la corrosion peut provoquer des fissurations dans les enrobages en béton, et par conséquent, la dégradation de la structure et sa capacité de la résistance. La sécurité et la durabilité de la structure sont alors menacées. La présente étude a été menée pour bien comprendre et bien maîtriser cette pathologie dans les structures en béton précontraint. On étudiera la capacité de résistance de poutres en béton précontraint en prenant en compte l'influence de la corrosion. Ce mémoire est composé de 6 chapitres.

D'abord, une analyse bibliographique est menée dans le premier chapitre. Puis, dans le chapitre deux, la relation entre l'ouverture des fissures et le taux de remplissage du produit corrodé dans les fissures a été établie par une approche expérimentale, notamment par l'essai de corrosion accélérée. Cette équation empirique est validée par des données expérimentales. Les résultats expérimentaux montrent que le taux de remplissage du produit de corrosion a un fort lien avec l'ouverture de la fissure, jusqu'à une valeur critique. Lorsque l'armature transversale est utilisée, l'ouverture critique diminue de 20% par rapport au cas sans armature transversale.

Ensuite, dans le chapitre trois, l'influence du niveau de précontrainte sur l'ouverture de fissuration est étudiée à la fois par des approches expérimentales et analytiques. On présentera d'abord les essais de corrosion accélérée sur des poutres avec différents niveaux de précontrainte. Puis un modèle analytique prenant en compte les effets couplés de la précontrainte et de la corrosion des armatures, est proposé pour prédire le processus global de fissuration de l'enrobage. Les résultats montrent que la

précontrainte peut accélérer le processus de fissuration induit par la corrosion. En faisant varier la précontrainte de 0 à 75% de la résistance d'armature, le temps correspondant à l'amorçage de fissuration diminue de 22% et le taux de propagation de la fissure augmente de 9%.

Dans le chapitre quatre, un modèle est proposé pour prédire la perte de précontrainte à cause de la corrosion dans les poutres en béton précontraint. Des essais de flexion à quatre points ont été réalisés sur huit poutres en béton précontraint sous différents niveaux de précontrainte, avec des armatures corrodées. Les résultats expérimentaux sont utilisés pour valider le modèle proposé. La chute de précontrainte dans les poutres et la résistance mécanique ont un fort lien avec la corrosion. Lorsque le niveau de corrosion est inférieur à 6,6%, il n'y a pas de perte de résistance significative. Puis, avec l'augmentation du taux de corrosion, la résistance des liaisons béton-armature et la précontrainte effective diminuent progressivement, jusqu'à zéro lorsque le niveau de corrosion atteint 34%.

Finalement, dans le cinquième chapitre, un modèle analytique pour prédire la résistance en flexion de poutres en béton précontraint corrodées a été proposé. Dans ce modèle, la réduction de la section d'armature, la détérioration des matériaux, la fissuration du béton et la dégradation des liaisons entre béton et armature ont été pris en compte. Le modèle proposé est validé par les résultats expérimentaux. A partir de 5,5%, la résistance en flexion a été fortement perturbée par la corrosion d'armature. Le dernier chapitre présente les conclusions générales et les perspectives.

**Mots clés : Ponts ; Poutres en béton précontraint ; Corrosion ; Fissuration ; Chute de précontrainte ; Résistance en flexion**

# ABSTRACT

Bridges, as the structures built to cross obstacles and generally has a relative larger span, play a key role in the road traffic. Pre-tensioned concrete structure is widely used in the bridge construction due to its superiority and advantages. However, with the mass exchange of its environment (water, CO<sub>2</sub> and other chemical agents), the prestressing strand would be easy to corrode. Strand corrosion can cause concrete cracking, degrade the bond performance at the strand-concrete interface, lead to prestress loss, and deteriorate the capacity of beams. The present study mainly focuses on the concrete cracking, prestress loss and flexural capacity of pre-tensioned concrete beams after strand corrosion. The main research works are as follows:

(1) The relationship between corrosion-induced crack widths and filling proportion of corrosion products has been established. The effect of stirrups on corrosion-induced cracking has also been investigated. An empirical model for crack width, considering the filling proportion of corrosion products and twisting shape of strand, is developed. The proposed model is validated by experimental data. Results show that the filling of corrosion products extends with crack propagation until a critical width. Beyond the critical width, the rust filling extent keeps stable. When the stirrups are used, the critical crack width decreases by 20%, comparing to that without stirrups.

(2) The influence of prestress on the strand corrosion-induced concrete cracking is investigated by both experimental and analytical approaches. Experimental data on the critical time of cover cracking, crack width and corrosion loss obtained from the accelerated corrosion test are presented. An analytical model, incorporating the coupled effects of prestress and strand corrosion, is proposed to predict the global process of concrete cracking from initiation to propagation. Results show that prestress can accelerate the corrosion-induced cracking process. By varying prestress from 0 to 75% of strand tensile strength, the critical time of cover cracking decreases by 22% and the crack propagation rate increases by 9%. It is found that the proposed model is accurate

in predicting corrosion-induced crack width in prestressed concrete beams.

(3) A novel model is proposed to predict the corrosion-induced prestress loss in pre-tensioned concrete beams. The coupling effects of concrete cracking and bond degradation are included into the model. The effective prestress in eight corroded pre-tensioned concrete beams under various stress levels is conducted by the four-point flexural test. Experimental results are employed to verify the proposed model. Prestress loss in corroded pre-tensioned concrete beams depends on corrosion level. Corrosion-induced concrete cracking may not degrade bond strength and effective prestress unless the corrosion level exceeds 6.6%. As corrosion further progresses, bond strength and effective prestress reduce monotonically, and then decrease to zero when the corrosion level reaches 34.0%.

(4) An analytical model, incorporating the effects of strand cross-section reduction, material deterioration, concrete cracking and bond degradation, is developed to predict the flexural capacity of corroded prestressed concrete beams. Additionally, the effects of flexural cracks are also included in the model. An equivalent bond stress concept is introduced to consider the effect of flexural cracks, which is further implemented into the flexural capacity prediction of corroded PC beams. The proposed model is validated by the experimental results collected from the previous studies. The flexural capacity deterioration of prestressed concrete beams depends on corrosion degree. Strand corrosion less than 5.5% leads to a slight decrement of flexural capacity. As corrosion progresses, the flexural capacity will exhibit a significant deterioration.

**Key Words: Bridge engineering; Pre-tensioned concrete beams; Corrosion; Corrosion-induced cracking; Prestress loss; Flexural capacity**

# TABLE OF CONTENTS

RESUME .....	I
ABSTRACT.....	III
TABLE OF CONTENTS .....	V
Chapter 1. Introduction .....	1
1.1 Backgrounds and significances .....	1
1.2 Literatures review .....	5
1.2.1 Corrosion morphology of strands .....	5
1.2.2 Corrosion-induced concrete cracking .....	7
1.2.3 Bond strength degradation of corroded strands .....	10
1.2.4 Corrosion-induced prestress loss .....	13
1.2.5 Flexural capacity of corroded PC beams .....	14
1.3 Discussions of existing researches .....	15
1.4 Layout of the dissertation.....	16
1.5 Summary .....	17
Chapter 2. Concrete Cracking Prediction Including the Filling Proportion of Strand Corrosion Products.....	19
2.1 Introduction.....	19
2.2 Experimental program .....	21
2.2.1 Specimen details .....	21
2.2.2 Accelerated corrosion of the strand.....	22
2.2.3 Crack width and corrosion loss measurement .....	23
2.3 Experimental results and discussions.....	25
2.3.1 Corrosion morphology, cracking propagation, and corrosion loss .....	25
2.3.2 Filling of corrosion products in cracks .....	31
2.4 Prediction model of crack propagation .....	35
2.4.1 Corrosion products at the micro-crack formation.....	35

2.4.2 Crack width on the concrete surface .....	38
2.4.3 Validation of the prediction model.....	39
2.5. Conclusions.....	40
Chapter 3 Crack Width Prediction under Combined Prestress and Strand Corrosion.	42
3.1 Introduction.....	42
3.2 Experimental program .....	44
3.2.1 Details of specimens .....	44
3.2.2 Accelerated corrosion and corrosion product measurement .....	45
3.2.3 Measurement of crack width and corrosion loss.....	47
3.3 Experimental results and discussions.....	47
3.3.1 Expansion ratio of strand corrosion products .....	47
3.3.2 Crack propagation under various prestress .....	50
3.4 Prediction of corrosion-induced cracking in PC beams.....	52
3.4.1 Model for corrosion-induced cracking.....	53
3.4.2 Model validation .....	59
3.5 Conclusions.....	60
Chapter 4 Prestress Loss Prediction in Pre-tensioned Concrete Structures with Corrosive Cracking .....	62
4.1 Introduction.....	62
4.2 Model for prestress loss in corroded PT structures.....	63
4.2.1 Concrete cracking induced by strand corrosion.....	64
4.2.2 Bond degradation due to strand corrosion .....	67
4.2.3 Corrosion-induced prestress loss .....	68
4.3 Evaluation of effective prestress in corroded PT beams .....	72
4.3.1 Specimen details .....	72
4.3.2 Accelerated corrosion and corrosion loss measurement .....	73
4.3.3 Effective prestress evaluation under various stress levels .....	74
4.3.4 Validation on prestress loss model .....	76

4.4 Conclusions.....	79
Chapter 5 Flexural Capacity Prediction of Corroded PC Beams Incorporating Bond Degradation.....	81
5.1 Introduction.....	81
5.2 Concept of flexural capacity model .....	82
5.3 Bond strength of corroded strand considering flexural cracks .....	84
5.3.1 Corrosion-induced cracking and bond degradation .....	84
5.3.2 Equivalent bond strength considering flexural cracks .....	88
5.4 Calculation procedure of flexural capacity .....	89
5.5 Model validation .....	94
5.6 Conclusions.....	99
Chapter 6 Conclusions and Perspectives .....	100
6.1 Conclusions.....	100
6.2 Perspectives.....	102
References.....	103
Acknowledgments.....	116
Publications and Projects .....	117

# Chapter 1 Introduction

## 1.1 Backgrounds and significances

Bridges, as the structures built to cross road obstacles, play a key role in the normal operation of road traffic. With the rapid development of social economy, bridge engineering has been unprecedentedly developed, showing a thriving scene. There are more than 830, 000 highway bridges and 10, 000 kilometers of high-speed railway bridges in China in 2018. Prestressed concrete has been widely used in bridge construction because of its high strength, good compactness, small cracks and superior spanning ability [1]. According to the construction technology, prestressed concrete bridges can be divided into pre-tensioned and post-tensioned concrete bridges.

Pre-tensioned concrete bridge is widely used in small/medium span bridge due to its superiority of convenient construction and mass precasting. However, the durability degradation of these bridges, caused by the bad construction quality, environmental erosion and material deterioration, has been gradually found during the serviceability period [2]. Additionally, the pre-tensioned concrete bridge has a small size and a thin protective concrete cover. Without the protection of corrugated pipe, the prestressing strand would be easy to corrode. Strand corrosion can cause concrete cracking, degrade bond performance at the strand-concrete interface, lead to prestress loss, and deteriorate the capacity of bridges [3], as shown in Fig. 1.1. Therefore, it has an important economic and academic values to study the durability and remaining service life of corroded pre-tensioned concrete bridges for ensuring their normal operation and safety utilization.

Strand corrosion is one of the main reasons for the performance deterioration of PC bridges. In worldwide, safety accidents of PC bridges caused by corrosion have been widely reported. A footbridge collapsed suddenly in Hampshire, England in 1967. A large number of corroded prestressing tendons in the Angell Road Bridge, North

London, was found in 1980. The Welsh bridge, United States, suddenly failed due to strand corrosion at the joint positions in 1985. The Ynys-Gwaa Bridge in the UK collapsed in 1985 due to the corrosion of post-tensioning tendons at the segment joints after only 32 years of service [4]. Additionally, Italy's Saint Stefano Bridge failed in 1999, after 40 years of service, due to pitting corrosion of the prestressing steel near the box girder joints. The collapse of Lake View Drive Bridge in the United States in 2005 was caused by strand corrosion [5].

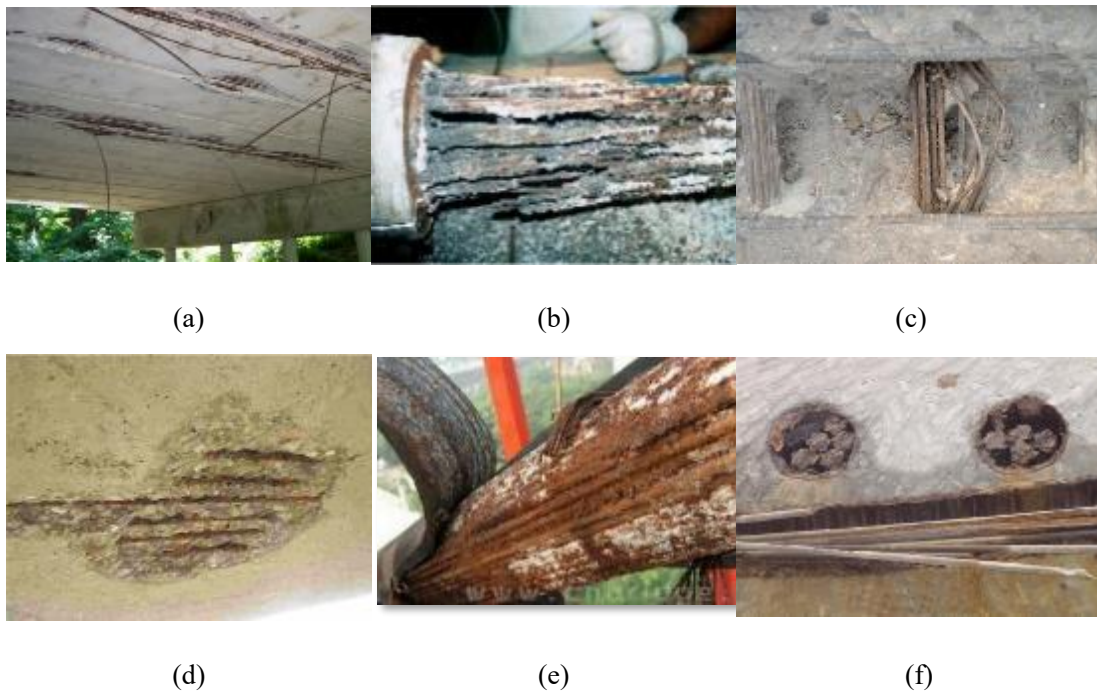


**Fig. 1.1. Corrosion of prestressed tendons in bridges**

It is found that more than 200 durability problems caused by prestressing tendon corrosion had been reported in worldwide during 1951-1979, which caused huge economic losses. A survey in 1982 indicated that 10 safety accidents caused by strand corrosion had been reported in USA during 1978-1982 [6]. Fig. 1.2 shows the failure of bridges due to the corrosion.

In China, with the economic development, a large number of PC bridges has been built. The durability of PC bridges has been gradually emerged under the combined effects of traffic growth and environment worsening during the serviceability, as shown in Fig. 1.3. Reports from the railway department in 1994 indicated that more than 6,000 defective concrete bridges were under the operation in China, accounting for 18.8% of

the total number. Structural deterioration caused by corrosion has cause huge economic losses, which needs to be paid high attention.



(a) Ynys-Y-Gwas Bridge, British (b) Lake View Bridge, USA (c) Saint Stefano Bridge, Italy



(d) Illinois Bridge, American (e) Lowe's Footbridge, USA (f) Bob Graham Bridge, USA

**Fig. 1.2. Corroded prestressed concrete bridges in worldwide**

Strand corrosion has been found to be one of the mostly common problems in prestressed concrete (PC) bridges [7, 8]. Corrosion can reduce the strand section area, the mechanical strength and bond properties of strand. These factors would lead to the structure deterioration. The failure of prestressed concrete bridges would exhibit brittle characteristic without warning owing to the high stress state of strand, which leads to a seriously economic loss. Existing investigations are mainly focus on the corrosion of reinforced concrete structures, and the related corrosion mechanism of ordinary steel has been studied extensively [9-11]. Very few works on strand corrosion have been reported.

The corrosion morphology of strand is more complicated than that of ordinary steel due to the combined effects of electrochemical corrosion, stress corrosion and crevice corrosion [12]. First, the corrosion rate of strand is faster than that of steel due to high stress state. Second, prestressing strand in bridges are usually made of multiple steel wires, the gap between the steel wires will provide a channel for the longitudinal

migration of erosion medium, which promotes the corrosion propagation. How does strand corrosion evolve? What is the effect of high stress on corrosion-induced cracking? How does the bond between strand and concrete degrade? How to evaluate the effective prestress of strand after corrosion? How do these factors affect the bearing capacity of corroded PC beams? These problems need to be resolved.



(a) Ziya Bridge, Tianjin

(b) Qianjiang Third Bridge

(c) A bridge in Jiangsu



(d) Xiaonanmen Bridge



(e) A bridge in Sichuan



(f) Lucun Bridge

**Fig. 1.3. Corrosion of prestressed concrete bridge in China**

The corrosion mechanism between the pre-tensioned and post-tensioned concrete bridges may be difference due to the construction techniques [12]. Post-tensioned concrete bridge bridges will exist the grouting defect due to bleeding and construction problems [13]. This defect not only reduces the ability of strand and concrete to work together, but also reduces the strand protection, causing it be corroded by erosion medium [14]. Strands in pre-tensioned concrete bridges are easily to be corroded without the bellow protection. Strand corrosion causes concrete cracking and bond degradation. Additionally, prestressing strand in pre-tensioned concrete beams transmits the prestressing force to concrete through interface bond stress, the effective bond is especially important compared with other concrete structures [15]. Corrosion-

induced bond degradation not only weakens the ability of strand to work together with concrete, but also affects the stress transfer, which can be easy to cause the anchorage failure of beams [16]. As mentioned above, the mechanical properties of corroded pre-tensioned and post-tensioned concrete structures are different, which needs to be discussed separately.

The present study mainly focuses on investigating the prestress and flexural capacity loss of pre-tensioned concrete beams with corrosion cracks. The paper is organized as follows. First, the filling effect of strand corrosion products and crack propagation are studied. Then, the prediction model of strand corrosion-induced cracking is proposed. Next, the prestress loss of pre-tensioned concrete beams with corrosive cracking is evaluated. Finally, the flexural capacity model of corroded pre-tensioned concrete beams is developed. This work will provide some scientific evidences for improving the durability evaluation theory, and guiding the repair and reinforcement decision-making of existing prestressed concrete bridges. Relevant investigations have important academic and engineering values.

## **1.2 Literatures review**

### **1.2.1 Corrosion morphology of strands**

Corrosion morphology of strands is very complicated, and relates to many factors [17]. The internal environment of PC structures is alkaline under normal circumstances first. This condition provides a dense passivation film on the strand surface, which can prevent the strand from corrosion. When the external erosive medium penetrates into the PC structures, the pH value inside concrete decreases, which would destroy the passivation film on the strand surface. With the existence of water and oxygen, the prestressing strands would be oxidized, causing electrochemical corrosion [13].

The electrochemical corrosion of strand can cause the uniform or pit corrosion. Once corrosion occurs, the strand surface would form a small anode region and a large cathode region. The oxygen in the cathode region is generally sufficient, which causes

the chemical reaction of iron element at the anode position. This reaction will generally lead to pit corrosion of strand [18]. The uniform corrosion appears once the large concentration of chloride ions exist on strand surface [19]. In addition, the twisting shape of strands causes crevice corrosion, which is different from ordinary steel. The corrosion rate of twisting wire at the strand-concrete interface is significantly faster than that on other positions [19, 20].

Except for the above-mentioned electrochemical and crevice corrosion, stress corrosion may also occur in strand under high stress state [21]. The unexpected sudden failure of metals subjected to stress corrosion cracking (SCC) will occur, especially at elevated temperature. The corrosion rate of strands under the high stress conditions is faster than the unstressed state [22, 23]. Toribio et al. [24, 25] investigated the residual stress of prestressing steel wire. It was found that the stress corrosion changed from hydrogen induced cracking to anode dissolution with the increase of corrosion potential. Valiente et al. [26] proposed a new method for evaluating SCC based on the fracture theory. This method showed that the small-scale yield of metal at the crack tip position was the main cause for the SCC. Vehovar et al. [22] investigated the corrosion state of prestressing steel wire in a 22-year-old viaduct bridge. It was pointed out that stress corrosion and hydrogen embrittlement could lead to the cleavage fracture of wire in the brittle region, and the region area of cleavage fracture increases with corrosion degree increases.

Stress corrosion of steel needs a specific electrochemical state, and the high stress state is a prerequisite for stress corrosion. Some theories have been proposed to explain the mechanism of stress corrosion of steel, which can be concluded as: Hydrogen embrittlement theory; three-stage theory of environmental rupture; mechanical-electrochemical mechanism theory; anodic dissolution theory; and stress adsorption theory [24, 27]. Although the above mentioned theories can explain the metal stress corrosion to some extent, the widely accepted theory has not been found yet.

For the stress corrosion mechanism of prestressing strands, the commonly accepted

theories are anodic dissolution (AD) and hydrogen induced cracking (HIC) mechanism. The AD mechanism indicates that the continuous exchange of metal cation with the anion can cause the passivation film destruction on the strand surface. A large tensile stress will be generated at the strand interface during this process, which cause a local plastic deformation. When the local plastic deformation exceeds a certain critical condition, micro cracks induced by stress corrosion will occur. HIC theory indicates that strands will absorb the hydrogen during the manufacturing process (or the cathode will release the hydrogen during the corrosion process) [25]. Once the hydrogen atoms diffuse to crack tip, the material may exhibit brittle properties, causing the hydrogen embrittlement fracture [27].

Under the coupling effects of stress state and corrosive environment, the micro crack and void may appear on the strand surface, which can damage the material microstructure [7]. Corrosion can change the elastic modulus, ultimate strength, and elongation of strand. Vu et al. [28] investigated the stress corrosion cracking of steel wires, and pointed out that the micro-cracks would cause a 25% decrease of elasticity modulus. Naito et al. [29] measured the mechanical properties of corroded prestressing tendons in Lake View Drive Bridge. Data indicated that the pit corrosion (corrosion loss greater than 20%) caused a 30% decrease of strand tensile strength. Gardoni et al. [12, 13] investigated the effects of grouting, salt spray and chloride ion on the mechanical properties of corroded prestressing strand, and established a time-varying probability model of resistance of corroded prestressing strands. Li et al. [30] carried out fatigue-loading tests on corroded prestressing stay cables serviced for 18 years. The fatigue life of stay cables had been obtained based on Monte Carlo sampling.

### **1.2.2 Corrosion-induced concrete cracking**

The volume expansion of strand corrosion products will be confined by the surrounding concrete, which can generate expansive pressure and lead to concrete cover cracking. Corrosion-induced cracking will further provide a path for the erosion ion to the internal concrete, which promote the corrosion rate of strand. Investigation shows

that the diameter, shape, material properties and corrosion morphology of strands can affect the corrosion-induced cracking process [31, 32]. Corrosion-induced cover cracking is an important indicator for the durability limit state of concrete structures. Therefore, it has an academic and practical values to clarify the mechanism of corrosion-induced cracking.

Many researches have been carried out to investigate the corrosion-induced cracking of reinforced concrete structures, which can be summarized as: the experimental, analytical and numerical studies. The experimental studies on the corrosion-induced cracking are the critical condition of cover cracking and crack propagation [33-35]. Coronelli et al. [36] considered the influences of the corrosion of longitudinal steels and stirrups on concrete cracking. The X-ray attenuation theory had also been employed to monitor the development of corrosion products and cracks [37]. The empirical formulas to predict the critical time of cover cracking and crack width have also been proposed. These formulas can provide a reasonable prediction under a certain condition, but the applicability of empirical formulas is still a problem. In addition, the corrosion-induced cracking of concrete structures is affected by many factors, such as the environment conditions and material properties. It is often difficult to comprehensively consider all factors in the empirical formula. Furthermore, the different test methods may lead to the differences of empirical models. The commonly used accelerated corrosion methods have dry-wet circulation, salt corrosion and electrochemical corrosion. How to use a unified empirical formula to evaluate the corrosion-induced cracking still needs to be studied further.

The analytical models for corrosion-induced cracking of RC structures have been proposed. Based on the theory of elastic or fracture mechanics, the critical corrosion loss of cover cracking can be obtained with a single-layer cylinder model or double-layer cylinder model [31, 38, 39]. Some scholars introduced a smeared crack concept to consider the softening behavior of cracked concrete, and derived the prediction model of crack widths. The concept of degradation factor had also been introduced to

consider the stiffness degradation of cracked concrete [40]. With the further development of theoretical research, the concrete cracking under the combined effects of non-uniform corrosion and external load was investigated. Studies indicate that the non-uniform corrosion can more veritably reflect the steel corrosion than the uniform corrosion, and the assumption of uniform corrosion may underestimate the internal stress generated by corrosion products [41]. Reale et al. [42] compared the existing theoretical models for corrosion-induced cracking, and discussed the defects and characteristics of each model. The existing theoretical model can reasonably describe the corrosion-induced cracking behavior of reinforced concrete structures, while how to accurately consider the material characteristics, the non-uniform corrosion and load effects in the model is still a problem.

Finite element simulation is another effective tool to model corrosion-induced concrete cracking in RC structures. The main advantage of numerical simulation is that it can effectively simulate the effect of pit corrosion on concrete cracking. The expansive pressure induced by pit corrosion can be simulated by the virtual internal pressure, temperature expansion ring or radial displacement. After that, the corrosion expansion force and cracking behavior of concrete cover can be obtained. The two-dimensional lattice model and the embedded finite element model had been proposed to model the corrosion-induced cracking [43, 44]. Du et al. [45] used the three-phase composite materials (i.e. aggregate, cement mortar matrix and interface transition zone) to simulate the concrete cracking with the uniform corrosion assumption. A plastic damage model was employed to investigate the mechanical behavior of mortar matrix and interface transition zone. The concept of fracture mechanics was used to consider the anisotropy of cracked concrete and the failure mode of concrete cover [46]. Some scholars compared the difference of the finite element nonlinear model, the single-layer cylinder model and the double-layer cylinder model, and pointed out the applicable conditions of each model [40]. Zhao et al. [47] measured the thickness of the rust layer on the steel surface, and employed the Gaussian function to describe the non-uniform

corrosion of steel.

In the numerical simulation, how to obtain the distribution of corrosion products and corrosive expansion pressure at the steel-concrete interface is the key factors to establish the model. The existing numerical simulation usually used a two-dimensional model to simulate the stress and strain distribution of the cracked concrete, which can effectively simplify the calculation process of cracking analysis. However, the two-dimensional model cannot consider the development of corrosive cracks in the longitudinal direction, and impossible to model the concrete spalling. Some scholars proposed the three-dimensional model to simulate concrete cracking for overcoming these defects. However, the relevant theory is still in the exploration stage, which needs the further study.

As mentioned above, numerous literatures have been undertaken to study the corrosion-induced concrete cracking in RC structures, few researches on PC structures have been reported yet. In addition, the twisting shape of the prestressing strands can cause the pit and crevice corrosion, which will lead to the accumulation and development of the corrosion products at strand-concrete interface to be more complicated. Thus, the researches on corrosion-induced cracking of prestressed concrete should be studied further.

### **1.2.3 Bond strength degradation of corroded strands**

Corrosion-induced cracking reduces the protective effect of cover on strand, and degrades the interlock, friction and bond properties between strand and concrete, which degrades the bond strength of strand. For PC structures, especially pre-tensioned concrete structures, the effective bond strength is a key factor to ensure the strand and concrete working together.

Many researches have been undertaken to investigate the bond behavior of corroded steels in RC structures, which can be concluded as: experimental research, theoretical analysis and numerical simulation [48]. Some scholars experimentally explored the bond-slip behavior of corroded steels with stirrup constraints [49-51]. Almusallam et al.

[52] studied the bond strength and failure modes of corroded reinforced concrete beams with the pull-out tests. The effects of relevant parameters (concrete cover thickness, steel diameter, concrete strength, type of stirrups and crack widths) on bond performance of corroded steels have been discussed [53, 54]. Al-Hammoud et al. [55] compared the difference of bonding properties of corroded reinforced concrete beams under static and dynamic loads. Choi et al. [56] discussed the difference of the bond properties of concrete structures under natural corrosion and accelerated corrosion, and pointed out that the accelerated corrosion method may underestimate the effect of corrosion on the bond degradation. Additionally, some scholars had also discussed the bond degradation behavior of corroded reinforced concrete with common aggregates and recycled aggregates [57].

Some analytical models have also been proposed to predict the bond performance of corroded reinforced concrete beams. Wang et al. [58] pointed out that the bond strength between corroded steel and concrete was affected by many factors, such as the corrosion degree, bar type, the adjacent bar spacing and the number of stirrups. Among these factors, the corrosion degree is most significant to affect the bond strength. Coccia et al. [59] considered the relationship between corrosion depth of steel and the radial displacement of concrete, and proposed a model to predict the bond strength of corroded steel based on the thick-walled theory. Chen et al. [48] proposed a model to predict the bond strength of corroded RC beams, incorporating the softening behavior of cracked concrete.

Some scholars have employed the finite element software to numerically simulate the bond behavior of corroded RC beams. Lee et al. [60] used the bond plane unit and bond interface unit to numerically model the bonding properties of corroded RC beams. Berto et al. [61] simulated the bond properties of corroded RC beams with two numerical methods, i.e. the friction type method and damage type method. Lundgren et al. [62] discussed the influences of corrosion on the bonding properties of ribbed and plain bars, respectively. Grass et al. [63] used the Lattice approaches to simulate the

bond properties of corroded RC beams, which can reasonably model the influence of filling extent of corrosion products in cracks.

The degradation law of bond performance after steel corrosion has been clarified. Abosrra et al. [64] indicated that the bond performance of steel would increase at the early stage of corrosion. As corrosion further increases, the bond performance of steel will gradually decrease. Kearsley et al. [65] pointed out that corrosion would lead to an increase in the bond strength when the corrosion loss of steel is less than 2%, and the bond strength decreases when the corrosion loss is greater than 2%. However, some other scholars indicated that a 2% diameter loss of steel would cause an 80% bond degradation. Chung et al. [66] pointed out that the critical corrosion loss of steel bond degradation was 3%. Wu et al. [67] showed that the failure mode of the corroded concrete members would change from the fracture failure of steel to the concrete crushing with corrosion increases. Bhargava et al. [68] reviewed the existing literatures on bond-slip of corroded steels, and proposed an empirical formula to predict the bond degradation of corroded RC beams.

Compared with the studies on the bond performance of corroded steels, the researches on the bond degradation of corroded strands are relatively rare. Morcous et al. [69] preliminarily explored the effect of corrosion pits on the bond properties of strands. Li et al. [23] conducted an experimental study to investigate the local bond-slip behavior of corroded strands. Wang et al. [70] established a bond-slip model of corroded strand based on the experimental results. Although some studies have been conducted to investigate the bond behavior of corroded strand, the relative mechanism has not been clarified yet.

As mentioned above, the bond behavior of prestressing strand is more complicated than the ordinary steels due to the twisting shape and material characteristic of strand. Additionally, the prestressing strands exist the rotate behavior during the pull-out process. Furthermore, the corrosion of prestressing strands under high stress state may be different from that of steel. Existing bond degradation laws of corroded steels may

not be applicable to predict the bond strength of corroded prestressing strands. The mechanism of bond degradation of corroded prestressing strands still needs to be studied further.

#### **1.2.4 Corrosion-induced prestress loss**

The effective prestress in PC structures is an important factor to ensure its serviceability and safety. The prestress loss in existing PC structures relates to many factors, such as concrete shrinkage and creep, stress relaxation and strand corrosion. These influencing factors are often interactive, and it is very difficult to reasonably evaluate the prestress loss in prestressing strands.

Existing researches mainly focus on investigating the effects of concrete shrinkage, concrete creep and stress relaxation of prestressing strand on long-term prestress loss. Caro et al. [71] studied the time-varying prestress losses caused by the shrinkage and creep of concrete. Asamoto et al. [72] evaluated the effect of early creep of concrete on prestress loss. Youakim et al. [73] evaluated the long-term prestress loss of prestressed concrete structures based on the coordination principles of strain and the force balance. Kottari et al. [74] further improved the calculation method of prestress loss proposed by AASHTO-LRFD specification, and investigated the sensitivity of parameters, such as concrete strength, the number of steel, the relative humidity and concrete age. Barr et al. [75] studied the prestress loss of high-performance prestressed concrete beams, and found that the method recommended by AASHTO-LRFD specification may overestimate the prestress loss.

As mentioned above, the existing researches mainly focus on investigating long-term prestress loss, and corrosion-induced prestress loss is rarely reported. Cavell and Waldron [76] used the strain compatibility method to estimate the residual prestress in post-tensioned concrete beams after tendon failure. Castel et al. [77] indicated that the prestressing force loss in post-tensioned concrete beams was proportional to the cross-section reduction of corroded strand.

The above researches evaluate the effect of cross-section area reduction of

corroded strands on the prestress loss in post-tensioned concrete beams. Corrosion-induced prestress loss is a very complicated problem. Except for the cross-sectional area reduction of strand, concrete cracking and bond degradation may induce the prestress loss. Additionally, the effective prestress of post-tensioned concrete structures depends on the anchor system at the beam end, while pre-tensioned concrete structures transfers prestress through bond stress at the strand-concrete interface. These lead to the corrosion-induced prestress loss in pre-tensioned concrete structures and post-tensioned concrete structures will be difference, which needs to be investigated separately.

### **1.2.5 Flexural capacity of corroded PC beams**

Strand corrosion in concrete is one of the main factors for the degradation of structural performance. Corrosion can lead to the section area reduction of strand, the deterioration of mechanical properties of materials, concrete cracking and bond degradation. These factors will weaken the bearing capacity of concrete structures. Additionally, corroded PC beams often exhibit the brittle failure without warnings under high stress state, which is more danger than RC members. It is significant to investigate the flexural capacity of corroded PC beams for ensuring its safety operation.

Many experimental studies have been carried out to study the bending performance degradation of corroded RC beams. The failure mode of specimens changes from the bending failure to the shear failure with corrosion increases [78-80]. Relative to the studies on the flexural capacity of corroded RC beams, the researches on the flexural capacity of corroded PC beams is relatively rare. Some experimental studies investigate the effect of corrosion on cracking, stiffness, ultimate strength, ductility and failure mode of PC members [81]. It is found that corrosion can reduce the number of bending cracks and increase the crack spacing, and decrease the ultimate load of beams [76]. The bearing capacity decreased by 67% when the corrosion loss reached 20% [82].

Corrosion can reduce the section area of strand, deteriorate the material property,

induce concrete cracking and degrade bond strength, which can further decrease the bearing capacity of PC beams. The bending capacity prediction model should reasonably consider the combined effects of these factors. Additionally, the aforementioned models fail to consider the effect of load cracks on the bending capacity of PC beams. The load cracks may change the bond strength in the longitudinal direction, which will affect the bending capacity. Neglecting the effect of flexural cracks may overestimate the flexural capacity of corroded PC beams. How to reasonably consider the aforementioned factors on the flexural capacity of corroded PC beams still needs to be studied further.

### **1.3 Discussions of existing researches**

As mentioned above, several literatures have studied the prestress and flexural capacity loss of pre-tensioned concrete structures due to corrosion cracks. Although some useful conclusions have been obtained, the relevant analysis theories are still not mature. Several technical problems still need to be studied further:

- [1] The filling extent of strand corrosion products in cracks has not been clarified. The filling of corrosion products relates to corrosion degree, the steel type and thickness of concrete cover. Additionally, strands are made of several twisting steel wires, which have a complicated cross-section. The filling of strand corrosion products in cracks may be different from that of ordinary steel. How to quantify the filling of strand corrosion products in cracks still needs to be studied further.
- [2] Prediction models for corrosion-induced cracking are concentrated on reinforced concrete structures. Corrosion-induced cracking of prestressed concrete may be different from that of reinforced concrete due to the prestressing force and twisting shape of strand. How to establish the prediction model for the corrosion-induced cracking of prestressing concrete is still a problem.
- [3] The effective prestress of strand is an important factor for ensuring the serviceability of pre-tensioned concrete beams. Corrosion-induced prestress loss is a complicated

problem. Corrosion can reduce the cross-sectional area of strand, cause concrete cracking, degrade bond strength, and lead to prestress loss. How to evaluate the corrosion-induced prestress loss in pre-tensioned concrete members needs to be studied further.

[4] Corrosion can reduce the section area of strand, deteriorate the material property, induce concrete cracking and degrade bond strength, which further deteriorate the bearing capacity of PC beams. Additionally, the load cracks change the bond strength in the longitudinal direction, which may affect the flexural capacity of PC beams. A model for the flexural capacity of corroded PC members, considering all of the aforementioned factors, is needed.

## **1.4 Layout of the dissertation**

The dissertation conducts a series of experimental and theoretical researches on the prestress and flexural capacity loss of pre-tensioned concrete structures due to corrosion cracks. The main work is as follows:

### **(1) Concrete Cracking Prediction Including the Filling Proportion of Strand Corrosion Products (Chapter 2)**

Strand corrosion can induce concrete cracking. Twelve cracked concrete beams with/without stirrups are obtained based on the accelerated corrosion test. The corrosion morphology of strands is observed. The filling extent of strand corrosion products in cracked concrete with/without stirrups is discussed, and the crack propagation in concrete is clarified. An empirical model for strand corrosion-induced crack widths is proposed based on the volume equivalent principle of corrosion products, considering the effects of stirrups, filling of corrosion products. The model is verified with the experimental results.

### **(2) Crack Width Prediction under Combined Prestress and Strand Corrosion (Chapter 3)**

Strand corrosion-induced concrete cracking under various prestress is investigated

experimentally and analytically. Experimental data on the critical time of cover cracking, crack width and corrosion loss obtained from the accelerated corrosion test are presented. An analytical model, incorporating the coupled effects of prestress and strand corrosion, is proposed to predict the global process of concrete cracking from initiation to propagation. The model is verified with the experimental results.

### **(3) Prestress Loss Prediction in Pre-tensioned Concrete Structures with Corrosive Cracking (Chapter 4)**

A novel model is proposed to predict the corrosion-induced prestress loss in pre-tensioned concrete beams. The coupling effects of concrete cracking and bond deterioration are incorporated into the model. The effective prestress in eight corroded pre-tensioned concrete beams under various stress levels is explored by the four-point flexural test. The experimental results are employed to verify the proposed model.

### **(5) Flexural Capacity Prediction of Corroded PC Beams Incorporating Bond Degradation (Chapter 5)**

An analytical model, incorporating the effects of strand cross-section reduction, material deterioration, concrete cracking and bond degradation, is developed to predict the flexural capacity of corroded prestressed concrete beams. Additionally, the effects of flexural cracks are also included in the model. An equivalent bond stress concept is introduced to consider the effect of flexural cracks, which is further implemented into the flexural capacity prediction of corroded PC beams. The proposed model is validated by the experimental results collected from the previous studies.

## **1.5 Summary**

This chapter first introduces the background and significance of this dissertation. Next, the literature review on the corrosion morphology of strand, corrosion-induced cracking, bond strength of corroded strand and flexural capacity of corroded PC beams, is introduced in detail. The shortcomings of existing researches are discussed. Then, the main research contents of this paper are given: (1) concrete cracking prediction

including the filling proportion of strand corrosion products (Chapter 2); concrete cracking prediction under combined prestress and strand corrosion (Chapter 3); prestress loss prediction in pre-tensioned concrete structures with corrosive cracking (Chapter 4); flexural capacity prediction of corroded pc beams incorporating bond degradation (Chapter 5).

# **Chapter 2 Concrete Cracking Prediction**

## **Including the Filling Proportion of Strand Corrosion Products**

### **2.1 Introduction**

Steel corrosion has been identified as one of the most deteriorating factors in concrete structures [83, 84]. During the corrosion process, the metallic iron is transformed to corrosion products [85, 86]. This reaction would create an expansive pressure around the concrete, and lead to concrete cracking [41]. The corrosion solution can easily diffuse to steel surface through the concrete cracks, which would further accelerate steel corrosion [87]. In addition, concrete cracking also weakens the bond between steel and concrete [88, 89]. These coupling effects decrease the durability and safety of concrete structures. Cover cracking has been considered as an important indicator of the service life end for the existing concrete structures [90].

A considerable number of studies have been undertaken on corrosion-induced cracking of reinforced concrete (RC) structures. The amount of corrosion products penetrating into cracks have also attracted attention. In early studies, some researchers considered that corrosion products fully filled cracks before cover cracking [91]. The recent detections of some existing structures, however, indicate that corrosion products could not fully fill cracks. This fully filled consideration may overestimate the filling effect of corrosion products. Zhao et al. [33, 34] found that corrosion products did not fill cracks inside concrete. Lu et al. [92] reported that the cracks were not completely filled by corrosion products, and a deduction coefficient was introduced to quantify the filling of corrosion products. These studies focus on the filling of corrosion products before cover cracking. After cover cracking, non-destructive studies were used to monitor the distribution of corrosion products [93]. Cracks were being filled with corrosion products gradually over time [94]. The composition and distribution of chloride-induced corrosion products in cracked concrete subjected to different loading

conditions were also investigated [95]. The filling of corrosion products depends on many parameters, such as corrosion degree, steel type, and cover thickness [31]. How to quantify the filling of corrosion products is still under discussion.

Predicting crack width with corrosion loss is another important issue to investigate concrete cracking. Torres-Acosta et al. [87, 96] established an empirical relationship between crack width and corrosion loss based on experimental data. The analytical crack width model considering the combined effects of steel corrosion and applied load was also derived [97]. Khan et al. [98] predicted the steel corrosion with crack width for a 26-year-old corroded RC beam. These studies aimed to investigate concrete cracking induced by corrosion of steel bars. Strand consists of several outer wires twisted around a core wire and has a flower-like cross-section. Concrete cracking caused by strand corrosion may be different from that caused by steel corrosion. For concrete structures reinforced with strands, Dai et al. [99] assumed the filling proportion of corrosion products as a constant and proposed a model to predict corrosion-induced cracking. A summary of studies on strand corrosion and crack filling are given in Table 2.1. With further work, the present study aims to quantify the filling proportion of corrosion products and develop a prediction model of crack width.

**Table 2.1. Summary of studies on strand corrosion and crack filling**

References	Specimens	Investigation
Vu et al. [28]	Steel wires	Stress corrosion cracking on stress-strain response of steel wires
Darmawan et al. [100]	Pre-stressing wires	Effect of pitting corrosion on capacity of pre-stressing wires
Vélez et al. [20]	Pre-tensioned concrete beams	Electrochemical characterization of early corrosion in pre-stressed concrete
Pillai et al. [13]	Strand	Probabilistic models for the tensile strength of corroding strands
Li et al. [23]	Post-tensioned concrete beams	Corrosion propagation of pre-stressing steel strands in concrete subject to chloride attack
Rinaldi et al. [82]	Pre-tensioned concrete beams	Influence of strand corrosion on flexural behavior of pre-stressed concrete beams
Li et al. [30]	Wire cables	Fatigue properties of corroded parallel wire cables
Dai et al. [99]	Post-tensioned concrete beams	Corrosion-induced cracking induced by strand corrosion

The proposed study investigates the filling of strand corrosion products during

concrete cracking. A prediction model of crack width is developed to consider the filling proportion of corrosion products and the twisting shape of strand. This chapter is organized as follows: first, the experimental design, including material properties, geometry dimensions, accelerated corrosion, and crack width and corrosion loss measurements are introduced; next, the filling of corrosion products and crack widths are discussed based on the experimental results; following this, a model is proposed to predict crack widths incorporating the filling proportion of corrosion products and the twisting shape of strand; finally, some conclusions are drawn based on the experimental results and theoretical analysis.

## 2.2 Experimental program

In this section, the details of specimens are given first. Next, the accelerated corrosion test is employed to obtain various crack widths. Following this, the measurement methods of crack widths, corrosion products and corrosion losses are exhibited. Details are shown below.

### 2.2.1 Specimen details

Twelve specimens were designed with a square cross-section of 150 mm × 150 mm, and 1200 mm in length. The specimens were divided into two groups: group S and group RS. Each group consisted of six beams. In the group RS, stirrups with 8 mm diameter and 150 mm spacing were arranged. Group S had no stirrups. The details of beams are shown in Fig. 2.1.

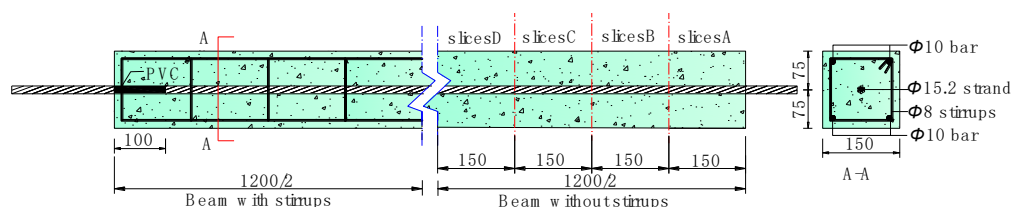


**Fig. 2.1. Details of the beam (unit: mm)**

The specimens were arranged with a 15.2 mm diameter, seven-wire steel strand. Four deformed bars with 10 mm diameters were used as the hanger bars at the corners of beams. The covers of strand and reinforcements were 67.4 and 30 mm, respectively. A 100 mm polyvinyl chloride (PVC) drive pipe was used to prevent the corrosion

solution flowing out from the beam end. Tables 2.2 and 2.3 show the chemical compositions and mechanical characteristics of steel.

**Table 2.2. Chemical compositions (wt %) of steel.**

Type	C	Mn	Si	P	S	Cr	Cu	Ni	Ti	Al
Strand	0.82	0.74	0.21	0.012	0.006	0.17	0.09	0.03	0.03	0.03
Deformed bars	0.2	1.34	0.55	0.033	0.028	/	/	/	/	/

**Table 2.3. Mechanical characteristics of steel.**

Type	Diameter (mm)	Yield Strength (Mpa)	Elastic Modulus (Gpa)
Strand	15.2	1830	195
Deformed bars (HRB335)	10	335	200
Deformed bars (HRB335)	8	335	200

The cement used in concrete was the Type 32.5 Portland cement. The Portland cement mainly contains CaO, SiO<sub>2</sub>, Fe<sub>2</sub>O<sub>3</sub>, and Al<sub>2</sub>O<sub>3</sub>. The concrete of group S and group RS was cast separately. The mix proportion and 28-day compressive strength of concrete are given in Tables 2.4 and 2.5.

**Table 2.4. Concrete mix proportion.**

Water to Cement Ratio	Cement (kg/m <sup>3</sup> )	Water (kg/m <sup>3</sup> )	Sand (kg/m <sup>3</sup> )	Stone (kg/m <sup>3</sup> )
0.43	417	179	676	1026

**Table 2.5. Twenty-eight-day compressive strength of concrete.**

Beams	S6, S9, S10, S11, S12, S13	RS3, RS7, RS9, RS10, RS11, RS12
Concrete strength (MPa)	32.5	35.5

### 2.2.2 Accelerated corrosion of the strand

The artificially-accelerated corrosion method was employed to obtain various crack widths in the beams [70]. To clarify the effect of strand corrosion on concrete cracking independently, reinforcement was protected with epoxy resin to prevent it from corrosion. The specimens were immersed in the 5% sodium chloride (NaCl) solution in a designed tank. The corrosion system consisted of a direct current potentiostat and a stainless steel plate. The strand acted as the anode, and the stainless steel plate served as the cathode. The direct current flowed from the positive terminals of potentiostat to the strand, and then through saturated concrete and saline solution to

the stainless steel plate, and finally back to the negative terminals of the potentiostat. Fig. 2.2 shows the accelerated corrosion system.

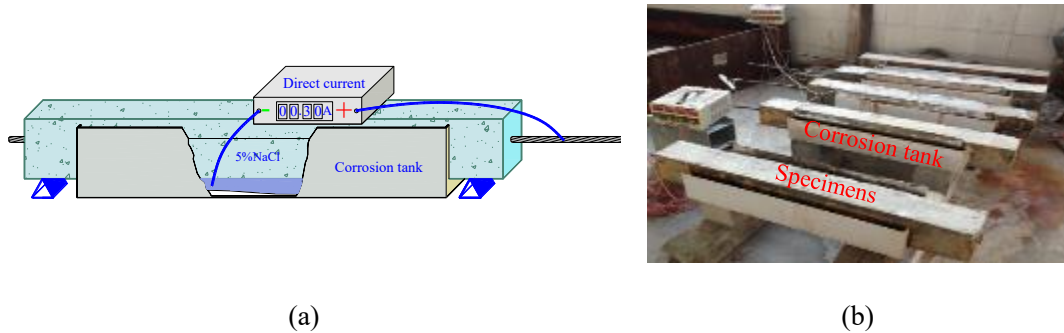


**Fig. 2.2. Accelerated corrosion device: (a) schematic diagram; and (b) photo**

The test specimens were immersed in the saline solution for three days before the accelerated corrosion. The corrosion rate was determined by the current density. The corrosion current in the total process was controlled at a constant of 0.3 A. The corresponding current density was about  $270 \mu\text{A}/\text{cm}^2$ . The theoretical mass loss was roughly estimated based on Faraday's law. The corrosion times were referred based on the relationship between the current intensity and mass loss. The accelerated corrosion time for all the specimens were given in Table 2.6.

**Table 2.6. Accelerated time of specimens**

Beams	S6	S9	S10	S11	S12	S13	RS3	RS7	RS9	RS10	RS11	RS12
Corrosion time (days)	2	9	7	3	5	6	7	8	14	9	3	3

### 2.2.3 Crack width and corrosion loss measurement

Micro cracks form, firstly, in the cross-section when tangential stress exceeds the concrete tensile strength. With increasing corrosion loss, the internal cracks could propagate to the concrete surface. The outer cracks on the concrete surface usually extend and join together to be a continuous crack along the specimen, which is named a longitudinal crack in the present study. After the accelerated corrosion test, the longitudinal cracks were observed on the concrete surface. The longitudinal cracks have different widths in various regions due to the uncertainty of corrosion and material properties. A portable microscope with the resolution of 0.01 mm was used to measure crack widths.

To investigate the crack patterns in the radial direction and the filling of corrosion

products in cracks, four 15 mm-thick cross-sectional slices were cut out from each beam after the accelerated corrosion. The location of the four slices is shown in Fig. 2.1 and labeled as A, B, C, and D, respectively. For example, the four slices of S6 are named as S6A, S6B, S6C, and S6D, respectively. The total number of slices was 48. The cracking angle was used to describe the crack distribution in the radial direction. Since the filling of corrosion products in cracks varied at different positions, the average rust-filling depth was used to reflect the filling of corrosion products in cracks.

The cracking angle was measured using a contour gauge. In the present testing, the maximum crack was selected to calculate the cracking angle. The measurement program was as follows: first, the contour shapes of cracks in the radial direction were painted to graph paper; next, the sketch maps of cracks were scanned into the computer. The cracking angle was defined as the angle of two sides of the crack; finally, the cracking angles were calculated by the aided drafting program. More details on the contour gauge can be seen in Higgins and Farrow [101]. The rust-filling depth was also measured using similar methods.

Strand corrosion exhibited variability in various regions. Local area loss and average mass loss were commonly used to evaluate the corrosion degree of strand. Some experimental studies showed that the average mass loss correlated well with the corrosion-induced crack widths for slightly corroded reinforcement [102]. In the present experimental testing, slight corrosion loss was found to induce cover cracking due to the large diameter of strand. Therefore, the average mass loss of the strand in 10 mm lengths was also employed to evaluate the corrosion degree.

The mass loss was measured after the accelerated corrosion, and the program was as follows. First, concrete cover was removed by the destructive method. Next, the strand was taken out and the concrete on its surface was removed by slightly knocking. Following this, the corroded strand was cleaned by 12% hydrochloric acid solution and then neutralized with alkali [103]. The strand was kept in the dry environment (relative humidity less than 25%). Finally, the average mass loss of the strand in 10 mm length was measured.

## 2.3 Experimental results and discussions

### 2.3.1 Corrosion morphology, cracking propagation, and corrosion loss

#### 2.3.1.1 Corrosion morphology of strand

Strand used in the present study includes the core wire and six outer wires. Fig. 2.3 shows the corrosion morphology of the strand. The strand showed pitting and crevice corrosion. Some small corrosion pits were observed on the strand surface. These corrosion pits exhibited oval or circle and their depths were small. Additionally, the gaps existed between the core wire and outer wires and could provide a path for the flow of aggressive liquid, resulting in crevice corrosion.

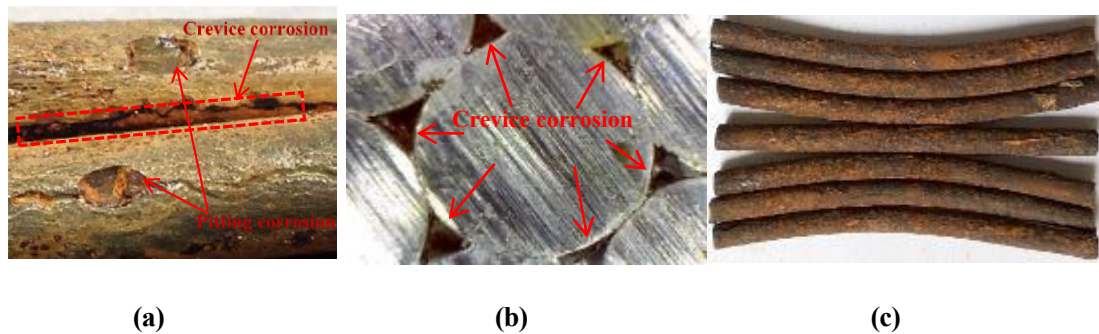


**Fig. 2.3. Corrosion morphology of strand: (a) pitting and crevice corrosion; (b) crevice corrosion; and (c) wire corrosion**

The movement of corrosive liquid along the crevices can lead to the range extension of corrosion along the strand, which will accelerate the corrosion rate of the strand. Corrosion loss in the strand can be higher than in steel reinforcement due to crevice effects, resulting in a larger corroding area per unit length. The corrosion rate of the steel increases with the increase of current density. The uniform corrosion occurred with a low current density. For a high current density, pitting corrosion occurred extensively on the steel surface [104]. In the present test, the current density was designed as the constant value. More studies on various current densities are needed in the future.

#### 2.3.1.2 Crack width and corrosion loss

With corrosion propagation, the first visible crack was found through the portable microscope. The crack then widened and extended along the corroded strand. Some corrosion products were found to flow out from the longitudinal cracks. Fig. 2.4 shows

corrosion products on the concrete surface from 10 mm to 110 mm for S6, S11, and S9, respectively. The average crack widths of S6, S11, and S9 are 0.13, 0.48, and 0.83 mm, respectively. Scarce corrosion products were found to flow out from the narrow longitudinal cracks. With cracking propagation, more corrosion products appeared on the concrete surface. The filling of corrosion products propagates with the widening crack.

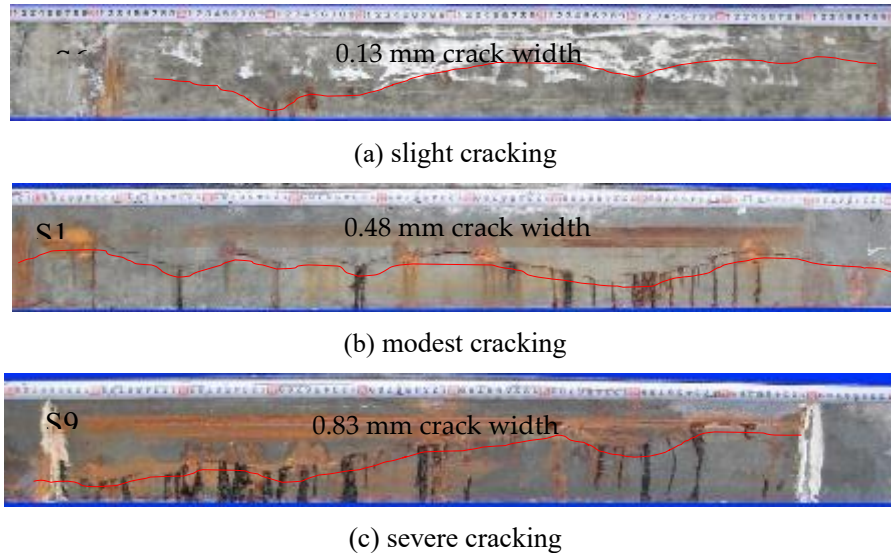


**Fig. 2.4. Longitudinal crack and corrosion products on concrete surface**

The beam ends were not immersed in the saline solution. Some radial cracks were still found at the specimen ends due to the movement of corrosive liquid. Fig. 2.5 shows the radial crack at the beam end. The radial crack is vertically inclined to the concrete surface.

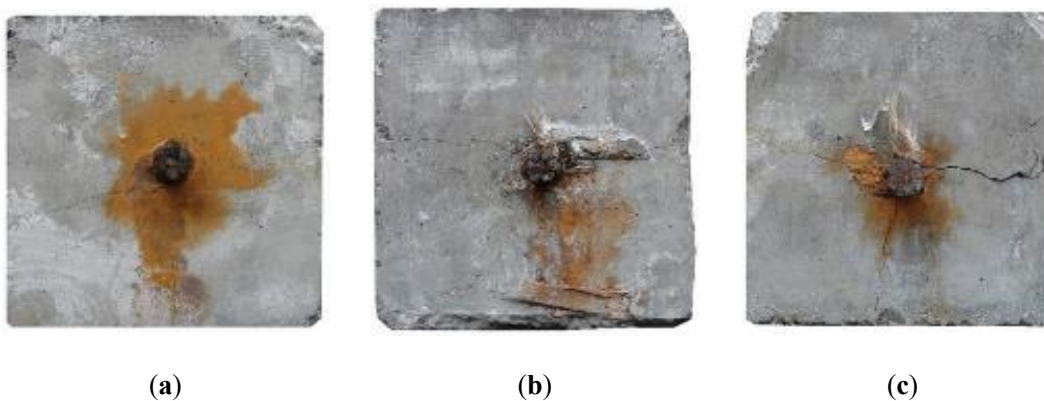


**Fig. 2.5. Radial cracks at beam end: (a) One crack; (b) two cracks; and (c) three cracks**

Strand corrosion prediction is one of the most important procedures for structural degradation evaluation. Corrosion loss is usually difficult to measure in terms of strands embedded into concrete. Correspondingly, crack widths on the concrete surface are easy

to obtain. Khan et al. [98] indicated that crack width could correlate well with corrosion loss. In the present study, crack widths are employed to identify the corrosion degree of strand. Crack width and corrosion loss were measured in 10 mm length. Fig. 2.6 and 2.7 show the relationship between crack width and corrosion loss for both groups, respectively.

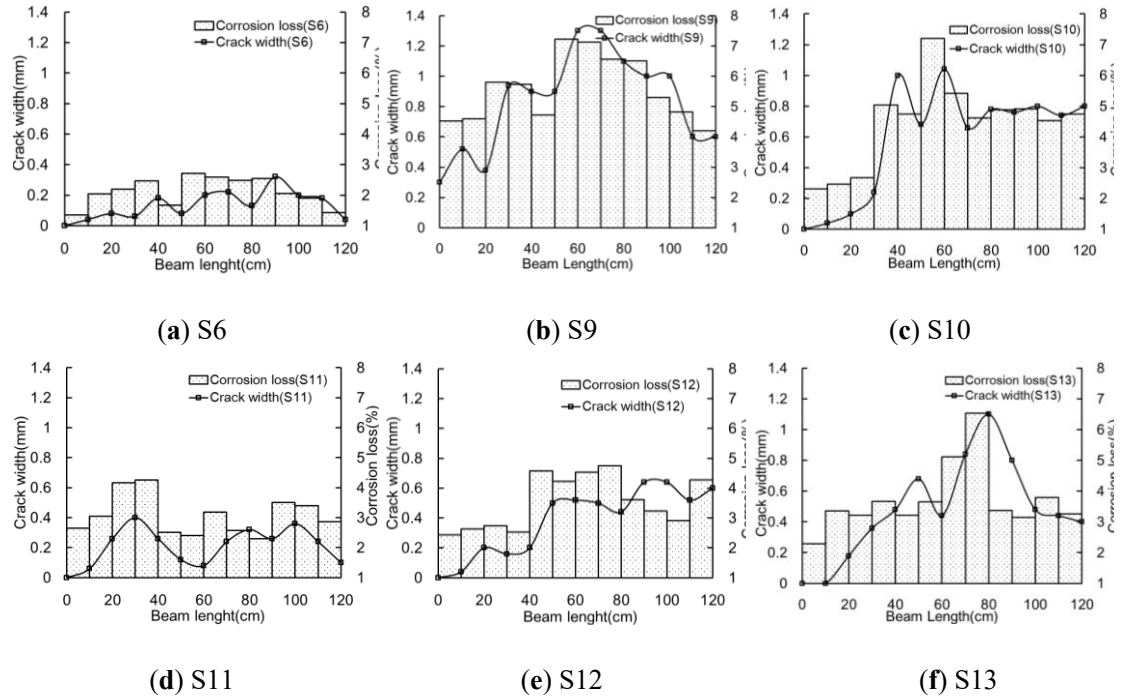


**Fig. 2.6. Crack width and corrosion loss (group S)**

The variation of crack width along beam length depends on corrosion degree. Under low corrosion loss, the variation of crack width is small. With future increasing corrosion, the variation of crack width increases. Additionally, it can be also found that the cracks in the middle span are usually wider than that in the beam ends. The reason for this phenomenon is that just the middle span of the beam has been immersed in the 5% sodium chloride (NaCl) solution during the accelerated corrosion. The corrosion degrees of the strand at the end regions are smaller than that in the middle span. Therefore, the crack in the middle span is wider than at the ends of the samples.

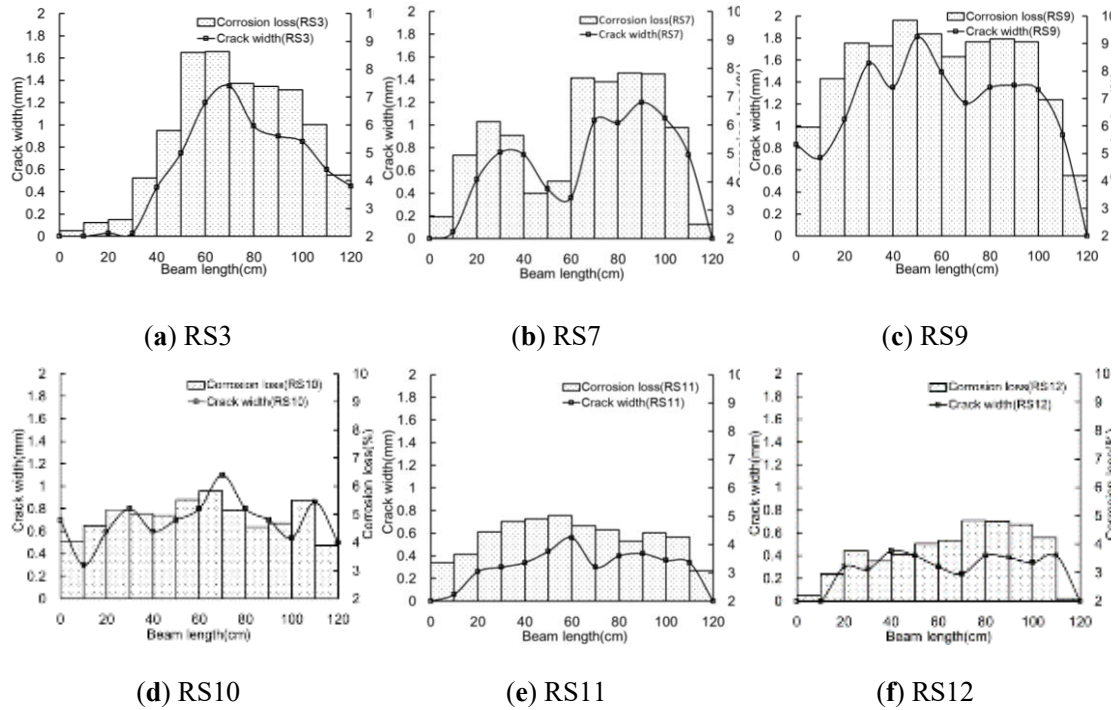


**Fig. 2.7. Crack width and corrosion loss (group RS)**

To analyze the effect of stirrups on crack width, the linear regression was used to describe the relation between crack width and corrosion loss and given in Fig. 2.8.

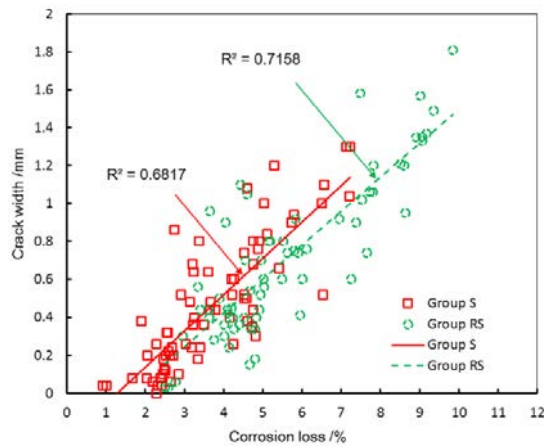


**Fig. 2.8. Summary of crack width and corrosion loss.**

As Fig. 2.8 shows, stirrups exhibit a significant restraint effect on corrosion-induced cracking. The cracks of Group S are wider than that of Group RS in the similar corrosion loss. The stirrups can bear the tangential stress induced by expansive pressure. Using stirrups decreases the corrosion-induced crack width. This indicates that increasing the amount of stirrups can restrain the crack extension in practical engineering.

Strand corrosion easily leads to concrete cover cracking. Some studies have been

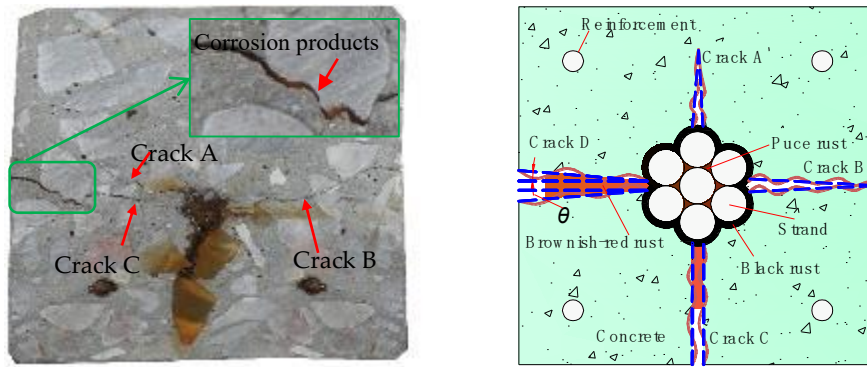
performed to improve the cracking resistance behavior of concrete [105, 106]. It has been reported that the supplementary cementing materials can significantly improve the concrete resistance against chloride ingress, lengthening the corrosion initiation time and cracking time of concrete structures under chloride-affected environment.

### **2.3.1.3 Cracking propagation**

The crack feature inside concrete is an important issue to investigate cover cracking. Crack propagation inside concrete is usually difficult to observe. To analyze the crack feature in the radial direction, specimens were cut into 15 mm-thick slices. Fig. 2.9(a) shows three cracks in a slice and named as: crack A, crack B, and crack C.

As Fig. 2.9 shows, crack A and crack C are the two forks of one crack in the cross-section. This separation of the crack could be attributed to the existing aggregate near the bifurcation point. Crack A is located in the inner concrete and did not extend to the concrete surface. Both cracks B and C propagated to the concrete surface. Crack B varied small along the radial direction. Crack C was the widest in the three cracks and it widened with the radius.

Cracks exhibit various width under different corrosion degrees. Fig. 2.9(b) gives the schematic diagram of crack propagation. Cracks exhibit three types of shapes at the different stages: the triangle, rectangle, and trapezoid. The similar crack shapes were also observed in the literature [33]. Before cover cracking, the crack inside concrete seems like a triangle, shown as crack A. With increasing corrosion, the crack propagates to the concrete surface, shown as crack B. This crack shape can still be considered as a triangle. After the crack appears on the concrete surface, it widens and exhibits the similar width in the radial direction. In this case, the crack shape is taken as a rectangle, shown as crack C. With the future increase of corrosion degree, the crack becomes wider along the radial direction. The crack shape is simplified as a trapezoid, shown as crack D. Corrosion products would accumulate at the strand-concrete interface and migrate from the interface to the concrete surface, which induce the crack shapes to transform from the triangular to the rectangle.



(a) crack distribution

(b) simplified crack propagation

**Fig. 2.9. Schematic diagrams of the crack propagation**

As mentioned previously, each beam was cut into four 15 mm-thick cross-sectional slices. The total number of slices was 48. The schematic diagram of cracking angle,  $\theta$ , was given in Figure 2.9(b). The cracking angle mainly represents the variation of crack width in the radial direction. When the crack narrows along the radius, the cracking angle is less than zero. With cracking propagation, the cracking angle equals zero when the crack width is similar in the radial direction. After that, the crack width on the concrete surface is larger than that at the interface. The cracking angle in this situation is larger than zero. Fig. 2.10 shows the linear regression and polynomial regression between  $\tan\theta$  and corrosion loss.

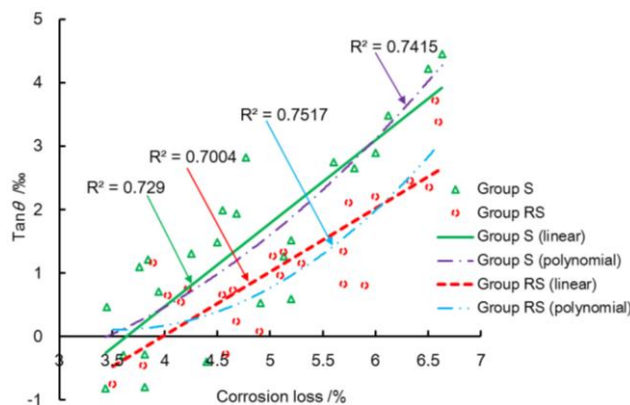


**Fig. 2.10. Tangent of cracking angle and corrosion loss**

The tangent of cracking angle increases with increasing corrosion degree. The discreteness of the correlation between  $\tan\theta$  and the corrosion loss may be attributed to the measurement uncertainty of the crack width and the corrosion loss. Concrete is a heterogeneous material. The variability of cracking propagation is inevitable. As Fig. 2.10 shows, the fitting precision of linear regression and polynomial regression are

similar. In the present study, the linear regression was used to describe the relation between  $\tan\theta$  and corrosion loss and given as follows:

$$\tan\theta = a\rho - b \quad (2.1)$$

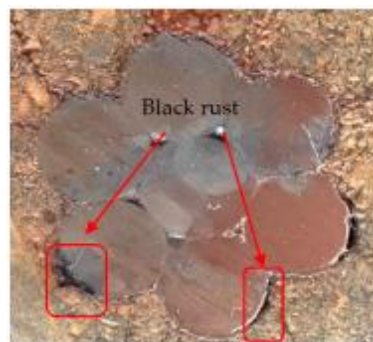
where  $a$  and  $b$  are the constants, for Group S,  $a = 0.1309$ ,  $b = 0.0048$ , for Group RS,  $a = 0.0999$ ,  $b = 0.0040$ ; and  $\rho$  is the corrosion loss of strand.

### 2.3.2 Filling of corrosion products in cracks

#### 2.3.2.1 Composition of corrosion products

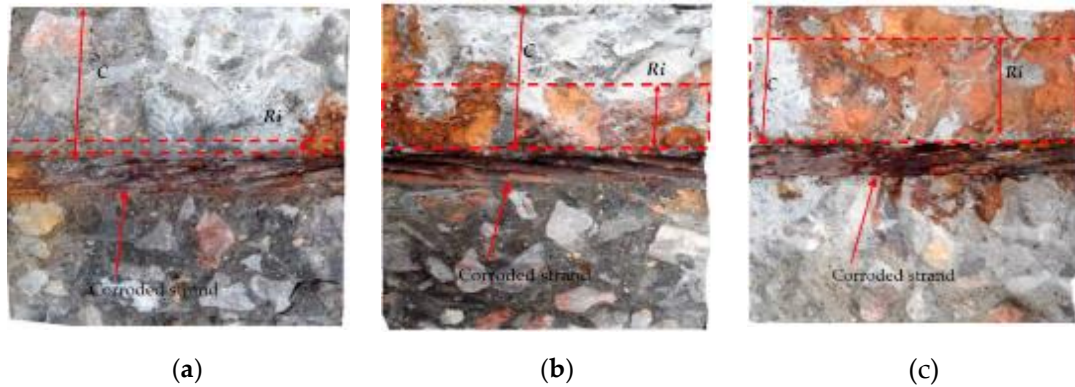
The compositions of corrosion products depends on the alkalinity degree, the oxygen supply, and the moisture content [107]. Corrosion products also exhibit various colors at different regions in the present study. Three colors of corrosion products were observed: black, brownish-red, and puce.

Fig. 2.11 shows the black rust at the strand-concrete interface. The cover prevents the oxygen to reach the strand-concrete interface. For the reaction with some oxygen, the main compositions of corrosion products are ferrous oxide (FeO) and ferroferric oxide (Fe<sub>3</sub>O<sub>4</sub>) [33, 95]. The colors of FeO and Fe<sub>3</sub>O<sub>4</sub> are black. FeO is unstable and can easily become Fe<sub>3</sub>O<sub>4</sub> in air. Therefore, Fe<sub>3</sub>O<sub>4</sub> is considered as the primarily composition of black rust.



**Fig. 2.11. The black rust at the strand-concrete interface.**

Fig. 2.12 shows the brownish-red rust in cracks. Cracks provide a path for oxygen to the inner concrete. The oxygen supply is sufficient in cracks. The color of iron oxide (Fe<sub>2</sub>O<sub>3</sub>) is brownish-red, and Fe<sub>2</sub>O<sub>3</sub> is regarded as the main composition of the brownish-red rust [33].



**Fig. 2.12. Filling of corrosion products in cracks: (a) Slight filling of rust; (b) partial filling of rust; and (c) vast filling of rust.**

As Fig. 2.3 shows, the puce rust was found in the gaps between the core wire and outer wires. The oxygen can reach the gaps with the flow of aggressive liquid. The oxygen supply in the gaps may be lower than those in cracks, and higher than that at the strand-concrete interface. Therefore, the color of rust in the gaps is between the black and the brownish-red.

### 2.3.2.2 Filling of corrosion products

The slices were broken down to observe the filling of corrosion products in cracks. Fig. 2.12 shows the slices profiles of S6B, S9A, and S9C, respectively. Concrete slice profiles were broken down along the widest cracks. Corrosion products filled principally in the widest crack. In another small crack, a few corrosion products were found. The similar experimental observations were also found by Šavija et al. [93]. In their study, the micro-computed X-ray tomography technique (CT-scanning) was used to monitor corrosion products formation during corrosion process. The scanning results showed that corrosion products principally penetrated into the widest crack, and few corrosion products were observed in other small cracks. This phenomenon is similar to the experimental observation obtained in the present study.

Fig. 2.12 shows the profiles of concrete slices along the widest cracks. It should be noted that the upper part of the profile is the position of the widest crack and the bottom part is the broken surface obtained by the destruction method. As mentioned before, the corrosion products mainly filled in the widest cracks. The salt water can also immerse into the cracks. Therefore, the upper part is overlaid by the corrosion products and salt powders. Additionally, no aggregates can clearly be observed in that region.

The bottom part, however, is a new surface. Very few, or no, corrosion products can be found, but the aggregates are clear in that region.

The filling of corrosion products depends on crack widths. The crack widths of the three slices in Fig. 2.12 are 0.08, 0.39, and 0.91 mm, respectively. The filling of corrosion products is slight in the narrow crack. Corrosion products principally fill in the wide crack. Corrosion products propagate with increasing crack width. The filling of corrosion products varies at different positions.

In the experimental testing, the volume of corrosion products is difficult to measure. Correspondingly, the filling depth of corrosion products is easy to obtain. Based on the geometric formula conversion, the volume of corrosion products can be obtained with the rust-filling depth. Therefore, the rust-filling depth was used to describe the rust-filling ratio in the experimental testing. The average rust-filling depth is used to represent the filling of corrosion products in the slice. The rust-filling ratio, defined as the ratio of average rust-filling depth to cover, is employed to reflect the filling of corrosion products:

$$f = \frac{R_i}{C} \quad (2.2)$$

where  $f$  is the rust-filling ratio;  $R_i$  is the average rust-filling depth; and  $C$  is the concrete cover.

Before corrosion products full fill cracks, concrete cover would have cracked. From the experimental testing, it can be found that corrosion products cannot fully fill cracks, even with severe cracking. The rust-filling ratio is defined as the ratio of the average rust-filling depth to the cover. Therefore, the rust-filling ratio is less than 1.0. Fig. 2.13 shows the linear regression and polynomial regression of rust-filling ratio and crack width. The rust-filling ratio increases with increasing crack width until a critical value. After that, the rust-filling ratio can be taken as a constant. This constant is less than one and considered as the maximum rust-filling ratio in the present study. The maximum rust-filling ratios of group S and group RS are 0.85 and 0.88, respectively. The critical widths of maximum rust-filling ratio are 0.79 mm and 0.63 mm in group S and group RS, respectively.

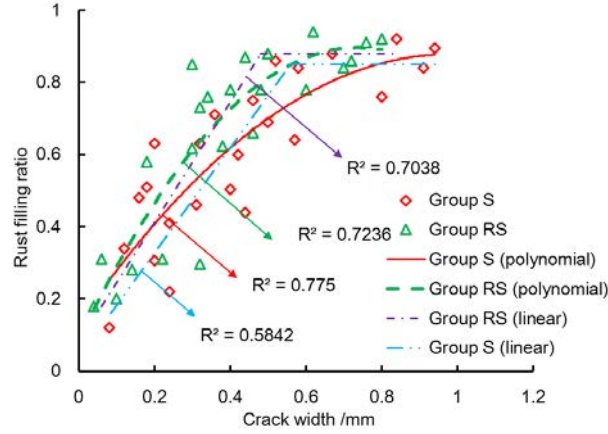


**Fig. 2.13. Rust-filling ratio and crack width.**

As Fig. 2.13 shows, the rust-filling ratio increases faster in the specimens with stirrups than that in the specimens without stirrups. The volume of corrosion products can be obtained with the crack width and rust-filling ratio. In the similar corrosion loss, the volumes of corrosion products in Group S and Group RS are the same. The stirrups can bear the tangential stress and decrease the crack width, which would lead to the large rust-filling ratio.

The discreteness of correlation between the rust-filling ratio and crack width may be attributed to the measurement uncertainty of crack width and corrosion loss. As Fig. 2.13 shows, the fitting precision of polynomial regression is larger than that of linear regression. The polynomial regression was used to describe the relation between crack width and rust-filling ratio in the present study. Two regressed curves of the rust-filling ratio are proposed for the both groups as follows:

$$f_s = \begin{cases} -0.773w_s^2 + 1.515w_s + 0.1353; & w_s \leq 0.79 \text{ mm} \\ 0.85; & w_s > 0.79 \text{ mm} \end{cases} \quad (2.3a)$$

$$f_r = \begin{cases} -1.4938w_r^2 + 2.2011w_r + 0.085; & w_r \leq 0.63 \text{ mm} \\ 0.88; & w_r > 0.63 \text{ mm} \end{cases} \quad (2.3b)$$

where  $f_s$  and  $f_r$  are the rust-filling ratios of group S and group RS, respectively; and  $w_s$  and  $w_r$  are the crack widths of group S and group RS, respectively.

The specimens in the present study were immersed in the saline solution and accelerated by the electrochemical corrosion. The rust-filling ratio obtained in this situation may be different from that in natural corrosion. The longer corrosion time can induce the higher corrosion degree, which would lead to the larger crack width and the deeper rust-filling depth.

It should be pointed out that cover depth, crack extension, corrosion rate, and corrosion environment are size-dependent and can affect the filling of corrosion products. The different concrete covers might induce the various filling extent of corrosion products[103]. Different corrosion rate may lead to the various filling extent of corrosion products. The rust-filling ratio obtained in the electrochemical corrosion may be different from that in natural corrosion. More studies on the filling of corrosion products in cracks are required.

## **2.4 Prediction model of crack propagation**

In this section, a model is proposed to predict the crack propagation based on corrosion loss. The filling of corrosion products and geometric properties of the strand are incorporated in the model. During the corrosion process, corrosion products first fill the pores around the strand-concrete interface and then contribute to the expansive pressure. After that, it would fill the corrosion-induced cracks. With the principle of volume equal to the corrosion products, the relationship between the crack width and corrosion loss can be obtained. Details are shown below.

### **2.4.1 Corrosion products at the micro-crack formation**

The accumulation of corrosion products would create expansive pressure at the strand-concrete interface. When the tangential stress reaches the concrete tensile strength, some micro-cracks would form. Based on the radial deformation at the strand-concrete interface, the volume of corrosion products at the micro-crack formation can be obtained.

The strand usually has a relative large diameter and slight corrosion may induce cover cracking [99]. The distribution of corrosion products around the strand surface relates to the corrosion degrees. Corrosion products are relatively uniform around the strand surface when the corrosion degree is low [88]. With increasing corrosion loss, the strand corrosion products may exhibit the non-uniform distribution. Non-uniform corrosion, compared with uniform corrosion, would induce the large expansive pressure and accelerate the concrete cracking process. In the present experimental observation,

the strand corrosion degree was low and the depths of corrosion pits were small. In terms of this phenomenon, corrosion products are simplified to uniformly distribute around the strand in the prediction model. The expansion of corrosion products would produce a uniform pressure on the surrounding concrete. Fig. 2.14 shows the expansive deformation at the strand-concrete interface caused by corrosion.

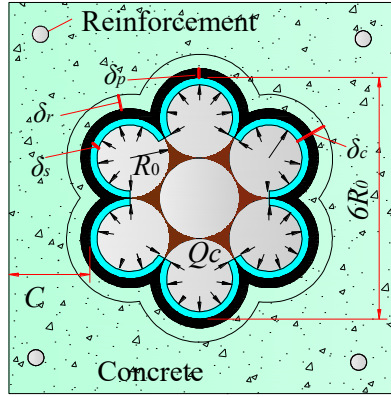


**Fig. 2.14. Expansive deformation at the strand-concrete interface.**

The thick-walled cylinder model has been frequently employed to analyze the corrosion-induced concrete cracking [89, 97]. This model can be considered as an axisymmetric problem subject to the uniform pressure, which can be further modeled as the plane stress problem under the symmetric conditions [108]. The governing stress equilibrium in the radial direction is:

$$\frac{d\sigma_r}{dr} + \frac{\sigma_r - \sigma_\theta}{r} = 0 \quad (2.4)$$

where  $\sigma_r$  and  $\sigma_\theta$  are the radial stress and the tangential stress at any radius  $r$ .

For the plane stress problem under the symmetric conditions, the strain-displacement equation is given as:

$$\varepsilon_r = \frac{du}{dr} \quad (2.5a)$$

$$\varepsilon_\theta = \frac{u}{r} \quad (2.5b)$$

where  $\varepsilon_r$ ,  $\varepsilon_\theta$ , and  $u$  are the radial strain, tangential strain, and radial displacement at any radius  $r$ .

The constitutive relationship between concrete stress and strain is:

$$\sigma_r = \frac{E_c}{(1 - \nu_c^2)} (\varepsilon_r + \nu_c \varepsilon_\theta) \quad (2.6a)$$

$$\sigma_{\theta} = \frac{E_c}{(1 - \nu_c^2)} (\varepsilon_{\theta} + \nu_c \varepsilon_r) \quad (2.6b)$$

where  $E_c$  is the elastic modulus of concrete;  $\nu_c$  is the Poisson's ratio of concrete.

Since concrete is a heterogeneous material, a porous zone surrounds the strand-concrete interface. Corrosion products first diffuse into the porous zone [109]. As corrosion products exceed the quantity needed to fill the porous zone, these products generate expansive pressure. The radial pressure will produce a concrete displacement. Combing Eqs. (2.4)-(2.6), the concrete displacement,  $\delta_r$ , is:

$$\delta_r = \frac{(R_0 + \delta_p)}{E_c} (1 + k + \nu_c) Q_c \quad (2.7)$$

where  $k$  is a constant,  $k = 2(R_0 + \delta_p)^2 / [C^2 + 2C(R_0 + \delta_p)]$ ;  $Q_c$  is the expansive pressure;  $R_0$  is the radius of the wire;  $C$  is the concrete cover; and  $\delta_p$  is the thickness of the porous zone,  $\delta_p = 10\text{--}20 \mu\text{m}$  [31].

Considering the geometric relationship, the volume of corrosion products per units of length at the micro-crack formation,  $V_m$ , is:

$$V_m = \frac{4\pi n}{n - 1} [(R_0 + \delta_c - \delta_s)^2 - R_0^2] \quad (2.8)$$

where  $n$  is rust expansion ratio,  $n = 2\text{--}4$  [110];  $\delta_s$  is the radial loss of wire; and  $\delta_c$  is the thickness of corrosion products,  $\delta_c = \delta_s + \delta_p + \delta_r$ .

The units of  $R_0$  are millimeters, and the units of  $(\delta_p + \delta_r)$  are microns. The value of  $(\delta_p + \delta_r)$  is much smaller than that of  $R_0$ . The term,  $(\delta_p + \delta_r)^2$ , is neglected in the calculations. Eq. (2.8) is rewritten as:

$$V_m = \frac{4\pi n R_0}{n - 1} (\delta_p + \delta_r) \quad (2.9)$$

Combining Eqs. (2.7) and (2.9), the expansive pressure,  $Q_c$ , can be written as:

$$Q_c = \frac{E_c}{(1 + k + \nu_c)(R_0 + \delta_p)} \left( \frac{(n - 1)V_m}{4\pi n R_0} - \delta_p \right) \quad (2.10)$$

The micro-crack forms when the tangential stress exceeds the concrete tensile strength. The tangential stress is derived with an elastic mechanics axisymmetric stress solution. Then, the maximum expansive pressure at the micro-crack formation can be obtained. More details can be found in Dai et al. [28]. The maximum expansive pressure at the micro-crack formation is expressed as:

$$Q_{cmax} = (0.225 + 0.075 \frac{C}{R_0}) f_t \quad (2.11)$$

where  $f_t$  is the concrete tensile strength.

Combining Eqs. (2.10) and (2.11), the volume of corrosion products at the micro-crack formation,  $V_m$ , is:

$$V_m = \frac{\pi n R_0}{(n-1) E_c} \left[ \left( 0.9 + 0.3 \frac{C}{R_0} \right) f_t (1 + k + v_c) (R_0 + \delta_p) + E_c \delta_p \right] \quad (2.12)$$

#### 2.4.2 Crack width on the concrete surface

Crack widths can be observed after cover cracking. As described previously, some discrete cracks were small. Most corrosion products were located in the widest crack. The filling of corrosion products in the small cracks is ignored in the present study. The widest crack in the cross-section is selected as an analysis object. A simplified trapezoid model is proposed to reflect crack shape in the radial direction. Fig. 2.15 shows the schematic diagram of crack shape incorporating the filling of the corrosion product.

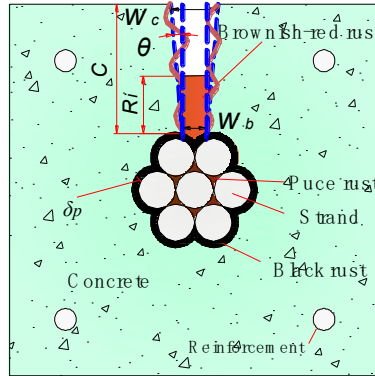


**Fig. 2.15. Simplified crack model.**

As observed in the previous experiment, the filling of corrosion products varies with increasing crack width. Crack width in the radial direction relates to the cracking angle. The cracking angle is employed to describe the volume of crack. Considering the filling of corrosion products and the cracking angle, the volume of corrosion products in the cracks,  $V_p$ , can be written as:

$$V_p = [w_c + C(f-2)\tan\theta] \times R_i \quad (2.13)$$

where  $w_c$  is the crack width on the concrete surface.

According to the geometric characteristic, the total volume of corrosion products can be expressed as:

$$V_c = n\rho V_s \quad (2.14)$$

where  $V_s$  is the strand volume per units of length.

With the equal principle of volume,  $V_c = V_m + V_p$ . Combining Eqs. (2.1) and (2.12)-(2.14), the crack width on concrete surface is:

$$w_c = C(f - 2)(b - a\rho) + \frac{nV_s\rho}{Cf} - \frac{\pi nR_0 \left[ \left(0.9 + 0.3 \frac{C}{R_0}\right) f_t (1 + k + v_c)(R_0 + \delta_p) + E_c \delta_p \right]}{(n - 1)E_c C f} \quad (2.15)$$

The relationship between crack width and the rust-filling ratio is given in Eq. (2.3). Combining Eqs. (2.3) and (2.15), crack width can be calculated by the corrosion loss. Equation shows that the filling of corrosion products, cover, rust expansion ratio, concrete tensile strength, and geometric properties of the strand can affect the corrosion-induced cracking. These parameters should be incorporated in the predicted model.

### 2.4.3 Validation of the prediction model

The proposed model was used to predict the corrosion-induced cracking in the present testing. Some parameters in the present model were selected as follows: the rust expansion ratio and the thickness of the porous zone were selected as 3 and 15  $\mu\text{m}$ , respectively; the proposed rust-filling ratio was incorporated into the prediction. Fig. 2.16 shows the comparison between the predicted and test crack widths. The predicted errors are 13.56% and 11.79% for group S and group RS, respectively. The average error of both groups is 12.68% and the variation coefficient is 0.175 with a 95% confidence interval.

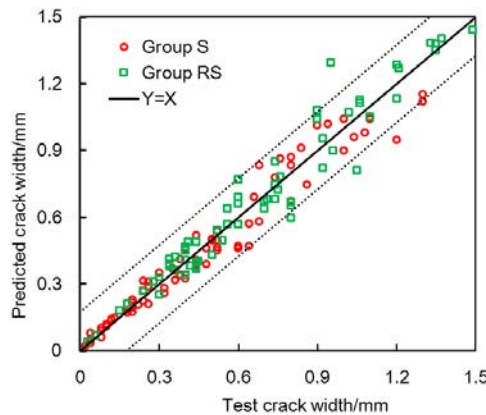


**Fig. 2.16. Predicted and test crack widths.**

The predicted errors may attribute to the measurement uncertainty of crack width,

corrosion loss, and cracking angle. Another reason is that the filling of corrosion products in the small cracks is ignored in the present model. Additionally, the heterogeneity and variability of materials may also affect the prediction. These errors can be accepted in view of the complexity of the corrosion-induced cracking process.

To clarify the filling effect of corrosion products, the theoretical crack widths under the various rust-filling ratios are also given in Fig. 2.17. As Fig. 2.17 shows, P1 and P2 represent the predicted results considering the rust-filling ratios as 1 and 0.5, respectively. The rust-filling ratio is a sensitive parameter for the proposed model. The P1 is smaller than the test value. The P2 is larger than the test result. The main cause of the discrepancy between the predicted values and the test results is the filling of corrosion products into cracks. To predict crack widths, it is essential to determine the rational amount of corrosion products penetrating into cracks.

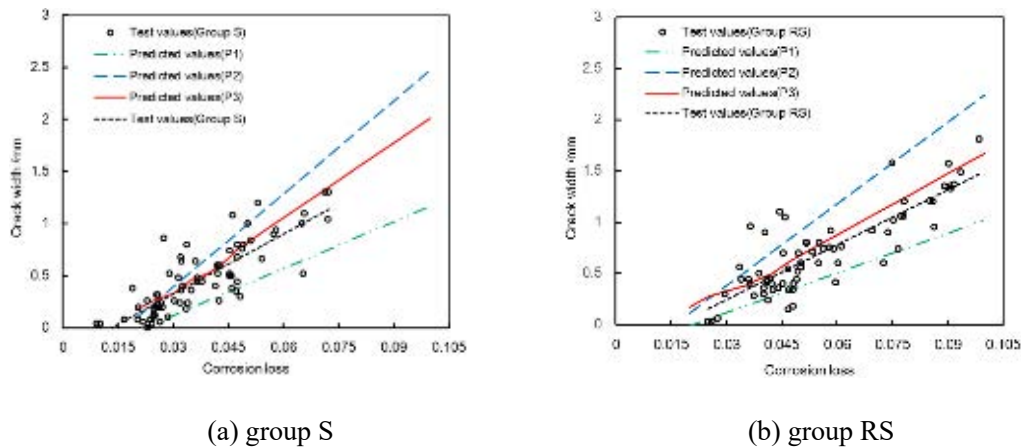


**Fig. 2.17. Predicted crack widths under the various rust-filling ratios**

The predicted values by the proposed method are expressed as the P3. As described previously, the filling of corrosion products varies with the crack width. By using the proposed rust-filling ratio, P3 agrees well with the test result. The filling of corrosion products has a significant influence on the predicted model. The corrosion-induced cracking model should incorporate the rational filling effect of corrosion products.

## 2.5. Conclusions

An experimental investigation is proposed to study the filling of strand corrosion products in cracked concrete. A prediction model of crack widths is developed

incorporating the filling proportion of corrosion products and the twisting shape of the strand. The following conclusions are drawn based on the experimental test and theoretical analysis:

- The filling extent of corrosion products varies with crack propagation. The rust-filling ratio increases with the propagating crack until a critical width. Beyond the critical width, the rust-filling extent remains stable. Using stirrups can decrease the critical crack width.
- Stirrups can restrict the corrosion-induced crack propagation. The tangent of cracking angle increases with the increasing corrosion degree. Using stirrups decreases the corrosion-induced crack width.
- The proposed model can provide a reasonable prediction for corrosion-induced crack width. The prediction of corrosion-induced cracks are sensitive to the rust-filling extent. The prediction model should incorporate the rational filling effect of corrosion products.

# Chapter 3 Crack Width Prediction under Combined Prestress and Strand Corrosion

## 3.1 Introduction

Prestressed concrete (PC) beams have been widely used due to their large spanning ability and favorable mechanical properties [111, 112]. Unfortunately, the long-term performance deterioration of PC beams has been discovered in recent decades. Strand corrosion is one of the major causes of deterioration of PC beams [7, 113]. Corrosion can decrease strand cross-sectional area, induce cover cracking, and change bond performance between strand and concrete [114, 115]. Additionally, strand corrosion under the high-stress level can increase the brittle failure probability of PC beams [116]. The corrosion-affect structural deterioration should be thoroughly investigated to ensure the serviceability and safety of PC beams. Corrosion-induced cover cracking is an early signal for the structural deterioration, which can be employed to evaluate the service life of corroded PC beams.

Rust-expansion ratio, defined as the ratio of the volume of corrosion products to that of consumed steel, is an essential factor for the corrosion-induced cracking investigation. Some existing studies have been undertaken to investigate the expansion ratio of reinforcement corrosion products [85, 117, 118]. The chemical composition of strand is different from that of reinforcement bar, which will lead to various expansion ratios [23]. In addition, the high-stress level can accelerate the corrosion rate of strand, which may change the composition of corrosion products [20, 23]. Studies on strand rust-expansion ratio have not been reported yet, and need to be studied further.

The establishment of the prediction model is another important issue for investigating corrosion-induced cracking. Many studies have been undertaken to predict corrosion-induced cracking in RC structures, which can be summarized as: empirical, numerical and analytical models. The empirical model is developed based on experimental data. The primary disadvantages of empirical model is that different

experimental methods can lead to a different model parameter [119-121]. For numerical method, the finite-element modeling is mostly used to numerically simulate the corrosion-induced cracking [122, 123]. However, the validation of numerical simulation is still a complex issue. For analytical models, corrosion-induced cracking is usually modeled by the thick-walled cylinder theory [108]. How to reasonably consider the anisotropy of material in the analytical model is still a problem. A detailed introduction of the prediction models can be found elsewhere [117]. The investigation of existing studies indicates that the corrosion-induced cracking process can be divided into two stages: crack initiation and propagation [124-126]. Crack initiation represents the stage from corrosion initiation to cover cracking, and crack propagation contains the stage from cover cracking to the critical crack width.

Studies regarding corrosion-affected cracking in prestressed concrete have been afforded little attention as compared to that in reinforced concrete. Dai et al. [99] proposed an analytical model to predict corrosion-induced cracking in prestressed concrete. In the model, the reinforcement rust-expansion ratio was used, and the residual stiffness of cracked concrete was neglected. Additionally, the model used two independent theories to predict the cracking from initiation to propagation, i.e. using a mechanical model to calculate the crack initiation and a geometrical relationship to describe the crack propagation. These non-global methods cannot reasonably explain the cracking process from initiation to propagation, which may cause that the micro-crack effects of concrete fail to coordinate with the macroscopic continuity. The effects of these factors on corrosion-induced cracking in prestressed concrete have not been clarified, and need to be studied further.

This study investigates the coupled effects of prestress and strand corrosion on concrete cracking experimentally and analytically. This chapter is organized as follows: first, an experimental study is performed to investigate strand corrosion-induced concrete cracking under various prestress; next, the expansion ratio of strand corrosion products and crack propagation under various prestress are discussed; then, an analytical model is proposed to predict the global process of prestressed concrete cracking from initiation to propagation; finally, several conclusions are drawn.

## 3.2 Experimental program

In this section, the details of PC beams are introduced at first. Next, the accelerated corrosion test and the measurement method of corrosion product compositions are exhibited. Then, the measurements of crack width and corrosion loss are presented.

### 3.2.1 Details of specimens

Twelve PC beams were designed with a rectangular cross-section of 130 mm × 150 mm, and 2000 mm in length. A 15.2 mm diameter seven-wire steel strand with concrete cover of 42.4 mm was used to reinforce the beam, and four deformed bars of HRB400 with concrete cover of 30.0 mm were employed as the hanger bars in the beam. Stirrups used in the beam have a 6 mm diameter and 100 mm spacing. Table 3.1 and Table 3.2 give the chemical composition and mechanical characteristic of steel, respectively [23]. Fig. 3.1 shows the details of the beam.

**Table 3.1. Chemical composition (wt. %) of steel**

Type	Fe	C	Mn	Si	P	S	Cr	Cu	Ni	Ti	Al
Strand	97.862	0.82	0.74	0.21	0.012	0.006	0.17	0.09	0.03	0.03	0.03
Reinforcement	97.849	0.2	1.34	0.55	0.033	0.028	/	/	/	/	/

**Table 3.2. Mechanical characteristic of steel**

Type	Diameter (mm)	Yield strength (MPa)	Ultimate strength (MPa)	Elastic modulus (GPa)
Strand	15.2	1830	1910	195
Deformed bars	6 (8)	400	540	200

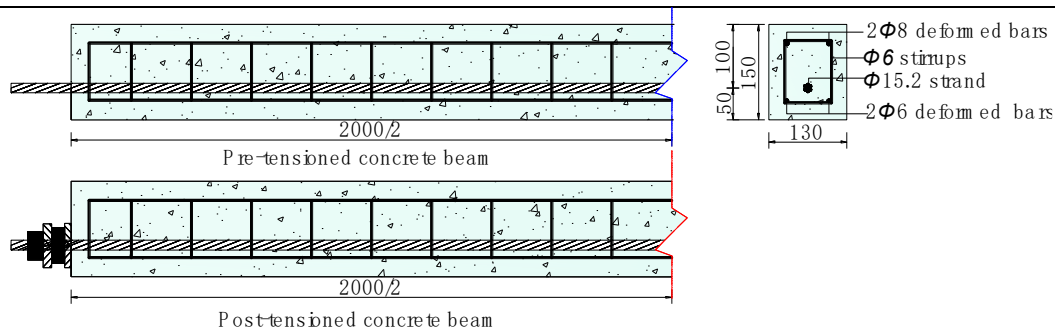


**Fig. 3.1. Details of the beams (Unit: mm)**

The detail parameters of specimens are given in Table 3.3. During the fabrication of specimens, the measurement of effective prestress in strand was a complicated

problem. In the present study, the initial tension stress of strand was used to reflect the prestress level, which was measured by a load cell during the tension process. To investigate corrosion-induced concrete cracking under various stress states, four prestress levels were designed as 0,  $0.25f_p$ ,  $0.5f_p$ , and  $0.75f_p$ , respectively, where  $f_p$  was 1860 MPa. According to the corrosion time and construction technology, the specimens were divided into three groups: group A (pre-tensioned concrete), group B (pre-tensioned concrete) and group C (post-tensioned concrete).

**Table 3.3. Parameters of specimens**

Type	Pre-tensioned concrete				Pre-tensioned concrete				Post-tensioned concrete			
	Group A				Group B				Group C			
Beam No.	PA0	PA1	PA2	PA3	PB0	PB1	PB2	PB3	PC0	PC1	PC2	PC3
Prestress (MPa)	0	$0.25f_p$	$0.5f_p$	$0.75f_p$	0	$0.25f_p$	$0.5f_p$	$0.75f_p$	0	$0.25f_p$	$0.5f_p$	$0.75f_p$

The cement used in the concrete was the Type 32.5 Portland cement. The concrete mix contained: 417 kg/m<sup>3</sup> cement, 676 kg/m<sup>3</sup> fine aggregates and 1026 kg/m<sup>3</sup> coarse aggregates. The water-cement ratio of concrete was 0.44. The sodium chloride (NaCl) with a 5% mass fraction of cement was used in the concrete to catalyze the corrosion process. The grout used in post-tensioned concrete beams consisted of cement, water and additive. After prestressing, the grout was injected into duct through the channels reserved at the end of the beam. The grout with high fluidity could flow along duct by gravity. The pre-tensioned and post-tensioned concrete beams were cast separately. The 28-day uniaxial compressive strengths of pre-tensioned and post-tensioned concrete were 44.1 MPa and 43.4 MPa, respectively.

### 3.2.2 Accelerated corrosion and corrosion product measurement

Crack widths in the specimens were caused by the artificially accelerated corrosion method. To investigate the effect of strand corrosion on concrete cracking alone, the reinforcement in concrete was protected with the epoxy resin to prevent corrosion. The corrosion device, shown in Fig. 3.2, was used to corrode the strand. The strand was linked to the anode, and the stainless steel plate dipped in the 10% NaCl solution was acted as the cathode. The direct current was imposed on the strand using a potentiostat.

The current density used in present test was determined based on the following two principles. First, according to the investigation of existing studies, it was found that Zhang et al. [127] used a current density of  $90 \text{ uA/cm}^2$  to accelerate the strand corrosion. Second, the preliminary experiment showed that the propagation rate of crack under the current density of  $90 \text{ uA/cm}^2$  was moderate, which was convenient to measure the experimental data. Therefore, the corrosion current in the present test was controlled as a constant of  $0.1 \text{ A}$ , and the corresponding current density was about  $90 \text{ uA/cm}^2$ . All the beams in the present test were subjected to the same corrosion current density.



**Fig. 3.2. Accelerated corrosion device**

The corrosion time of beams was determined based on corrosion-induced crack widths. The corrosion time of groups A and B were set to be 15 and 20 days, respectively, which were used to reflect crack widths in pre-tensioned concrete beams under the different corrosion time. The corrosion time of group C was set to be 20 days. Groups B and C represented the difference between pre-tensioned concrete cracking and post-tensioned concrete cracking under the same corrosion time.

Strand corrosion products were collected to evaluate the expansion ratio, and the measurement program was as follows. First, the samples were broken after the accelerated corrosion test, and the corroded strands were taken out from the concrete. Corrosion products on the strand surface were collected. Next, corrosion products were dried by the special baking box. Then, corrosion products were grinded to the powder using the planetary ball mill. After that, the compositions of corrosion products were measured with the infrared (IR) spectroscopy and thermal gravimetry (TG). The infrared spectroscopy was performed using a Nicolet 6700 FTIR spectrometer. The

thermal gravimetry (TG) was carried out on a DTG-60H thermal analyzer at a heating rate of 10 °C/min from 36 °C to 1000 °C.

### **3.2.3 Measurement of crack width and corrosion loss**

During the accelerated corrosion process, the crack propagation over time was recorded. After the accelerated corrosion, crack widths at 10 cm intervals in the longitudinal direction were measured by a portable microscope with a resolution of 0.01 mm.

Strand corrosion exhibited variability in various regions. The average mass loss of strand at 10 cm length was measured to reflect the corrosion degrees at the different positions, and the program was as follows. First, the corroded strand was taken out from the concrete. Next, corrosion products on the strand surface were cleaned with 12% hydrochloric acid solution, and then the strand was neutralized with alkali [128]. Following this, the strand was cut into 10 cm length, and the mass loss of segmental strand was measured.

## **3.3 Experimental results and discussions**

In this section, the composition and expansion ratio of strand corrosion products are firstly presented in terms of their effects on corrosion-induced cracking. Then, the crack propagation under various prestress is discussed.

### **3.3.1 Expansion ratio of strand corrosion products**

The expansion of strand corrosion products can induce concrete cracking. Strand rust-expansion ratio has not been studied well. For evaluating the expansion-ratio of strand corrosion products, the compositions of corrosion products and the proportions of corrosion product compositions are two key issues. The IR spectroscopy can be used to measure the compositions of corrosion products due to the fact that molecules absorb frequencies that are characteristic of their structures. The reason that the TG analysis can be employed to evaluate the proportions of corrosion product compositions is that iron hydroxide would be oxidized to iron oxide during heating process. More details about the IR spectroscopy and TG analysis can be seen in the following. Therefore, the

IR spectroscopy and TG analysis are utilized to evaluate the strand rust-expansion ratio in the present study.

The IR spectrums of the samples are shown in Fig. 3.3. The variation tendencies of curves in Fig. 3.3 are similar, and the distinction of each curve is that the magnitude of transmissivity is different. The reason for this phenomenon is that the composition proportion of corrosion products in each sample is different. The standard spectra of various rusts are given in Table 3.4 [129]. Based on the standard spectra,  $\alpha$ -Fe<sub>2</sub>O<sub>3</sub>, Fe<sub>3</sub>O<sub>4</sub>,  $\alpha$ -FeOOH,  $\beta$ -FeOOH and  $\gamma$ -FeOOH are confirmed in the samples. Each sample has the different proportions of iron oxide ( $\alpha$ -Fe<sub>2</sub>O<sub>3</sub> and Fe<sub>3</sub>O<sub>4</sub>) and iron hydroxide ( $\alpha$ -FeOOH,  $\beta$ -FeOOH and  $\gamma$ -FeOOH). This indicates that prestress cannot change the corrosion product composition, but affects the proportion of corrosion product composition.

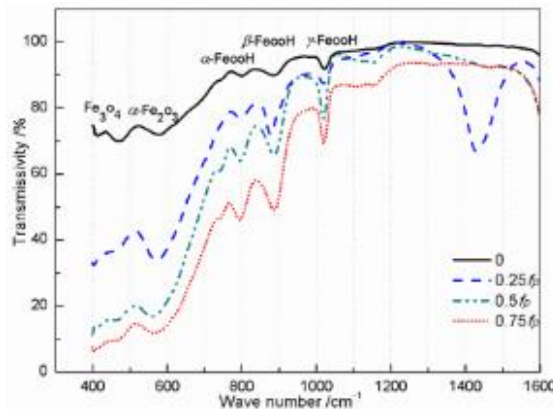


**Fig. 3.3. Infrared spectrums of corrosion products**

The hydroxyl in iron hydroxide would be oxidized during heating process, which would lead to the mass change in the samples. Based on this phenomenon, the TG analysis can be employed to analyze the proportions of iron oxide and iron hydroxide in the samples. The derivative thermogravimetry (DTG) is also utilized to evaluate the weight loss ratio of corrosion products during heating process. Fig. 3.4 shows the TG and DTG curves of the samples.

As Fig. 3.4 shows, the weight losses of corrosion products are principally found at the temperatures of 36~200°C and 200~400°C during heating process. The weight loss of corrosion products at 36~200°C is larger than that at 200~400°C. The evaporation of adsorbed water is the main reason that causing the weight loss of corrosion products at 36~200°C. The decomposition temperature of hydroxyl in iron hydroxide is 200~400°C

[118]. During this stage, the iron hydroxide would be oxidized to the iron oxide. Table 3.5 gives the weight losses of samples at 200~400°C. With the mass conservation law, the mass percentages of iron hydroxide and iron oxide in the samples can be determined, and are given in Table 3.5. It is found that prestress can increase the proportion of iron oxide and decrease the proportion of iron hydroxide in the samples.

**Table 3.4. Standard spectra and expansion ratio of rusts**

Types	Peaks (cm <sup>-1</sup> ), (Relative Intensity)	Rust expansion ratio
$\alpha$ -FeOOH	1399(M), 1260(VM), 881(S), 793(S), 608(W), 463(B,VW)	2.95
$\beta$ -FeOOH	858(B,S), 670(B,S), (300~500) (B,S)	3.53
$\gamma$ -FeOOH	1152(B,M), 1017(S), 737(VW), 487(VB,W)	3.07
$\delta$ -FeOOH	1110(B,S), 880(S), 786(VW), 617(B,VW), 493(B,W)	2.99
$\alpha$ -Fe <sub>2</sub> O <sub>3</sub>	535(S), 464(M)	2.15
$\gamma$ -Fe <sub>2</sub> O <sub>3</sub>	690(S), 682(S), 550(VS), 475(W), 437(W), 418(VW)	2.32
FeO	492(VB,W)	1.71
Fe <sub>3</sub> O <sub>4</sub>	556(500~700)(B,W), 404(300~500)(VB,W)	2.10

Note: S is strong peak; M is medium peak; W is weak peak; VS is relative strong peak; VW is relative weak peak; B is broad band; VB is relative broad band.

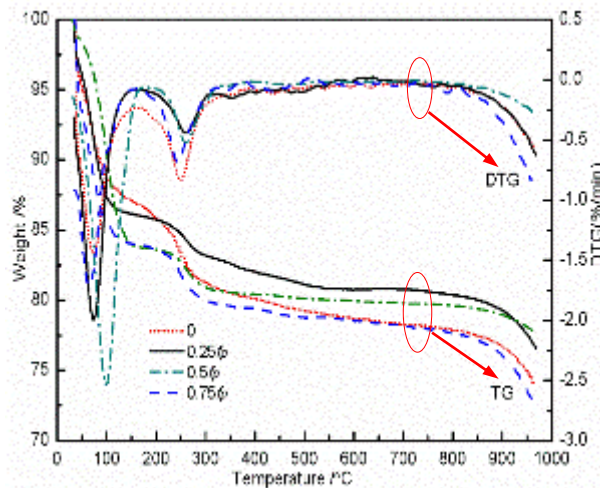


**Fig. 3.4. TG and DTG curves of corrosion products**

The standard expansion ratios of rusts are given in Table 3.4 [130]. In the present study, the expansion ratio of iron oxide is considered as the average expansion ratio of  $\alpha$ -Fe<sub>2</sub>O<sub>3</sub> and Fe<sub>3</sub>O<sub>4</sub>, and the expansion ratio of iron hydroxide is selected as the average

value of  $\alpha$ -FeOOH,  $\beta$ -FeOOH and  $\gamma$ -FeOOH for simplifying the analysis. Based on the proportions of iron oxide and iron hydroxide, the expansion ratios of strand corrosion products can be evaluated, and are given in Table 3.5.

**Table 3.5. Parameters of corrosion products**

Prestress (Mpa)	Weight loss at 200~400°C (%)	Mass percentage of iron hydroxide (%)	Mass percentage of iron oxide (%)	Rust expansion ratio
0	7	69	31	2.96
$0.25f_p$	4	40	60	2.68
$0.5f_p$	4	40	60	2.68
$0.75f_p$	5	49	51	2.78
Average rust expansion ratio				2.78

Comparing with experimental data in Table 3.5, it is found that strand rust-expansion ratios under various prestress range from 2.68 to 2.96. This indicates that strand rust-expansion ratios under various prestress are similar. Changing prestress has a slight effect on the expansion ratios of strand corrosion products. Therefore, the effect of prestress on strand rust-expansion ratio is neglected in the present study, and the strand rust-expansion ratio under various prestress in electrochemically accelerated corrosion condition is considered as the average value (2.78).

### 3.3.2 Crack propagation under various prestress

For evaluating corrosion-induced cracking, the critical time of cover cracking and corrosion-induced crack widths are two key issues. Thus, this part contains two contents: the critical time of cover cracking under various prestress; the relationship between crack width and corrosion loss under various prestress.

To evaluate the effect of prestress on cover cracking, the critical time of cover cracking is given in Table 3.6. Experimental data in Table 3.6 indicate that increasing prestress can shorten the critical time of cover cracking. By varying prestress from 0 to  $0.75f_p$ , the average decrement for the critical time of cover cracking is 22%. To further clarify the effect of prestress on crack propagation, the widest crack propagation over time is shown in Fig. 3.5.

**Table 3.6. Critical time of cover cracking**

Beam No. / Prestress	PA0 / 0	PA1 / $0.25f_p$	PA2 / $0.5f_p$	PA3 / $0.75f_p$	PB0 / 0	PB1 / $0.25f_p$	PB2 / $0.5f_p$	PB3 / $0.75f_p$	PC0 / 0	PC1 / $0.25f_p$	PC2 / $0.5f_p$	PC3 / $0.75f_p$
Time of cover cracking (h)	149	147	125	121	154	146	132	112	175	162	150	138
Cracking time decrement (%)	NA	1	16	19	NA	5	14	27	NA	7	14	21

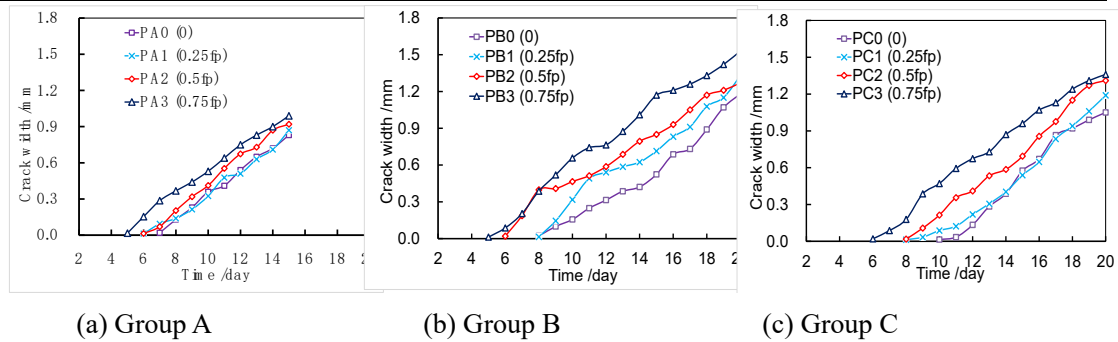


**Fig. 3.5. Crack propagation over time: (a); (b); (c)**

As Fig. 3.5 shows, crack widths increase with increasing prestress under the same corrosion time. By varying prestress from 0 to  $0.75f_p$ , the maximum crack widths in groups A, B and C increase 19%, 30% and 30%, respectively. Comparing with experimental data in Fig. 3.5, it can be found that crack width in pre-tensioned concrete beams is usually larger than that in post-tensioned concrete beams under the same corrosion time. For post-tensioned concrete beams, the grout is used to fill the duct. The use of grout leads to the concrete cover becoming the non-continuous material, which contains the internal region of grout and external region of concrete. Strand corrosion would firstly induce the internal grout cracking before it could affect the external concrete. This may be the reason that post-tensioned concrete beams have a smaller crack width than pre-tensioned concrete beams under the same corrosion time.

After the accelerated corrosion, the longitudinal cracks, shown in Fig. 3.6, were observed on the bottom of beam. Crack widths and mass losses are presented in Fig. 3.7 to reflect the effect of prestress on corrosion-induced crack width. Some studies indicate that corrosion-induced crack width associates well with the average mass loss [131, 132]. Therefore, the linear regressions between crack widths and mass losses are employed to reflect the crack propagation rate.



**Fig. 3.6. Longitudinal crack of specimen**

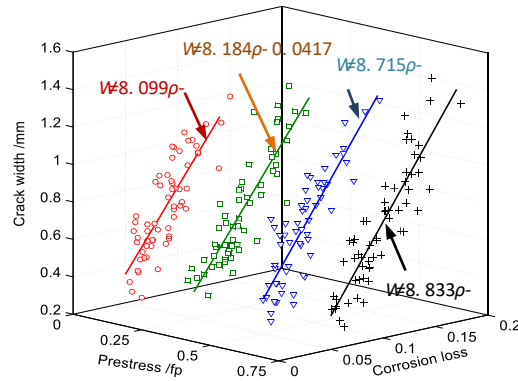


**Fig. 3.7. Crack widths and corrosion losses**

As Fig. 3.7 shows, slight strand corrosion can induce cover cracking, and corrosion-induced crack width increases with increasing prestress. For the non-prestressed concrete, a corrosion loss of 10% can induce a 0.76 mm crack width. With the same corrosion degree, crack widths increase 3%, 7% and 11%, respectively, when the prestress are  $0.25f_p$ ,  $0.5f_p$  and  $0.75f_p$ . The slope of curve in Fig. 3.7 is employed to reflect the crack propagation rate of the specimens. By varying prestress from 0 to  $0.75f_p$ , the crack propagation rate increases about 9%. This indicates that prestress can accelerate the crack propagation rate.

### 3.4 Prediction of corrosion-induced cracking in PC beams

For RC beams, concrete around steel rebar would suffer with expansive pressure during the corrosion process. Concrete cracks when the tensile stress induced by expansive pressure exceeds the concrete tensile strength. For PC beams, concrete around prestressing strand would suffer with expansive pressure and prestress during the corrosion process. The high stress levels in strand can accelerate the corrosion-induced cracking process. Additionally, strand consists of several outer wires spiraled around a core wire, and has a flower-like cross-section. Due to the specific cross-section feature of strand, the strand corrosion-induced cracking mechanism may be different

from that of steel rebar. These effects should be included in the prediction of corrosion-induced cracking in PC beams.

In this section, a model is proposed to predict corrosion-induced crack widths in PC beams. The strand rust-expansion ratio and the residual stiffness of cracked concrete are incorporated into the model. The superiority of the present model is that it can predict the global process of prestressed concrete cracking from initiation to propagation by transforming the boundary conditions.

### 3.4.1 Model for corrosion-induced cracking

During the corrosion process, prestressed concrete would suffer with the prestress and expansive pressure. Fig. 3.8 shows the stress distribution at the strand-concrete interface in PC beams. In the present experimental test, it is found that slight strand corrosion can induce cover cracking. For the slight corrosion, corrosion products are considered to be uniformly distributed around strand.

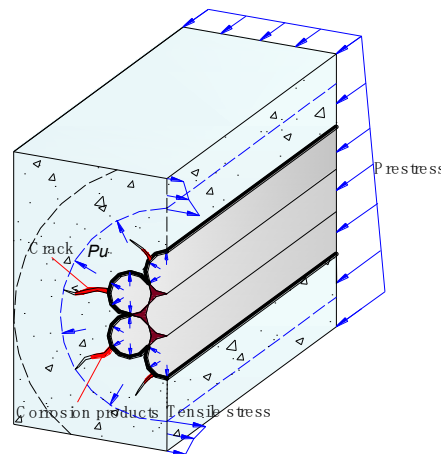


**Fig. 3.8. Stress distribution at the strand-concrete interface in PC beams**

The thick-walled cylinder theory is employed to model corrosion-induced concrete cracking in the present model. When the tensile stress induced by expansive pressure exceeds the concrete tensile strength, concrete is considered to crack. Before cover cracking, the concrete cover contains two parts: a cracked inner region and an uncracked outer region. Concrete cracking due to strand corrosion is shown in Fig. 3.9.

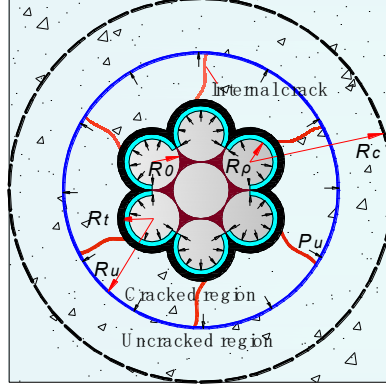


**Fig. 3.9. Concrete cracking due to strand corrosion**

The seven-wire steel strand is generally used in PC beams, and is selected as the analysis object in the present model. The outer wires are considered to corrode firstly when the strand is subjected to corrosion. The corrosion loss of strand,  $\rho$ , can be expressed as

$$\rho = 4\pi(R_o^2 - R_\rho^2)/A_p \quad (3.1)$$

where  $R_o$  and  $R_\rho$  are the radiuses of wire before and after corrosion, respectively;  $A_p$  is the strand cross-sectional area.

Strand corrosion products have a larger volume than the consumed iron, which would induce the corrosion expansion. During the corrosion process, some corrosion products would fill pores and cracks, and others contribute to the expansive pressure. With the constant volume principle, the total volume of strand corrosion products,  $\Delta V_r$ , can be expressed as

$$\Delta V_r = \Delta V_w + \Delta V_c + \Delta V_p \quad (3.2)$$

where  $\Delta V_r = n\Delta V_w$ ,  $n$  is the strand rust-expansion ratio;  $\Delta V_w$  is the volume change of wires;  $\Delta V_c$  is the volume change of concrete induced by expansive pressure;  $\Delta V_p$  is the volume of corrosion products that fill cracks and pores.

Based on the geometrical relationship, the volume change of wires,  $\Delta V_w$ , and the volume change of concrete induced by expansive pressure,  $\Delta V_c$ , respectively, are

$$\Delta V_w = \frac{2}{3}\pi(R_o^2 - R_\rho^2) \quad (3.3a)$$

$$\Delta V_c = \frac{2}{3}\pi(R_t^2 - R_o^2) \quad (3.3b)$$

where  $R_t$  is the radius of wire with corrosion products.

The volume of corrosion products that fill cracks and pores,  $\Delta V_p$ , can be written as [133]

$$\Delta V_p = \frac{2}{3}\pi(R_t - R_o)(R_u - R_t) \quad (3.4)$$

where  $R_u$  is the radius of the cracked region.

Combing Eqs. (3.1-3.4), the displacement of concrete at the strand-concrete interface,  $u_c$ , is

$$u_c = R_t - R_o = \frac{(n-1)A_p\rho}{4\pi(R_u+R_o)} \quad (3.5)$$

The experimental investigation indicates that prestress can accelerate the corrosion-induced concrete cracking process. For PC beams, the concrete would be under the biaxial stress state during corrosion process, i.e. the tensile stress induced by corrosion expansion and the compressive stress caused by prestress. The biaxial stress state of concrete can be expressed as [134]

$$\frac{\sigma_p}{f_{ck}} = \frac{1}{1+KS} \quad (3.6)$$

where  $K = f_t/\sigma_p$ ,  $f_t$  is the concrete tensile strength under the biaxial stress state,  $\sigma_p$  is the compressive stress of concrete at the strand location;  $S = f_{ck}/f_{tk}$ ,  $f_{ck}$  and  $f_{tk}$  are the uniaxial tensile and compressive strengths of concrete, respectively.

The compressive stress of concrete induced by the prestress,  $\sigma(y)$ , can be expressed as

$$\sigma(y) = \frac{N_p}{A} + \frac{N_p e_p}{I} y \quad (3.7)$$

where  $N_p$  is the prestressing force of strand;  $A$  is the cross-sectional area of concrete;  $I$  is the moment of inertia of the concrete cross-section;  $e_p$  is the eccentricity of strand;  $y$  is the distance from the position of concrete to the section centroid of concrete.

The concrete tensile strength under the biaxial stress state,  $f_t$ , can be evaluated by Eqs. (3.6-3.7). Concrete would crack when the tangential stress induced by expansive pressure exceeds the concrete tensile strength. Assuming the smeared cracks in the cracked region are distributed uniformly. A reduction factor,  $a$ , is employed to reflect the residual tangential stiffness in cracked concrete, and is defined as [135]

$$a = \frac{f_t \exp(-\lambda(\bar{\varepsilon}_\theta - \bar{\varepsilon}_\theta^c))}{\bar{\varepsilon}_\theta E_c} \quad (3.8)$$

where  $\lambda$  is the material constant,  $\lambda = \pi \frac{f_t}{G_t} (R_0 + R_u)$ ;  $G_t$  is the fracture energy;  $\overline{\varepsilon}_\theta$  is the average residual tangential strain of cracked concrete;  $\overline{\varepsilon}_\theta^c$  is the average tangential strain of uncracked concrete;  $E_c$  is the elastic modulus of concrete.

The cracked concrete is an anisotropic material. The elastic modulus and Poisson's ratio of cracked concrete in the tangential and radial directions are different [133, 135]. The radial and tangential stresses of cracked concrete,  $\sigma_r(r)$  and  $\sigma_\theta(r)$ , respectively, can be expressed as

$$\sigma_r(r) = \frac{E_c}{1-v_c^2} (\varepsilon_r(r) + v_c \sqrt{a} \varepsilon_\theta(r)) \quad (3.9a)$$

$$\sigma_\theta(r) = \frac{E_c}{1-v_c^2} (a \varepsilon_\theta(r) + v_c \sqrt{a} \varepsilon_r(r)) \quad (3.9b)$$

where  $r$  is the radius of concrete at the cracked region,  $R_0 \leq r \leq R_u$ ;  $\varepsilon_r(r)$  and  $\varepsilon_\theta(r)$  are the radial and tangential strains of concrete, respectively;  $v_c = \sqrt{v_1 v_2}$ ,  $v_1$  and  $v_2$  are the Poisson's ratios of concrete in the radial and tangential directions, respectively.

For the cracked region, the concrete stress in the radial direction should satisfy the equilibrium equation, which can be expressed as

$$\frac{\partial \sigma_r(r)}{\partial r} + \frac{\sigma_r(r) - \sigma_\theta(r)}{r} = 0 \quad (3.10)$$

The strain-displacement compatibilities are  $\varepsilon_r(r) = \frac{du(r)}{dr}$  and  $\varepsilon_\theta(r) = \frac{u(r)}{r}$ , where  $u(r)$  is the displacement in cracked concrete. The governing equation for the displacement in the cracked concrete cylinder can be expressed as

$$\frac{d^2 u(r)}{dr^2} + \frac{1}{r} \frac{du(r)}{dr} - a \frac{u(r)}{r^2} = 0 \quad (3.11)$$

The displacement in cracked concrete,  $u(r)$ , can be calculated as

$$u(r) = b_1(r) r^{\sqrt{a}} + b_2(r) r^{-\sqrt{a}} \quad (3.12)$$

where  $b_1(r)$  and  $b_2(r)$  are the unknown parameters.

Combing Eqs. (3.9) and (3.12), the radial and tangential stresses of cracked concrete,  $\sigma_r(r)$  and  $\sigma_\theta(r)$ , respectively, can be rewritten as

$$\sigma_r(r) = \frac{\sqrt{a}E_c}{1-v_c^2} [b_1(r)(1+v_c)r^{\sqrt{a}-1} - b_2(r)(1-v_c)r^{-\sqrt{a}-1}] \quad (3.13a)$$

$$\sigma_\theta(r) = \frac{aE_c}{1-v_c^2} [b_1(r)(1+v_c)r^{\sqrt{a}-1} + b_2(r)(1-v_c)r^{-\sqrt{a}-1}] \quad (3.13b)$$

For the uncracked region, the stress state in concrete can still be modeled by the elasticity theory. The radial stress,  $\sigma_r(t)$ , tangential stress,  $\sigma_\theta(t)$ , and radial displacement,  $u(t)$ , in uncracked concrete, respectively, are

$$\sigma_r(t) = \frac{R_u^2 P_u}{(R_c^2 - R_u^2)} \left(1 - \frac{R_c^2}{t^2}\right) \quad (3.14a)$$

$$\sigma_\theta(t) = \frac{R_u^2 P_u}{(R_c^2 - R_u^2)} \left(1 + \frac{R_c^2}{t^2}\right) \quad (3.14b)$$

$$u(t) = \frac{(1+v_c)R_u^2 P_u}{E_c(R_c^2 - R_u^2)} \left[\frac{R_c^2}{t} + (1 - 2v_c)t\right] \quad (3.14c)$$

where  $t$  is the radius of concrete at the uncracked region,  $R_u \leq t \leq R_c$ ;  $R_c = R_0 + C$ ,  $C$  is the concrete cover;  $P_u$  is the expansive pressure at the interface between the cracked and uncracked regions.

According to the equivalence principle of tangential stress at the same location, the tensile stress at the interface between the cracked and uncracked regions should be equal to the concrete tensile strength, i.e.  $\sigma_\theta(R_u) = f_t$ . Then, the expansive pressure at the interface between the cracked and un-cracked regions,  $P_u$ , can be expressed as

$$P_u = f_t \frac{R_c^2 - R_u^2}{R_c^2 + R_u^2} \quad (3.15)$$

In addition, the radial stress and deformation at the interface between the cracked and uncracked regions should also satisfy the coordination relationship, i.e.  $u(t) = u(r)$  and  $\sigma_r(t) = \sigma_r(r)$ . Then,  $b_1(r)$  and  $b_2(r)$  can be obtained as

$$b_1(r) = \frac{(1-v_c)m + P_u(1-v_c^2)/(\sqrt{a}E_c)}{2R_u^{\sqrt{a}-1}} \quad (3.16a)$$

$$b_2(r) = \frac{(1+v_c)m + P_u(1-v_c^2)/(\sqrt{a}E_c)}{2R_u^{-\sqrt{a}-1}} \quad (3.16b)$$

where  $m$  is the parameter,  $m = \frac{(1+v_c)f_t}{E_c(R_c^2 + R_u^2)} [R_c^2 + (1 - 2v_c)R_u^2]$ .

The average tangential strain of uncracked concrete,  $\overline{\varepsilon_\theta^c}$ , and the average residual tangential strain of cracked concrete,  $\overline{\varepsilon_\theta}$ , in Eq. (3.8) over  $[R_0, R_u]$ , respectively, are

$$\overline{\varepsilon_\theta^c} = \frac{1}{R_u - R_0} \int_{R_0}^{R_u} \frac{u(t)}{t} dt \quad (3.17a)$$

$$\overline{\varepsilon_\theta} = \frac{1}{R_u - R_0} \int_{R_0}^{R_u} \frac{u(r)}{r} dr \quad (3.17b)$$

Combining Eqs. (3.8) and (3.17), the stiffness reduction factor,  $a$ , can be computed. Then, the corrosion loss of strand can be determined by Eqs. (3.5) and (3.12), and is expressed as

$$\rho = \frac{4\pi(R_u+R_0)[b_1(R_t)R_t^{\sqrt{a}}+b_2(R_t)R_t^{-\sqrt{a}}]}{(n-1)A_p} \quad (3.18)$$

When crack propagates to the concrete surface, the concrete would fracture completely, i.e.  $R_u = R_c$ , and the corresponding corrosion loss is called as the critical corrosion loss of cover cracking.

After cover cracking, crack shapes in the cross-section direction would exhibit the trapezoid, as shown in Fig. 3.10. The boundary conditions would be changed after concrete cracking, and the solution of Eq. (11) should be rewritten as

$$u(r) = b_3r^{\sqrt{a}} + b_4r^{-\sqrt{a}} \quad (3.19)$$

where  $b_3$  and  $b_4$  are the unknown parameters.

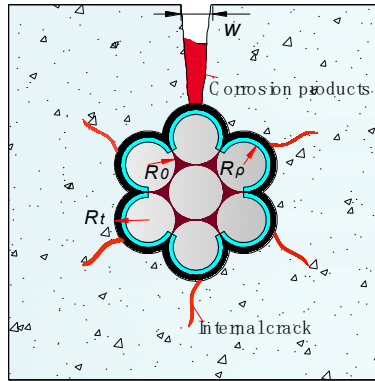


**Fig. 3.10. Crack propagates to concrete surface**

The new boundary conditions can be expressed as [136]

$$b_3(1 + \nu_c)R_c^{(\sqrt{a}-1)} - b_4(1 - \nu_c)R_c^{(-\sqrt{a}-1)} = 0 \quad (3.20a)$$

$$b_3R_0^{\sqrt{a}} + b_4R_0^{-\sqrt{a}} = R_t - R_0 \quad (3.20b)$$

The parameters of  $b_3$  and  $b_4$  can be calculated with Eq. (3.20). Then, crack width on the concrete surface,  $w_c$ , can be expressed as

$$w_c = 2\pi R_c \left[ \varepsilon_\theta(R_c) - \frac{f_t}{E_c} \right] \quad (3.21)$$

where  $\varepsilon_\theta(R_c)$  is the tangential strain of concrete on the concrete surface.

Combing Eqs. (3.19) and (3.21), crack width on the concrete surface can be

rewritten as [136]

$$w_c = \frac{4\pi(R_t - R_0)}{(1 - \nu_c)(R_0/R_c)^{\sqrt{a}} + (1 + \nu_c)(R_c/R_0)^{\sqrt{a}}} - \frac{2\pi R_c f_t}{E_c} \quad (3.22)$$

The relationship of crack width and corrosion loss can be estimated by Eqs. (3.5) and (3.22). The prediction of corrosion-induced cracking is sensitive to the rust-expansion ratio and prestress. The advantage of the present model, compared with existing models, is that it can consider the effect of prestress on corrosion-induced cracking. Additionally, the cross-section feature of strand can be also incorporated into the model.

### 3.4.2 Model validation

The proposed model is employed to predict corrosion-induced crack widths in PC beams. The values of basic variables used in the model are given in Table 3.7. Pantazopoulou and Papoulia [133] indicates that the fracture energy ranges between 0.065 and 0.088 N/mm. The fracture energy used in Li and Yang [23] is 0.088 N/mm. Thus, the fracture energy in the present model is selected as 0.088 N/mm. The predicted and experimental values are shown in Fig. 3.11.

**Table 3.7. Values of basic variables used in the model**

Symbol	Values	Sources
$A_p$ (mm <sup>2</sup> )	139	Present study
$C$ (mm)	42.4	Present study
$G_t$ (N/mm)	0.088	Li and Yang (2011)
$n$	2.78	Present study
$E_c$ (GPa)	32.5	MHURD (2010)
$f_{ck}$ (MPa)	44.1 (pre-tensioned concrete) 43.4 (post-tensioned concrete)	Present study
$\nu_c$	0.18	Liu and Weyers (1998)

As Fig. 3.11 shows, the predicted crack widths correlate well with the experimental values. The average error and standard deviation are 10.98% and 0.091, respectively. The prediction error in the present study is defined as  $\frac{|w_t - w_p|}{w_t}$ , where  $w_t$  and  $w_p$  are tested and predicted crack widths. The error may be ascribed to some

simplifications of the analytical model. Another reason for the error may be the measurement uncertainty of experimental data. Considering the complexity of corrosion process, the prediction error can be accepted. The proposed model, incorporating the coupled effects of strand corrosion and prestress, can provide an accurate prediction for corrosion-induced crack widths in PC beams.

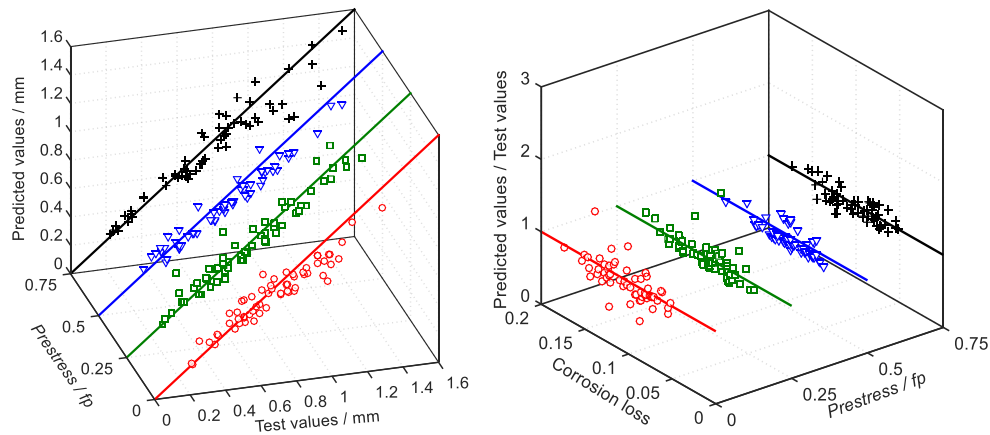


**Fig. 3.11. Verification: (a) Predicted and test values; (b) Crack width and corrosion loss**

### 3.5 Conclusions

An experimental study is performed to investigate the coupled effects of strand corrosion and prestress on concrete cracking. Then, an analytical model is proposed to predict the global process of prestressed concrete cracking from initiation to propagation. The following conclusions can be drawn from the experimental tests and theoretical analysis:

- Prestress can accelerate the corrosion-induced cracking process. By varying prestress from 0 to 75% strand tensile strength, the critical time of cover cracking decreases 22% and the crack propagation rate increases 9%.
- Prestress can increase the proportion of iron oxide and decrease the proportion of iron hydroxide in corrosion products. These changes have a slight effect on the expansion ratio of strand corrosion products. Strand rust expansion-ratio in the electrochemically accelerated corrosion conditions is proposed as 2.78.
- Strand corrosion in pre-tensioned concrete beams can more easily induce concrete cracking than that in post-tensioned concrete beams.

- The proposed model, incorporating the coupled effects of prestress and strand corrosion, can provide an accurate prediction for corrosion-induced crack widths. The prediction of corrosion-induced cracking is sensitive to the prestress and rust-expansion ratio.

# Chapter 4 Prestress Loss Prediction in Pre-tensioned Concrete Structures with Corrosive Cracking

## 4.1 Introduction

Prestressed concrete has been widely used in engineering structures due to its superior performances and high durability [137, 138]. Unfortunately, some recent failure cases raise concerns over the safety of existing PC structures [23, 139]. Strand corrosion is one of the main causes for the deterioration of PC structures [14, 140]. Corrosion can reduce strand cross-section, induce concrete cracking, degrade bond strength, lead to prestress loss and eventually deteriorate the capacity of PC structures [126, 141, 142]. For PC structures, the effective prestress is particularly important as compared with reinforced concrete members. The evaluation of prestress loss is necessary to ensure the serviceability and safety of existing PC structures.

Many factors can lead to prestress losses in existing PC structures, such as the creep and shrinkage of concrete, the stress relaxation of prestressed strand and corrosion. Numerous studies have been undertaken to assess the effects of concrete creep and shrinkage, and the stress relaxation of prestressed strands on long-term prestress losses [143, 144]. Some codes also propose the prediction methods to evaluate long-term prestress losses in PC structures [145-147]. As compared with researches on long-term prestress losses, studies regarding corrosion-induced prestress loss have been afforded little attention. Cavell and Waldron [76] used the strain compatibility method to estimate the residual prestress in post-tensioned concrete beams after tendon failure. Castel et al. [77] indicated that the prestressing force loss in post-tensioned concrete beams was proportional to the cross-section reduction of corroded strand.

The above mentioned studies focus on evaluating the effect of strand cross-section reduction on the prestress loss in corroded post-tensioned concrete beams. The evaluation of corrosion-induced prestress loss is a complicated issue. Except for the

cross-section reduction of corroded strand, concrete cracking and bond degradation can also cause prestress loss. Additionally, post-tensioned concrete members use the anchorage systems to transmit the prestress, while the prestress in pre-tensioned concrete (PT) structures is built through the bond stress at the strand-concrete interface. Corrosion-induced cracking and bond degradation should have a larger impact on the effective prestress in PT structures than that in post-tensioned concrete members. How to evaluate the prestress loss in PT structures caused by corrosive cracking still needs to be studied further.

The objective of this study is to propose an analytical model to evaluate the prestress loss in corroded PT structures, incorporating the coupling effects of concrete cracking and bond degradation. This chapter is organized as follows: first, an analytical model is proposed to evaluate the corrosion-induced prestress loss; next, the effective prestress in eight corroded PT beams under various stress levels is explored by the four-point flexural test; then, the proposed model is verified by the experimental results; finally, several conclusions are drawn.

## **4.2 Model for prestress loss in corroded PT structures**

Strand corrosion expansion can induce concrete cracking and degrade bond strength, which cause further the prestress loss in corroded PT structures. For the corrosion-induced prestress loss evaluation, how to consider the effects of concrete cracking and bond degradation is still a problem. In the present study, a novel model, including the coupling effects of concrete cracking and bond degradation, is proposed to predict the corrosion-induced prestress loss.

In this section, the corrosion-induced cracking is estimated considering the softening behaviors of cracked concrete at first; next, the bond strength of corroded strand is evaluated from the contributions of adhesion stress, confinement stress and expansive pressure; then, a prediction model for prestress loss in corroded PT structures is proposed, incorporating the coupling effects of concrete cracking and bond degradation.

#### 4.2.1 Concrete cracking induced by strand corrosion

Strand corrosion expansion can lead to cover cracking. Numerous studies indicate that the corrosion-induced cracking process can be reasonably explained with the thick-walled cylinder theory [39, 97, 99]. Therefore, the thick-walled cylinder theory is also employed to model concrete cracking in the present study. Dai et al. [99] experimentally investigated corrosion-induced cracking in PC beams, and indicated that slight strand corrosion could induce cover cracking. Experimental observation showed that corrosion products exhibited the uniform distribution at the strand-concrete interface under the slight corrosion. Thus, corrosion products are considered to be uniformly distributed around strand in the present model. When the tensile stress induced by strand corrosion expansion exceeds the concrete tensile strength, concrete is considered to crack. Fig. 4.1 shows concrete cracking due to strand corrosion.

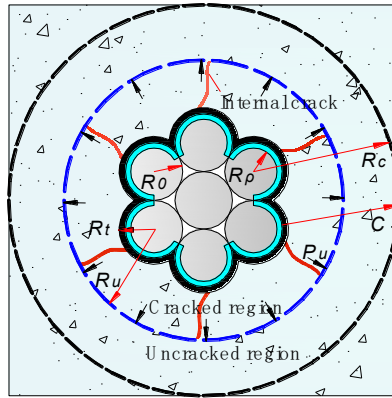


Fig. 4.1. Concrete cracking due to strand corrosion

The seven-wire steel strand is generally used in PC structures. The contact area between the outer wire and concrete is equal to two-thirds of the surface area. The outer wires would be corroded firstly when the strand is subjected to environmental erosion, as shown in Fig. 4.1. The corrosion loss of strand  $\rho$  can be expressed as

$$\rho = 6\Delta A/A_p \quad (4.1)$$

where  $\Delta A$  is the area loss of single wire,  $\Delta A = \frac{2}{3}\pi(R_0^2 - R_\rho^2)$ ,  $R_0$  and  $R_\rho$  are the radiuses of wire before and after corrosion, respectively;  $A_p$  is the cross-sectional area of un-corroded strand.

Corrosion products have the larger volume than the consumed iron, and would

expand outwardly during corrosion process. Some corrosion products fill pores and cracks, and others contribute to expansive pressure [39]. With the equivalent principle of volume, the volume reduction of strand  $\Delta V_w$  per unit length can be expressed as

$$\Delta V_w = \frac{1}{\gamma-1} (\Delta V_c + \Delta V_e) \quad (4.2)$$

where  $\gamma$  is the rust expansion ratio;  $\Delta V_w = 4\pi(R_0^2 - R_p^2)$ ;  $\Delta V_c$  is the volume of corrosion products per unit length that fill in cracks and pores;  $\Delta V_e$  is the volume change of concrete per unit length,  $\Delta V_e = 4\pi(R_t^2 - R_0^2)$ ,  $R_t$  is the wire radius with corrosion products.

The volume of corrosion products per unit length that fill in cracks and pores can be given as [39]

$$\Delta V_c = 4\pi(R_t - R_o)(R_u - R_t) \quad (4.3)$$

where  $R_u$  is the radius of cracked region.

The concrete displacement  $u_c$  induced by expansive pressure can be calculated with Eqs. (4.1-4.3), and is given as

$$u_c = R_t - R_0 = \frac{(\gamma-1)A_p\rho}{4\pi(R_u+R_0)} \quad (4.4)$$

As Fig. 4.1 shows, the concrete cover contains two parts before cover cracking: a cracked inner and an un-cracked outer regions. For the un-cracked concrete, the stress state of concrete can be described by the elasticity thick-walled cylinder theory. The hoop stress  $\sigma_\theta(t)$  and radial displacement  $u(t)$  in un-cracked concrete, respectively, are [58]

$$\sigma_\theta(t) = \frac{R_u^2 P_u}{(R_c^2 - R_u^2)} \left(1 + \frac{R_c^2}{t^2}\right) \quad (4.5a)$$

$$u(t) = \frac{R_u^2 P_u}{E_c(R_c^2 - R_u^2)} \left[ (1 + \nu_c) \frac{R_c^2}{t} + (1 - \nu_c)t \right] \quad (4.5b)$$

where  $t$  is the radius of concrete at the un-cracked region,  $R_u \leq t \leq R_c$ ,  $R_c = R_0 + C$ ,  $C$  is the concrete cover;  $P_u$  is the expansive pressure at the interface between cracked and un-cracked regions;  $E_c$  and  $\nu_c$  are the elastic modulus and Poisson ratio of concrete, respectively.

According to the equivalence principle of stress distribution at the same position, the tensile stress of concrete  $\sigma_\theta(R_u)$  at the interface between cracked and un-cracked

regions should be equal to the concrete tensile strength  $f_t$ , i.e.  $\sigma_\theta(R_u) = f_t$ . The expansive pressure at the interface between cracked and un-cracked regions can be obtained with Eq. (4.5a), and is written as

$$P_u = f_t \frac{R_c^2 - R_u^2}{R_c^2 + R_u^2} \quad (4.6)$$

Substituting Eq. (4.6) into Eq. (4.5b), the radial displacement  $u(t)$  in the un-cracked concrete can be calculated. Assuming that the radial displacement  $u(r)$  in the cracked concrete still satisfies the linear distribution principle, the radial displacement can be expressed as

$$u(r) = \frac{f_t R_u^2}{E_c (R_c^2 + R_u^2)} \left[ (1 + \nu_c) \frac{R_c^2}{r} + (1 - \nu_c) r \right] \quad (4.7)$$

where  $r$  is the radius of concrete at the cracked region,  $R_0 \leq r \leq R_u$ .

Cracks can lead to the tension softening of concrete. The bilinear softening curve is employed to describe the tension softening in the cracked concrete [133], and is shown in Fig. 4.2. Considering the softening behaviors of concrete, the hoop stress of cracked concrete can be written as [133]

$$\sigma_\theta(r) = \begin{cases} E_c \varepsilon_\theta(r), & \varepsilon_\theta(r) \leq \varepsilon_{ct} \\ f_t \left[ 1 - 0.85 \frac{\varepsilon_\theta(r) - \varepsilon_{ct}}{\varepsilon_1 - \varepsilon_{ct}} \right], & \varepsilon_{ct} < \varepsilon_\theta(r) \leq \varepsilon_1 \\ 0.15 f_t \left[ \frac{\varepsilon_u - \varepsilon_\theta(r)}{\varepsilon_u - \varepsilon_1} \right], & \varepsilon_1 < \varepsilon_\theta(r) \leq \varepsilon_u \end{cases} \quad (4.8)$$

where  $\sigma_\theta(r)$  and  $\varepsilon_\theta(r)$  are the hoop stress and hoop strain of concrete, respectively;  $\varepsilon_{ct}$  is the strain corresponding to concrete tensile strength;  $\varepsilon_1$  is the strain corresponding to 15% concrete tensile strength;  $\varepsilon_u$  is the ultimate strain of concrete.

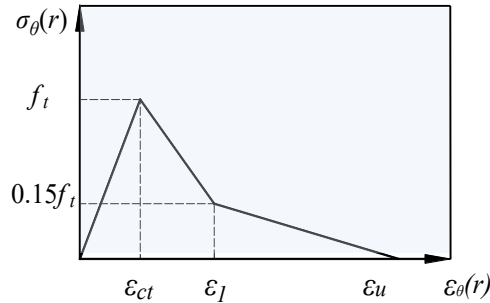


**Fig. 4.2. Stress-strain curve of concrete in tension**

Before cover cracking, the expansive pressure would be resisted by the residual tensile stress in the cracked concrete and the confining stress in the un-cracked concrete.

More details can be found in Wang et al. [58]. The expansive pressure  $P_c$  at the strand-concrete interface can be given as

$$P_c R_0 = P_u R_u + \int_{R_0}^{R_u} \sigma_\theta(r) dr \quad (4.9)$$

After cover cracking, the expansive pressure would be primarily resisted by the residual tensile strength in the cracked concrete. The expansive pressure at the strand-concrete interface can be rewritten as [148]

$$P_c R_0 = \int_{R_0}^{R_c} \sigma_\theta(r) dr \quad (4.10)$$

#### 4.2.2 Bond degradation due to strand corrosion

Corrosion can change the geometrical shape of strand. Corrosion-induced cracking can reduce the confinement effects of concrete. These factors would affect the bond behaviors of corroded strand. The strand's bond mechanism is very similar to that of deformed bar based on the experimental investigation performed by Wang et al. [149]. In the present study, a model proposed by Chen and Nepal [89], which is used to predict the bond stress of corroded deformed bar, is further developed to estimate the bond stress of corroded strand. The bond strength can be estimated from the contribution of the adhesion stress, confinement stress and expansive pressure. Considering the corrosion effects, the bond stress of corroded strand  $\tau_\eta$  can be written as

$$\tau_\eta = \tau_a + \tau_b + \tau_c \quad (4.11)$$

where  $\tau_a$  is the adhesion stress at the bond interface;  $\tau_b$  is the confinement stress from the surrounding concrete;  $\tau_c$  is the bond stress induced by expansive pressure.

The adhesion stress of corroded strand can be expressed as [89]

$$\tau_a = \frac{k A_r [\cot \delta + \tan(\delta + \theta)]}{\pi D s_r} f_{coh} \quad (4.12)$$

where  $k$  is the number of transverse ribs;  $A_r$  is the rib area in the plane at right angles to strand axis;  $D$  is the strand diameter;  $\delta$  is the rib orientation;  $\theta$  is the friction angle between strand and concrete;  $s_r$  is the rib spacing;  $f_{coh}$  is the coefficient of adhesion stress.

The confinement stress from the surrounding concrete can be given as [3]

$$\tau_b = \frac{kC_r \tan(\delta + \theta)}{\pi} p_x \quad (4.13)$$

where  $C_r$  is the shape factor constant;  $p_x$  is the maximum pressure at bond failure.

The bond stress induced by expansive pressure can be written as

$$\tau_c = k_c P_c \quad (4.14)$$

where  $k_c$  is the friction coefficient between corroded strand and cracked concrete.

Substituting Eqs. (4.12-4.14) into Eq. (4.11), the bond stress of corroded strand can be obtained. For PT structures, the prestress transfers from strand to concrete through the bond stress. The bond stress of corroded strand will be employed to evaluate the corrosion-induced prestress loss in the follow section.

#### 4.2.3 Corrosion-induced prestress loss

Since corrosive cracking and bond degradation have been estimated, a model for corrosion-induced prestress loss can be proposed. The corrosion-induced prestress loss in the present study is defined as the effective prestress in un-corroded strand minus that in corroded strand. The effective prestress in corroded strand could be evaluated based on the strain compatibility and force equilibrium equations.

When the prestressing force in PT structures is released, the strand prestress would transfer to the concrete through the bond stress. Fig. 4.3 shows the stress variation in corroded strand. One-half of the beam is discretized into several segments to analyze the stress variation in corroded strand.

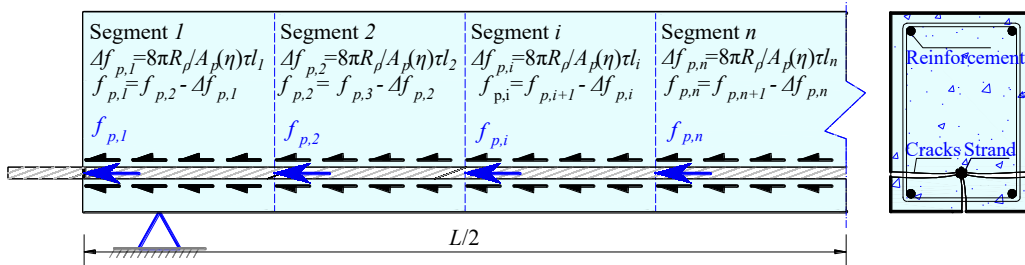


Fig. 4.3. Stress variation in corroded strand

As Fig. 4.3 shows, the segments of half beam are numbered from 1 to  $n$ . For an arbitrary segment  $i$ , the stress of strand  $f_{p,i}$  can be written as

$$f_{p,i} = f_{p,i+1} - \Delta f_{p,i} \quad (4.15)$$

where  $\Delta f_{p,i}$  is the local stress variation in corroded strand at the  $i$  segment,  $1 \leq i \leq n$ .

The contact area  $S$  between the outer wire and concrete is equal to two-thirds of the surface area, which can be expressed as  $S = \frac{4}{3}\pi R_{\rho,i} l_i$ ,  $R_{\rho,i}$  is the residual radius of corroded wire at the  $i$  segment,  $l_i$  is the segment length. The local stress variation in corroded strand can be given as

$$\Delta f_{p,i} = \frac{6S}{A_{p,i}(\eta)} \tau_{\eta} \quad (4.16)$$

where  $A_{p,i}(\eta)$  is the residual cross-sectional area of corroded strand at the  $i$  segment.

For corroded PT structures, the strand prestress at the beam end is zero, i.e.  $f_{p,1} =$

0. The tension force of corroded strand  $T_{p,i}$  can be computed as

$$T_{p,i} = f_{p,i} A_{p,i}(\eta) \quad (4.17)$$

After corrosion, the strain change in strand at  $i$  segment  $\Delta \varepsilon_{p,i}$  can be written as

$$\Delta \varepsilon_{p,i} = \frac{T_{pi}}{E_p A_p} - \frac{T_{p,i}}{E_p A_{p,i}(\eta)} \quad (4.18)$$

where  $T_{pi}$  is the initial prestressing force of un-corroded strand at the  $i$  segment;  $E_p$  is the elastic modulus of strand.

When the stress of corroded strand reaches the effective prestress, the strain change in concrete  $\Delta \varepsilon_{c,i}$  at the strand position should be equal to the strain change in corroded strand  $\Delta \varepsilon_{p,i}$  to maintain the strain compatibility, i.e.  $\Delta \varepsilon_{c,i} = \Delta \varepsilon_{p,i}$ . After corrosion, the concrete strain at the  $i$  segment  $\varepsilon_{cp,i}$  can be given as

$$\varepsilon_{cp,i} = \frac{T_{pi}}{E_c} \left( \frac{1}{A} + \frac{e_p^2}{I} \right) - \Delta \varepsilon_{c,i} \quad (4.19)$$

where  $e_p$  is the eccentricity of strand;  $A$  is the cross-sectional area of intact concrete;  $I$  is the inertia moment of gross section of intact concrete.

This study primarily investigates the prestress loss induced by strand corrosion, no corrosion is considered in the steel reinforcements. The strain distribution in the beam cross-section is shown in Fig. 4.4. Based on the plane section assumption, the strains of reinforcements in the tension and compression zones,  $\varepsilon_{s,i}$  and  $\varepsilon'_{s,i}$ , respectively, are

$$\varepsilon_{s,i} = \frac{h_x - a_s}{h_x - a_p} \varepsilon_{cp,i} \quad (4.20a)$$

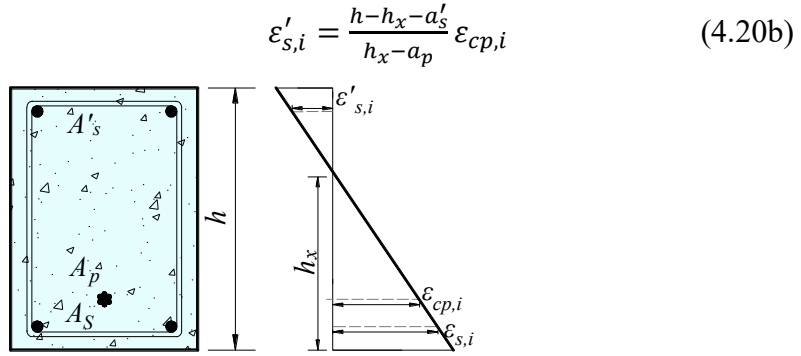


**Fig. 4.4. Strain distribution in the beam cross-section**

where  $h$  is the height of beam;  $h_x$ ,  $a_p$  and  $a_s$  are the distances from the beam gravity, strand center and tensile reinforcement center to the bottom of beam, respectively;  $a'_s$  is the distance from the compressive reinforcement center to the top of beam.

The stress-strain behaviors of reinforcements can be described by an elastic-plastic constitutive model [150], and is written as

$$f_s = \begin{cases} E_s \varepsilon_s & \varepsilon_s \leq \varepsilon_{sy} \\ f_{sy} + E_{sp}(\varepsilon_s - \varepsilon_{sy}) & \varepsilon_s > \varepsilon_{sy} \end{cases} \quad (4.21)$$

where  $f_s$  and  $\varepsilon_s$  are the stress and strain of reinforcement, respectively;  $E_s$  and  $E_{sp}$  are the elastic and hardening modulus of reinforcement, respectively;  $f_{sy}$  and  $\varepsilon_{sy}$  are the yield strength and yield strain of reinforcement, respectively.

The forces of reinforcements in the tension and compression zones,  $F_{s,i}$  and  $F'_{s,i}$ , respectively, are

$$F_{s,i} = A_s f_s(\varepsilon_{s,i}) \quad (4.22a)$$

$$F'_{s,i} = A'_s f_s(\varepsilon'_{s,i}) \quad (4.22b)$$

where  $A_s$  and  $A'_s$  are the section areas of reinforcements in the tension and compression zones, respectively;  $f_s(\varepsilon_{s,i})$  and  $f_s(\varepsilon'_{s,i})$  are the stresses of reinforcements in the tension and compression zones, respectively.

The mechanical behavior of concrete in tension can be modeled by a linear elastic constitutive law [151]. The nonlinear constitutive law of concrete proposed by Collins and Mitchell [152] is used to describe the mechanical behavior of concrete in compression. The stress-strain curve of concrete is expressed as

$$f_c = \begin{cases} f'_c \left[ 2 \left( \frac{\varepsilon_c}{\varepsilon_0} \right) - \left( \frac{\varepsilon_c}{\varepsilon_0} \right)^2 \right] & \text{in compression} \\ E_c \varepsilon_c & \text{in tension} \end{cases} \quad (23)$$

where  $f_c$  and  $\varepsilon_c$  are the stress and strain of concrete, respectively;  $f'_c$  is the concrete compressive strength, and  $\varepsilon_0$  is the strain corresponding to the concrete compressive strength and taken as 0.002.

The total force of concrete  $C_i$  can be written as

$$C_i = \int_{A_c} f_c d A_c \quad (4.24)$$

where  $A_c$  is the cross-sectional area of damaged concrete.

For corroded PT structures, the forces in prestressing strand, concrete and steel reinforcements should satisfy the equilibrium equation, which can be expressed as

$$C_i + F'_{s,i} - T_{p,i} - F_{s,i} = 0 \quad (4.25)$$

As mentioned above, a novel model, incorporating the coupling effects of concrete cracking and bond degradation, is proposed to evaluate the corrosion-induced prestress loss in PT structures. The calculation process of prestress loss can be performed as follow. First, the corrosion-induced cracking and bond degradation is estimated by Eqs. (4.1-4.14). Next, the stress variation in corroded strand at each segment is calculated by Eq. (4.16). Based on the step-by-step accumulation, the stress increment from zero to the effective prestress is obtained with Eq. (4.15). The accumulation process is terminated when the stress states of prestressing strand, concrete and steel reinforcements satisfy the strain compatibility and force equilibrium equations. Then, the effective prestress in corroded strand is evaluated with Eq. (4.17). The effective prestress in un-corroded strand can be calculated when the corrosion loss is defined as zero in the above procedure. The corrosion-induced prestress loss is equal to the effective prestress in un-corroded strand minus that in corroded strand. The calculation flow chart of prestress loss is shown in Fig. 4.5.

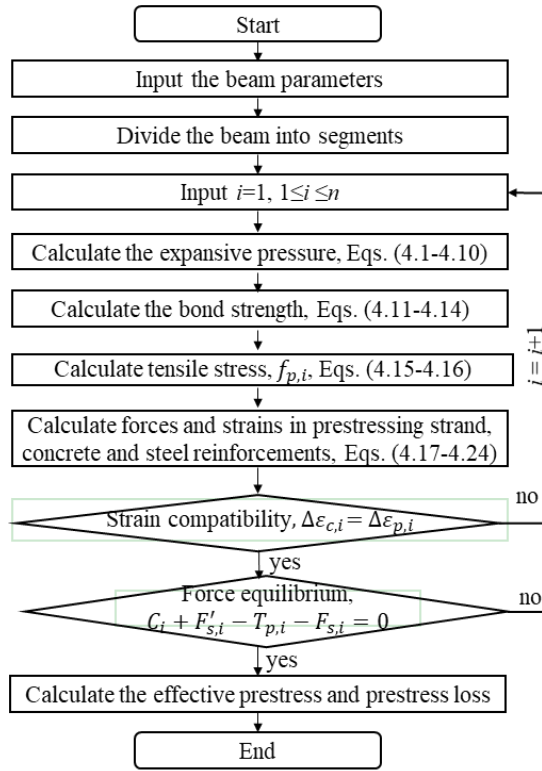


Fig. 4.5. Calculation flow chart of prestress loss

### 4.3 Evaluation of effective prestress in corroded PT beams

In this section, eight concrete beams under various stress levels were designed to evaluate the effect of strand corrosion on the effective prestress. The electrochemically accelerated method was employed to obtain the different corrosion levels of strand in PT beams. The effective prestress in corroded PT beams was evaluated by the four-point flexural test.

#### 4.3.1 Specimen details

Eight concrete beams were designed with a rectangular section of 130×150 mm, and 2000 mm in length. The beams were reinforced with a 15.2 mm diameter seven-wire steel strand. The yield and ultimate strengths of the strand were 1830 and 1910 MPa, respectively. Two 6 mm deformed bars were arranged as the longitudinal bars at the bottom of beam, two 8 mm deformed bars were employed as hanger bars at the top of beam, and 6 mm stirrups with 100 mm spacing were used in the beam. The yield and ultimate strengths of the deformed bars were 400 and 540 MPa, respectively. The covers

of reinforcements and strand were 30 mm and 42.4 mm, respectively. The specimen details are shown in Fig. 4.6.

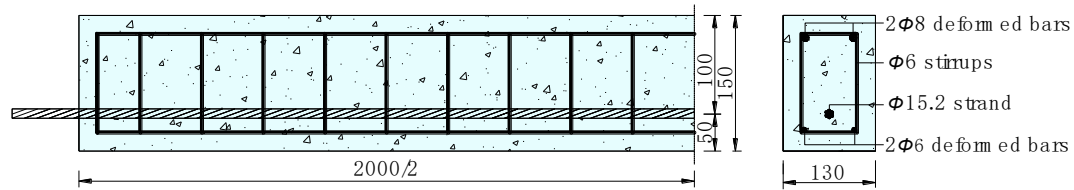


**Fig. 4.6. Details of specimen (Unit: mm)**

The testing parameters are presented in Table 4.1. To investigate the prestress loss under various stress and corrosion levels, four stress levels of strand were designed as 0,  $0.25f_p$ ,  $0.5f_p$ , and  $0.75f_p$ , respectively, where  $f_p$  was 1860 MPa. According to the corrosion time, the specimens were divided into two groups: group A and group B. The corrosion time in group A and group B were 15 and 20 days, respectively.

**Table 4.1. Testing parameters**

Beam No.	Group A				Group B			
	PA0	PA1	PA2	PA3	PB0	PB1	PB2	PB3
Prestress (MPa)	0	$0.25f_p$	$0.5f_p$	$0.75f_p$	0	$0.25f_p$	$0.5f_p$	$0.75f_p$
Corrosion time (Days)	15	15	15	15	20	20	20	20

The concrete was cast using the ordinary Portland cement. The concrete mix contained:  $417 \text{ kg/m}^3$  of cement,  $1026 \text{ kg/m}^3$  of coarse aggregates and  $676 \text{ kg/m}^3$  of fine aggregates. The water-cement ratio of concrete was 0.44. The sodium chloride (NaCl) with a 5% mass fraction of cement was used in the concrete to catalyze the corrosion process. The 28-day uniaxial compressive strength of concrete was 44.1 MPa.

#### 4.3.2 Accelerated corrosion and corrosion loss measurement

In the present testing, the electrochemically accelerated method was employed to obtain the different corrosion levels of strand. To clarify the effect of strand corrosion on the prestress loss alone, the steel reinforcements were protected with the epoxy resin to prevent corrosion. The corrosion device consisted of a direct current potentiostat and a stainless steel plate. The direct current was impressed on strand using the potentiostat. The corrosion current in the total process was 0.1 A. Fig. 4.7 shows the accelerated corrosion device.



**Fig. 4.7. Accelerated corrosion device**

The average mass loss of strand was employed to reflect corrosion level. The measurement of mass loss was performed after loading test, and the program was as follows. First, the concrete cover was removed by the destructive method, and the corroded strand was taken out. Next, the corroded strand was cleaned by 12% hydrochloric acid solution and neutralized with alkali [128]. Then, the average mass loss of the strand was measured, and is given in Table 4.2.

**Table 4.2. Summary of experimental results**

Beam No.	PA0	PA1	PA2	PA3	PB0	PB1	PB2	PB3
$\rho_c$ (%)	7.05	7.47	8.35	9.41	10.45	11.52	12.48	14.69
$F_c$ (kN)	5.0	8.5	11.5	14.0	4.5	7.0	9.5	11.5
$F_u$ (kN)	38.0	42.0	45.5	48.0	28.3	31.0	33.5	36.7
$F_{e,t}$ (kN)	0.0	52.6	89.7	120.7	0.0	37.5	56.4	74.0
$f_{e,t}$ (MPa)	0.0	409.0	704.1	958.5	0.0	304.9	463.6	624.0
Normalized prestress loss (%)	0.0	12.0	24.3	31.3	0.0	34.4	50.2	55.3

Note:  $\rho_c$  is the mass loss,  $F_c$  is the cracking load,  $F_u$  is the ultimate load,  $F_{e,t}$  is the prestressing force,  $f_{e,t}$  is the effective prestress.

### 4.3.3 Effective prestress evaluation under various stress levels

Existing studies indicate that several experimental techniques have been proposed to evaluate the effective prestress in PC structures, which can be divided into: (1) measuring longitudinal concrete strains over time at the gravity of prestressing strand; (2) determining the cracking load based on the load testing; (3) monitoring the strain

variation in strand by cutting it into a representative exposed length; (4) determining the side pressure to close cracks in a small cylindrical hole. More details about these methods can be seen in Caro et al. [153]. The aforementioned methods all require a reverse process from the testing results to calculate the prestress loss using the mechanical theory. For these methods, the cracking load test is one of the most commonly used technique, which will be employed to evaluate the effective prestress in corroded PT beams in the present testing.

A four-point flexural test was performed to obtain the load-deflection curves of corroded specimens. Fig. 4.8 shows the diagram of load testing. Each specimen had a clear span of 1800 mm and a bending span of 600 mm. Loads were applied monotonically and measured by a load cell. The displacements at the mid-span are employed to reflect the load-deflection curves of specimens, and are presented in Fig. 4.9.

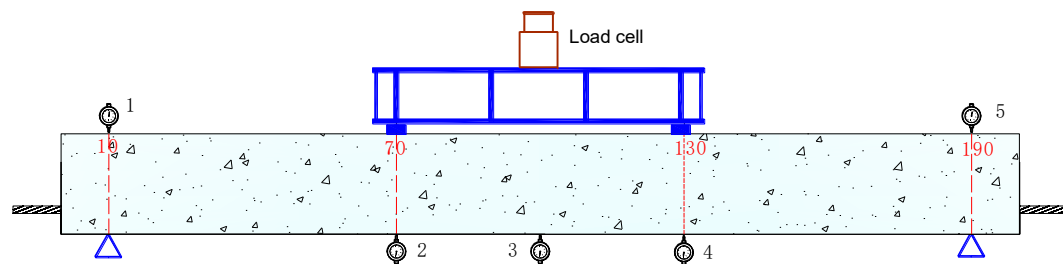


**Fig. 4.8. Diagram of load testing**

As Fig. 4.9 shows, the beam exhibits increasing deflection with increasing load before the maximum load. After that, the concrete crushing in the compression zone induces a sudden decrease of load, and leads to the beam failure. The cracking and ultimate loads are measured during the load testing, and are listed in Table 4.2. Comparing with the experimental data in Table 4.2, it is found that prestress can accelerate the mass loss of strand. The mass losses of PA0 and PA3 are 7.05% and 9.41%, respectively. The mass losses of PB0 and PB3 are 10.45% and 14.69%, respectively. By varying the stress level of strand from 0 to  $75\%f_p$ , the average increase rate of mass loss is 37.0% in the current experimental study.

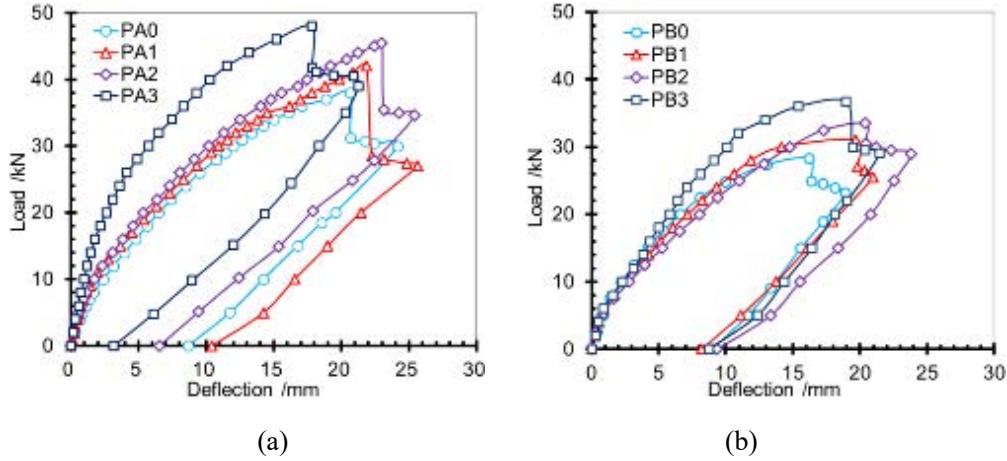


Fig. 4.9. Load-deflection curves: (a) Group A; (b) Group B

During the load testing, the tensile stress in the bottom of beam is conducted by three factors: the self-weight, effective prestress and applied load. Cracks would appear when the tensile stress at the bottom of beam exceeds the concrete tensile strength. The critical condition of concrete cracking can be expressed as

$$f_t = f_{p,\eta} A_p(\eta) \left( \frac{1}{A_c} + \frac{e_p}{I_c} y_b \right) - \frac{M_s}{I_c} y_b - \frac{M_c}{I_c} y_b \quad (4.26)$$

where  $f_{p,\eta}$  is the effective prestress in corroded PC beams;  $A_p(\eta)$  is the residual cross-sectional area of corroded strand;  $y_b$  is the distance from the neutral axis to the bottom of beam;  $M_s$  is the moment due to the self-weight of beam;  $M_c$  is the cracking moment;  $I_c$  is the inertia moment of gross section of damaged concrete.

Based on the cracking load and corrosion loss, the effective prestress and prestress loss in corroded PT beams can be evaluated, and are given in Table 4.2. The normalized prestress loss is defined as the ratio of prestress loss in corroded strand to effective prestress in un-corroded strand. Comparing with the prestress loss presented in Table 4.2, it is found that the high stress of strand can accelerate corrosion-induced prestress loss. The prestress losses of PA1 and PA3 are 12.0% and 31.3%, respectively. The prestress losses of PB1 and PB3 are 34.4% and 55.3%, respectively. By varying the stress level of strand from 25%  $f_p$  to 75%  $f_p$ , the corrosion-induced prestress loss increases 20.1% in the current experimental study.

#### 4.3.4 Validation on prestress loss model

The experimental results are employed to verify the proposed model in this section.

The relevant parameters are selected as follow. The rust expansion ratio  $\gamma$  varies from 2 to 4 [91], and is set as 3. The friction angle between corroded strand and concrete is expressed as  $k_c = 0.37 - 0.26(x - x_c)$  [3],  $x$  is the corrosion depth of strand,  $x_c$  is critical corrosion depth of cover cracking. The coefficient of adhesion stress is given as  $f_{coh} = 2 - 10(x - x_c)$  [89]. The shape factor constant  $C_r$  is taken as 0.8 [89].

For evaluating the corrosion-induced prestress loss, the bond degradation is the key factor and should be clarified first. To investigate the effect of strand corrosion on the bond strength, bond strengths under different corrosion levels are shown in Fig. 4.10. The normalized bond strength in Fig. 4.10 is defined as the bond strength ratio of corroded strand to un-corroded strand.

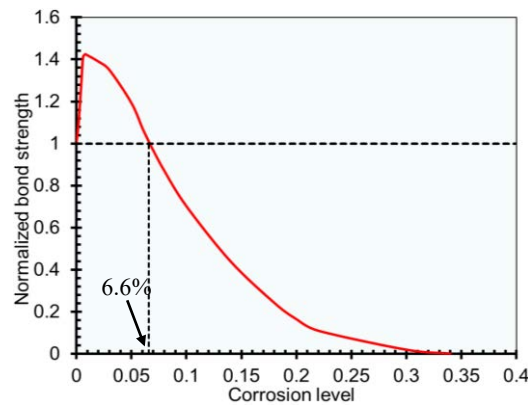


**Fig. 4.10. Bond strengths under different corrosion levels**

As Fig. 4.10 shows, strand corrosion less than 6.6% can increase the bond stress, and the further corrosion will lead to the bond stress deterioration. For the slight corrosion less than 6.6%, the accumulation of corrosion products increases the roughness of strand surface, and improves the friction and gear forces at the strand-concrete interface. Thus, the slight strand corrosion can increase the bond stress. Exceeding the corrosion level of 6.6%, corrosion would cause severe concrete cracking and reduce the confinement of concrete, which could lead to the bond stress deterioration.

The proposed model is employed to predict the experimental results. Fig. 4.11 shows the predicted effective prestress and experimental results. The normalized prestress in Fig. 4.11 is defined as the ratio of effective prestress in corroded strand to

$75\%f_p$ . For the prediction of effective prestress, the bond strength model is selected as follows. Slightly corroded strand (corrosion loss less than 6.6%) is considered to have the similar bond stress with the un-corroded strand for the safety reserve reasons. After that, the bond strength model proposed in the present study is employed to predict the effective prestress.

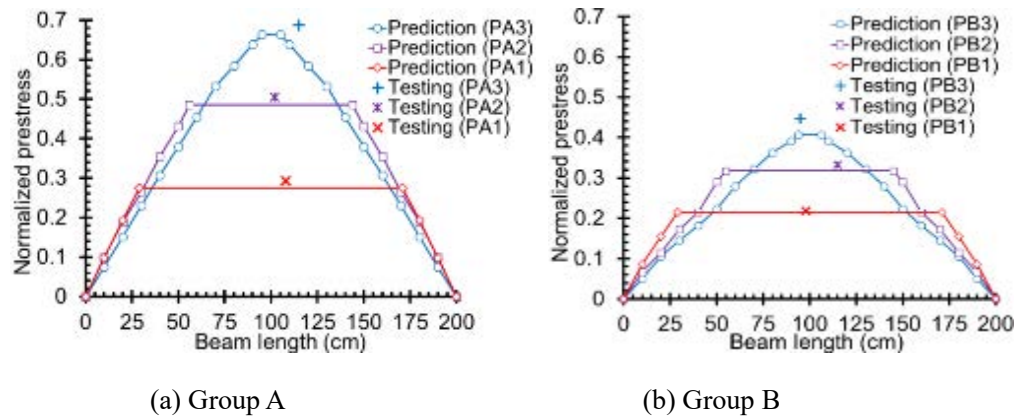


**Fig. 4.11. Experimental and predicted prestress**

As Fig. 4.11 shows, the average error and standard deviation of prediction are 4.8% and 0.02, respectively. The prediction error in the present study is defined as  $\frac{|P_t - P_p|}{P_t}$ , where  $P_t$  and  $P_p$  are tested and predicted effective prestress, respectively. The reason for the error may be ascribed to some simplifications of the analytical model. Another reason for the error is the measurement uncertainty of experimental data. Considering the complexity of corrosion process, the prediction error can be accepted. This indicates that the proposed model can provide an accurate prediction for the effective prestress in corroded PT structures.

To further clarify the applicability of the proposed model, the bond stress models proposed by the present study and Wang et al. [149] are employed to predict the corrosion-induced prestress loss, as shown in Fig. 4.12. Wang et al. [149] designed ten pull-out beams with various corrosion levels to investigate the bond degradation. Based on the experimental data, the empirical model is proposed to predict the bond strength and expressed as

$$R_\eta = \begin{cases} 1.0, & \eta \leq 6.0\% \\ 2.03e^{-11.8\eta}, & \eta > 6.0\% \end{cases} \quad (4.27)$$

where  $R_\eta$  is the bond stress ratio of corroded strand to un-corroded strand.

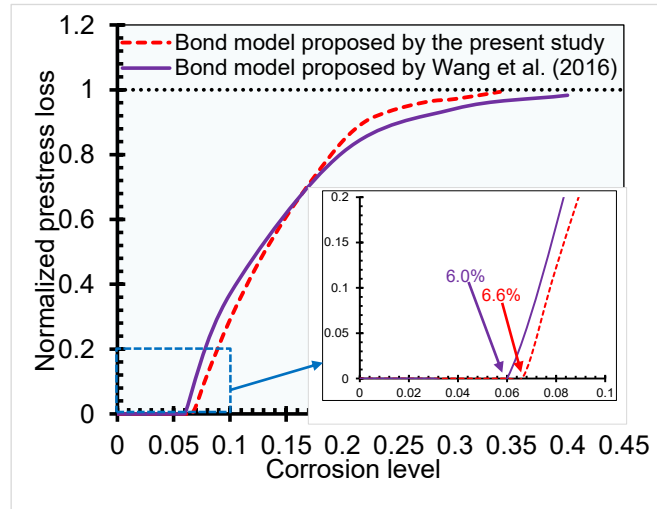


**Fig. 4.12. Prestress loss and corrosion level**

As Fig. 4.12 shows, prestress loss depends on corrosion level. When the corrosion level is less than the critical value, strand corrosion may lead to slight cracking of concrete, but would not degrade bond strength and effective prestress. The critical corrosion levels for the present model and Wang et al. [149] are 6.6% and 6.0%, respectively. Thus, strand corrosion less than the critical value would not cause prestress loss. Exceeding the critical corrosion level, strand corrosion can induce severe cracking of concrete, which can reduce bond strength and effective prestress. The curve obtained from the present model shows that the effective prestress would decrease to zero when the corrosion level is greater than 34.0%. The prediction tendencies of corrosion-induced prestress loss in Fig. 4.12 for both models are similar. This further indicates that the proposed model can be employed to predict the corrosion-induced prestress loss in PT structures.

## 4.4 Conclusions

A novel model is proposed to predict the prestress loss in corroded PT structures caused by corrosive cracking. The effective prestress in eight corroded PT beams under various stress levels is explored by the four-point flexural test. The proposed model is verified by the experimental results. The following conclusions can be drawn:

- The proposed model can provide an accurate prediction for corrosion-induced prestress loss in PT structures. The superiority of the present model is that it can consider the coupling effects of concrete cracking and bond degradation.

- Prestress loss depends on corrosion level. Corrosion-induced concrete cracking would not degrade bond strength and effective prestress unless the corrosion level exceeds 6.6%. As corrosion further progresses, bond strength and effective prestress decrease monotonically, and then reduce to zero when the corrosion level reaches 34.0%.
- The high stress of strand can accelerate corrosion-induced prestress loss. By varying the stress level of strand from 25% to 75% of strand tensile strength, corrosion-induced prestress loss increases by 20.1%.

# **Chapter 5 Flexural Capacity Prediction of Corroded PC Beams Incorporating Bond Degradation**

## **5.1 Introduction**

Steel corrosion in concrete has been considered as one of the main causes of structural deterioration [1, 141]. Due to the high-stress level of prestressing strand, the potential threat of corrosion in PC beams would be much more severe than that in reinforced concrete members [154-156]. The collapse of corroded PC beams usually exhibits brittle failure without warning, which would cause substantial economic losses. The effect of strand corrosion on flexural capacity should be thoroughly investigated to insure the serviceability and safety of corroded PC beams.

Some experimental studies have been undertaken to investigate the flexural behaviors of corroded PC beams [127, 157-159]. Based on the load testing, corrosion effects on concrete cracking, stiffness, ultimate capacity, ductility and failure mode of PC beams are evaluated. Analytical studies regarding flexural capacity of corroded PC beams have been afforded little attention as compared to experimental studies. Cavell et al. [76] neglected the effect of bond degradation, and used a strain compatibility method to study the residual flexural capacity of deteriorating PC beams after tendon failure. Wang et al. [160] proposed a strain-incompatibility theory to evaluate the flexural capacity of corroded PC members, but it failed to consider the effect of concrete cracking, and the bond model was obtained from the experimental results. The applicability of the empirical model is still a problem.

Corrosion can deteriorate the flexural capacity of PC beams by decreasing strand cross-section, causing material deterioration, inducing concrete cracking and degrading bond strength [112, 156, 161]. The investigation of existing methods shows that no model can incorporate all of these mentioned effects. Additionally, the aforementioned studies have not considered the effect of flexural cracks on flexural capacity. The flexural cracks can change the distribution of bond strength along beam length, and

further affect the flexural capacity of corroded PC beams. Neglecting the effect of flexural cracks may overestimate the flexural capacity. Therefore, a new analytical model for flexural capacity of corroded PC beams that can include all these effects is needed.

This study presents a new analytical model to predict the flexural capacity of corroded PC beams. The novelty of the model is that it can incorporate the effects of strand cross-section reduction, material deterioration, concrete cracking and bond degradation. Additionally, the effect of flexural cracks can be also included in the model. The chapter is organized as follows. First, an analytical model, incorporating all these effects, is proposed to predict the flexural capacity of corroded PC beams. And then, the proposed model is validated by the experimental results collected from the previous researches. Finally, some conclusions are given.

## **5.2 Concept of flexural capacity model**

For the flexural capacity prediction, the effects of strand cross-section reduction and material deterioration can be easily incorporated into the model with the corrosion loss and degraded constitutive law. How to consider the effects of corrosion-induced cracking and bond degradation is still a complicated problem. Additionally, the effect of flexural cracks has not been considered in the model. In the present study, an analytical model, incorporating these multi-factor effects, is proposed to evaluate the flexural capacity of corroded PC beams.

Corrosion affects the bond behavior by decreasing the strand cross-section and changing the geometrical shape of strand. Moreover, corrosion-induced cracking can degrade the bond strength by reducing the confinement effect of surrounding concrete. Wang et al. [149] indicated that the strand's bond mechanism was very similar to that of deformed bar. Therefore, a model proposed by Chen and Nepal [89], which is used to predict the bond stress of corroded deformed bar, is further developed to estimate the bond stress of corroded strand in the present study. The bond stress of corroded strand is established from the contributions of adhesion stress, confinement stress and expansive pressure.

Aggressive agents and material deterioration can lead to the stiffness degradation of PC beams. Load cracks may appear on PC beams under normal service conditions. How to consider the effect of flexural cracks is a key issue for the flexural capacity prediction. The flexural cracks can change the magnitude of expansive pressure along beam length, as shown in Fig. 5.1.

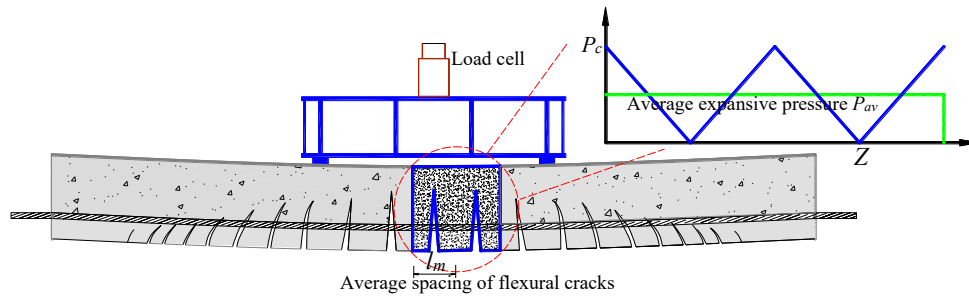


**Fig. 5.1. Distribution of expansive pressure along beam length**

As Fig. 5.1 shows, the expansive pressure ( $P_c$ ) would be fully effective at the middle point between adjacent flexural cracks, while it would totally release at the crack location. For the bond strength prediction, the expansive pressure distribution is idealized as the average expansive pressure ( $P_{av}$ ) along the beam length. Then, an equivalent bond stress concept is introduced to consider the effect of flexural cracks, which makes it possible to evaluate the bond force of corroded strand for the flexural capacity calculation.

During the loading test, the applied load on PC beams is mainly resisted by the tensile force of strand. Fig. 5.2 shows the transfer theory of strand force under the applied load. The tension force of prestressing strand ( $F_p$ ) depends on the effective bond force ( $F_{eb}$ ), residual bond force ( $F_{er}$ ) and effective prestressing force ( $F_{e\eta}$ ) [160].

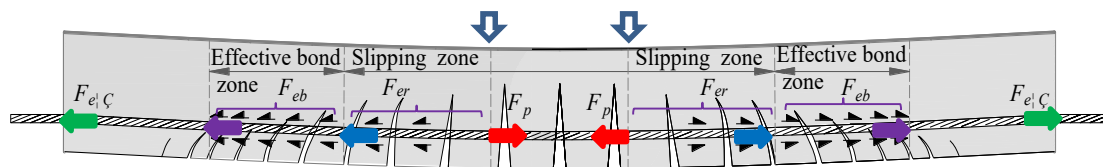


**Fig. 5.2. Schematic of strand force under applied load**

For un-corroded or slightly corroded PC beams, corrosion would not degrade the strand bond strength. The applied load under the ultimate state can be resisted by the effective prestressing force and effective bond force, and no slip between strand and

concrete would appear. Strand and surrounding concrete are considered to have the consistent strains during the whole loading test. The flexural capacity of un-corroded or slightly corroded PC beams can easily be estimated based on the force and moment equilibrium equations.

For severely corroded PC beams, corrosion would decrease the bond strength between strand and concrete. The applied load under the ultimate state is greater than the total of effective prestressing force and effective bond force. The effective bond zone would shift toward the beam ends to resist the applied loads, which leads to the mid-span of beam becoming the slipping zone. More details about the shifting theory of effective bond zone can be seen in Wang et al. [160]. The strain of corroded strand in the slipping zone would fail to follow the plane section assumption. Studies show that the incompatible strain between corroded strand and concrete can be quantified through introducing a compatibility coefficient [127, 160]. Considering the compatibility coefficient, the flexural capacity of corroded PC beams can be predicted.

## **5.3 Bond strength of corroded strand considering flexural cracks**

### **5.3.1 Corrosion-induced cracking and bond degradation**

Strand corrosion can lead to concrete cracking. Existing studies show that the thick-walled cylinder theory has been widely utilized to describe the corrosion-induced cracking process [39, 97, 162]. In the present model, the cover cracking process is also modeled by the thick-walled cylinder theory. Experimental studies indicate that the slight strand corrosion can lead to concrete cracking [94, 99]. For the slight corrosion degree, the uniform corrosion products can be observed at the strand-concrete interface. When the tensile stress induced by uniform corrosion products exceeds the concrete tensile strength, concrete is considered to crack. Fig. 5.3 displays the crack propagation and stress distribution in concrete.

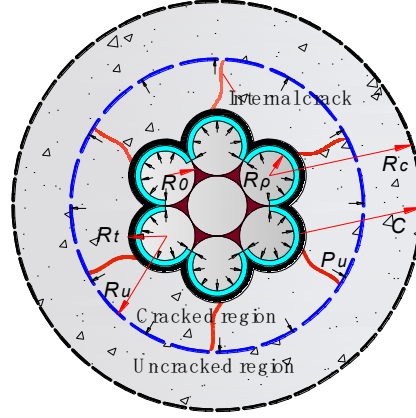


**Fig. 5.3. Crack propagation and stress distribution in concrete**

The seven-wire steel strand is used as the prestressed steel in the present model. The six outer wires would be corroded firstly when the strand is subjected to environmental erosion. The contact area between the outer wire and concrete is equal to two-thirds of the surface area of wire, and the area loss of single wire can be expressed as  $\frac{2}{3}\pi(R_0^2 - R_\rho^2)$ , where  $R_0$  and  $R_\rho$  are the radiuses of wire before and after corrosion, respectively. Then, the corrosion loss of strand  $\rho$  can be given as

$$\rho = 4\pi(R_0^2 - R_\rho^2)/A_p \quad (5.1)$$

where  $A_p$  is the cross-sectional area of un-corroded strand.

Strand corrosion products have larger volume than the consumed iron, which would expand outwardly during corrosion process. Some corrosion products fill pores and cracks, and others contribute to expansive pressure [39]. With the constant volume principle, the total volume of wire corrosion products per unit length  $\Delta V_t$  can be expressed as

$$\Delta V_t = \Delta V_w + \Delta V_e + \Delta V_c \quad (5.2)$$

where  $\Delta V_t = n\Delta V_w$ ,  $n$  is the rust expansion ratio;  $\Delta V_w$  is the volume change of wire per unit length,  $\Delta V_w = \frac{2}{3}\pi(R_0^2 - R_\rho^2)$ ;  $\Delta V_e$  is the volume change of concrete per unit length,  $\Delta V_e = \frac{2}{3}\pi(R_t^2 - R_0^2)$ ;  $R_t$  is the radius of wire with corrosion products;  $\Delta V_c$  is the volume of corrosion products per unit length that fill in cracks and pores.

The volume of corrosion products per unit length that fill in cracks and pores can be written as [39]

$$\Delta V_c = \frac{2}{3}\pi(R_t - R_o)(R_u - R_t) \quad (5.3)$$

where  $R_u$  is the radius of cracked region.

The concrete displacement  $u_c$  induced by expansive pressure can be calculated with Eqs. (5.1-5.3), and is expressed as

$$u_c = R_t - R_o = \frac{(n-1)A_p\rho}{4\pi(R_u+R_o)} \quad (5.4)$$

As Fig. 5.3 shows, before cover cracking occurs, the concrete consists of the cracked inner and uncracked outer regions. For the uncracked concrete, the stress state of concrete can be modeled by the elasticity theory. Based on the stress distribution and displacement boundary conditions in the axial symmetrical structures, the hoop stress  $\sigma_\theta(t)$  and the radial displacement  $u(t)$  in uncracked concrete, respectively, are

$$\sigma_\theta(t) = \frac{R_u^2 P_u}{(R_c^2 - R_u^2)} \left(1 + \frac{R_c^2}{t^2}\right) \quad (5.5a)$$

$$u(t) = \frac{R_u^2 P_u}{E_c (R_c^2 - R_u^2)} \left[ (1 + \nu_c) \frac{R_c^2}{t} + (1 - \nu_c) t \right] \quad (5.5b)$$

where  $t$  is the radius of concrete at the uncracked region,  $R_u \leq t \leq R_c$ ;  $R_c = R_o + C$ ,  $C$  is the concrete cover;  $P_u$  is the expansive pressure at the interface between cracked and uncracked regions;  $E_c$  and  $\nu_c$  are the elastic modulus and Poisson ratio of concrete, respectively.

According to the compatibility principle of stress distribution, the tensile stress of concrete  $\sigma_\theta(R_u)$  at the interface between cracked and uncracked regions should be equal to the concrete tensile strength  $f_t$ , i.e.  $\sigma_\theta(R_u) = f_t$ . With this principle, the expansive pressure  $P_u$  at the interface between cracked and uncracked regions can be obtained with Eq. 5.5(a). Then, the radial displacement  $u(t)$  in uncracked concrete region can be calculated with Eq. 5.5(b). Assuming the radial displacement  $u(r)$  in cracked concrete region still satisfies the linear distribution principle, which can be written as

$$u(r) = \frac{f_t R_u^2}{E_c (R_c^2 + R_u^2)} \left[ (1 + \nu_c) \frac{R_c^2}{r} + (1 - \nu_c) r \right] \quad (5.6)$$

where  $r$  is the radius of concrete at the cracked region,  $R_o \leq r \leq R_u$ .

For the partially cracked concrete, the expansive pressure would be resisted by the

residual tensile stress in cracked concrete and the confining stress in uncracked concrete. The residual tensile stress in cracked concrete can be estimated based on the tensile softening model proposed by Pantazopoulou and Papoulia [133]. Before cover cracking occurs, the expansive pressure  $P_c$  at the strand-concrete interface can be given as [58]

$$P_c R_0 = P_u R_u + \int_{R_0}^{R_u} \sigma_\theta(r) dr \quad (5.7)$$

where  $\sigma_\theta(r)$  is the hoop stress in cracked concrete.

The concrete cover would crack completely when cracks reach the concrete surface. After cover cracking occurs, the expansive pressure is mainly resisted by the residual tensile strength in cracked concrete. The expansive pressure at the strand-concrete interface should be rewritten as

$$P_c R_0 = \int_{R_0}^{R_c} \sigma_\theta(r) dr \quad (5.8)$$

Corrosion-induced cracking can degrade the bond strength by reducing the confinement effect of surrounding concrete. In the present study, a model proposed by Chen and Nepal [89], which is used to predict the bond stress of corroded deformed bar, is further developed to estimate the bond stress of corroded strand. The bond stress of corroded strand  $\tau_\eta$  can be evaluated with the adhesion stress, confinement stress and expansive pressure, and is expressed as

$$\tau_\eta = \tau_a + \tau_b + \tau_c \quad (5.9)$$

where  $\tau_a$  is the bond stress induced by expansive pressure;  $\tau_b$  is the adhesion stress at the bond interface;  $\tau_c$  is the confinement stress from the surrounding concrete.

The bond stress induced by expansive pressure can be given as

$$\tau_a = k_c P_c \quad (5.10)$$

where  $k_c$  is the friction coefficient between corroded strand and concrete.

The adhesion stress at the strand-concrete interface can be written as

$$\tau_b = \frac{k A_r [\cot \delta + \tan(\delta + \theta)]}{\pi D s_r} f_{coh} \quad (5.11)$$

where  $k$  is the number of transverse ribs;  $A_r$  is the rib area in the plane at right angles to bar axis;  $D$  is the strand diameter;  $\delta$  is the rib orientation;  $\theta$  is the friction angle between strand and concrete;  $s_r$  is the rib spacing;  $f_{coh}$  is the coefficient of adhesion

stress.

The confinement stress from the surrounding concrete is expressed as

$$\tau_c = \frac{kC_r \tan(\delta + \theta)}{\pi} p_x \quad (5.12)$$

where  $C_r$  is the shape factor constant;  $p_x$  is the maximum pressure at the bond fails.

### 5.3.2 Equivalent bond strength considering flexural cracks

The aforementioned bond model can be employed to evaluate the corrosion-induced bond degradation in PC beams without flexural cracks. However, when the applied load exceeds the cracking load of corroded PC beams, the flexural cracks would appear. The flexural cracks would change the distribution of bond strength along beam length. In the present study, an equivalent bond stress concept is introduced to consider the effect of flexural cracks.

After concrete cracking occurs, flexural cracks would appear on the beam surface, as shown in Fig. 5.1. To investigate the distribution of bond strength along beam length under the ultimate state, the beam is discretized into a series of elements. Each element is considered to have a single crack at the middle point, and the crack spacing is assumed as the constant.

As Fig. 5.1 shows, the expansive pressure at the crack location is zero, and it turns to  $P_c$  at the middle point between adjacent flexural cracks. A linear curve is employed to describe the distribution of expansive pressure between adjacent flexural cracks. The expansive pressure  $P_c(z)$  at a location  $z$  can be written as

$$P_c(z) = P_c \left(1 - \frac{2}{l_m} z\right) \quad 0 < z < \frac{l_m}{2} \quad (5.13)$$

where  $l_m$  is the average spacing of flexural cracks.

The average expansive pressure  $P_{av}$  can be expressed as

$$P_{av} = \frac{2}{l_m} \int_0^{l_m/2} P_c(z) dz \quad (5.14)$$

An equivalent bond stress concept is introduced to consider the distribution of bond strength along beam length [163]. Considering the effect of flexural cracks, the modified bond strength of corroded strand  $\tau_{a\eta}$  under the ultimate state can be written

as

$$\tau_{a\eta} = k_c P_{av} + \tau_b + \tau_c \quad (5.15)$$

The effective bond force of corroded strand  $F_{eb}$  under the ultimate state can be evaluated with the bond stress and contact area at the strand-concrete interface, which can be given as

$$F_{eb} = \tau_{a\eta} S L_{eb} \quad (5.16)$$

where  $S$  is the circumference of corroded strand;  $L_{eb}$  is the effective bond length.

## 5.4 Calculation procedure of flexural capacity

During the loading test, the applied load on PC beams is mainly resisted by the tensile force of strand. Fig. 5.2 shows the transfer theory of strand force under the applied load. The tension force of corroded prestressing strand  $F_p$  can be expressed as

$$F_p = F_{eb} + F_{er} + F_{e\eta} \quad (5.17)$$

Wang et al. [160] indicated that the residual bond stress could be considered as 40% of the effective bond stress. Then, the residual bond force of corroded strand  $F_{er}$  can be given as

$$F_{er} = 0.4 \tau_{a\eta} S L_{er} \quad (5.18)$$

where  $L_{er}$  is the length of slip region.

Zhang et al. [127] experimentally investigated the effective prestressing force of post-tensioned concrete beams under different corrosion degrees. Studies show that the effective prestressing force of corroded strand  $F_{e\eta}$  can be evaluated with the corrosion loss, which can be expressed as

$$F_{e\eta} = (1 - \rho) F_{pe} \quad (5.19)$$

where  $F_{pe}$  is the initial prestressing force of un-corroded strand.

The mechanical property of corroded strand has been studied by Wang et al. [160]. A constitutive law is proposed to describe the mechanical property of corroded strand, which can be given as

$$f_p = \begin{cases} E_p \varepsilon & \varepsilon \leq \varepsilon_y \\ f_y + E_{pp}(\varepsilon - \varepsilon_y) & \varepsilon_y < \varepsilon \leq \varepsilon_{pu} - \frac{\rho}{\rho_c}(\varepsilon_{pu} - \varepsilon_y) \\ E_p \varepsilon & \varepsilon \leq \varepsilon_y \end{cases} \quad \begin{matrix} \rho \leq \rho_c \\ \rho > \rho_c \end{matrix} \quad (5.20)$$

where  $f_p$  and  $\varepsilon$  are the stress and strain of corroded strand, respectively;  $\rho_c$  is the critical corrosion loss, and is considered as 11%;  $E_p$  and  $E_{pp}$  are the elastic and hardening modulus of un-corroded strand, respectively;  $f_y$  is the yield strength of un-corroded strand,  $\varepsilon_y$  and  $\varepsilon_{pu}$  are the yield and ultimate strains of un-corroded strand, respectively.

Combing Eqs. (5.17) and (5.20), the strand strain  $\varepsilon_p$  can be written as

$$\varepsilon_p = \begin{cases} \frac{F_p}{(1-\rho)A_p E_p} & F_p \leq (1-\rho)A_p f_y \\ \varepsilon_y + \frac{F_p}{(1-\rho)A_p E_{pp}} - \frac{f_y}{E_{pp}} & F_p > (1-\rho)A_p f_y \end{cases} \quad (5.21)$$

As mentioned above, corrosion can lead to the strain incompatibility between strand and concrete [127, 149]. A compatibility coefficient is introduced to quantify the incompatible strain between corroded strand and concrete under the ultimate state. Fig. 5.4 shows the strain distribution of strand and steel reinforcements in the cross-section. The concrete strain  $\varepsilon_{cp}$  at the strand location can be given as

$$\varepsilon_{cp} = \varepsilon_p / \delta \quad (5.22)$$

where  $\delta$  is the compatibility coefficient.

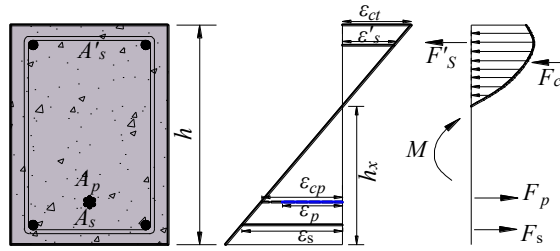


Fig. 5.4. Force and strain distribution in the cross-section

The present study only investigates the flexural capacity deterioration induced by strand corrosion, and no corrosion is considered in steel reinforcements. The steel reinforcements and surrounding concrete would have consistent strains under the applied load. As Fig. 5.4 shows, the strains of steel reinforcements in the tension and compression zones,  $\varepsilon_s$  and  $\varepsilon'_s$ , respectively, are

$$\varepsilon_s = \frac{\varepsilon_{cp} + \varepsilon_{ct}}{h_p} h_0 - \varepsilon_{ct} \quad (5.23a)$$

$$\varepsilon'_s = \varepsilon_{ct} - \frac{\varepsilon_{cp} + \varepsilon_{ct}}{h_p} a'_s \quad (5.23b)$$

where  $\varepsilon_{ct}$  is the concrete strain at the top of beam;  $h_p$ ,  $h_0$  and  $a'_s$  are the distances from the centers of strand, tensile steel reinforcements and compressive steel reinforcements to the top of beam, respectively.

The stress-strain curve of steel reinforcements can be described by a linear elastic-plastic model, and is written as

$$f_s = \begin{cases} E_s \varepsilon_{ss} & \varepsilon_{ss} \leq \varepsilon_{sy} \\ f_{sy} + E_{sp} (\varepsilon_{ss} - \varepsilon_{sy}) & \varepsilon_{ss} > \varepsilon_{sy} \end{cases} \quad (5.24)$$

where  $f_s$  and  $\varepsilon_{ss}$  are the stress and strain of steel reinforcements, respectively;  $E_s$  and  $E_{sp}$  are the elastic and hardening modulus of steel reinforcements, respectively;  $f_{sy}$  and  $\varepsilon_{sy}$  are the yield strength and yield strain of steel reinforcements, respectively.

The forces of steel reinforcements in the tension and compression zones,  $F_s$  and  $F'_s$ , respectively, are

$$F_s = A_s f_s(\varepsilon_s) \quad (5.25a)$$

$$F'_s = A'_s f_s(\varepsilon'_s) \quad (5.25b)$$

where  $A_s$  and  $A'_s$  are the section areas of steel reinforcements in the tension and compression zones, respectively;  $f_s(\varepsilon_s)$  and  $f_s(\varepsilon'_s)$  are the stresses of steel reinforcements in the tension and compression zones, respectively.

The constitutive law of concrete in compression can be modeled by a parabolic relationship, and is expressed as

$$f_c = f'_c \left[ \frac{2\varepsilon_c}{\varepsilon_0} - \left( \frac{\varepsilon_c}{\varepsilon_0} \right)^2 \right] \quad (5.26)$$

where  $f_c$  and  $\varepsilon_c$  are the stress and strain of concrete, respectively;  $f'_c$  is the concrete compressive strength, and  $\varepsilon_0$  is the concrete strain corresponding to the compressive strength.

The compressive force of concrete  $F_c$  and the distance from the centroid of concrete equivalent-stress-block to the top of beam  $y_c$  can be given as

$$F_c = \int_0^h f_c(\varepsilon_c) b dy \quad (5.27a)$$

$$y_c = \frac{\int_0^h f_c(\varepsilon_c) b y dy}{F_c} \quad (5.27b)$$

where  $f_c(\varepsilon_c)$  is the stress of concrete;  $b$  is the width of beam;  $h$  is the depth of beam;  $y$  is the distance from the arbitrary section of concrete to the top of beam.

For corroded PC beams, the forces of strand, steel reinforcements and concrete, and the bending moment on the section should satisfy the equilibrium equations, which can be expressed as

$$F_c + F'_s - F_p - F_s = 0 \quad (5.28)$$

$$M = F_c(h_p - y_c) + F_s(h_0 - h_p) + F'_s(h_p - a'_s) \quad (5.29)$$

where  $M$  is the bending moment.

As mentioned above, an analytical model has been proposed to predict the flexural capacity of corroded PC beams. Fig. 5.5 shows the calculation procedure of flexural capacity. Details are performed as follows:

- (1) Input the beam parameters and corrosion degrees;
- (2) Evaluate corrosion-induced cracking and bond degradation by Eqs. (5.1-5.15);
- (3) Assume the failure pattern of beam is concrete crushing, the concrete strains at the top of beam should reach the ultimate value, i.e.  $\varepsilon_{ct} = 0.0035$ ;
- (4) Assume a value of the length of slipping region ( $L_{er}$ );
- (5) Calculate the forces and strains of strand, steel reinforcements and concrete by Eqs. (5.16-5.27);
- (6) If the force equilibrium equation (Eq. 5.28) is satisfied, the procedure is ended; otherwise, revise the assumed length of slipping region ( $L_{er}$ ) and repeat the above procedure;
- (7) After that, if the strand strain is less than the ultimate strain, the failure pattern of beam is confirmed as concrete crushing; else the failure pattern of beam is defined

as strand rupture;

- (8) When the failure pattern of beam is strand rupture, the tensile strain of strand should reach the ultimate state before concrete crushing. Recalculate the forces and strains of strand, steel reinforcements and concrete by Eqs. (5.16-5.27);
- (9) Finally, the flexural capacity of corroded PC beams can be calculated with the moment equilibrium equation (Eq. 5.29).

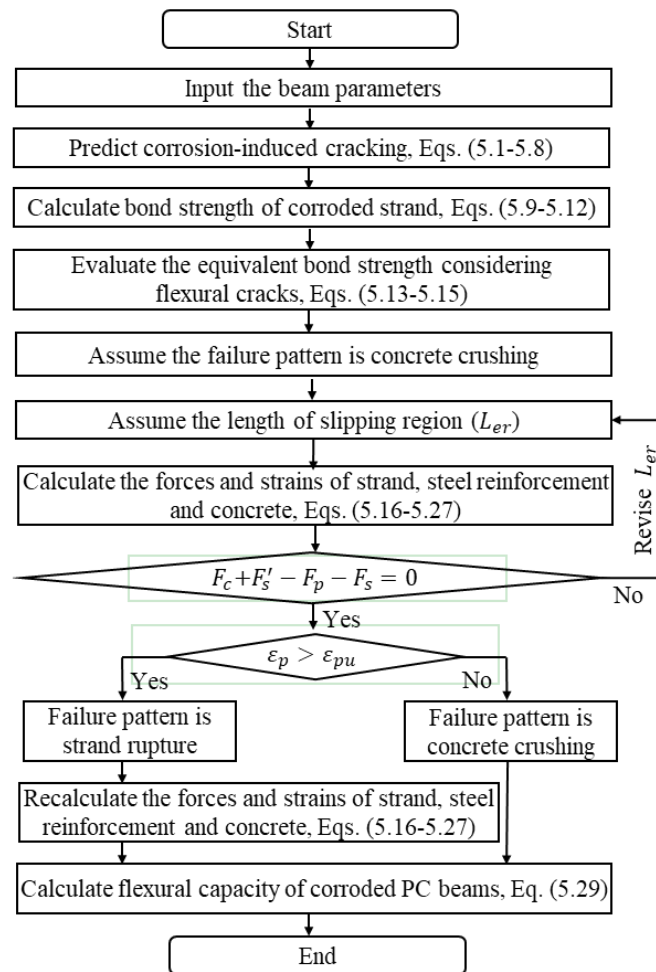


**Fig. 5.5. Calculation procedure of flexural capacity**

Flexural cracks provide aggressive agents (such as water, oxygen, carbon dioxide, and chloride) an easy access to steel reinforcements, which would influence the longitudinal distribution of reinforcement corrosion. Some experimental studies have been undertaken to investigate the effect of flexural cracks on steel corrosion (Otieno et al. 2016a). The effect of cracks on corrosion varies not only with their width, but also

with depth, frequency and distribution. Some empirical models have also been proposed to predict the chloride-induced corrosion rate in cracked reinforced concrete structures (Otieno et al. 2016b; Yu et al. 2015). The main purpose of the present study is to propose an analytical model to investigate the impact of flexural cracks on flexural capacity of corroded PC beams. The influence of flexural cracks on the longitudinal distribution of strand corrosion has not been considered in the model. How to consider this factor will be studied further.

## 5.5 Model validation

To validate the effectiveness of the proposed model for predicting the flexural capacity of corroded PC beams, some experimental results from Zhang et al. [127], Li and Yuan [164] and Zeng et al. [165] are collected.

Zhang et al. [127] designed eight bonded post-tensioned partially PC beams with a dimension of 150 mm × 220 mm × 2000 mm. A seven-wire steel strand was used to reinforce PC beams. The diameter, yield strength and ultimate strength of strand were 15.2 mm, 1830 MPa and 1910 MPa, respectively. The initial prestress of strand was 1395 MPa. Two 8 mm diameter plain bars were arranged as the tensile steel reinforcements. The compressive steel reinforcements consisted of two 12 mm diameter deformed bars. The stirrups were 8 mm diameter plain bars with a 90 mm spacing. The average compressive strength of concrete was 31.8 MPa.

An electrochemically accelerated method was employed to obtain different corrosion degrees of strand, and the current was 0.4 A. After the accelerated corrosion test, a four-point bending test was employed to investigate the flexural behaviors of corroded PC beams. The crack distribution of corroded PC beams was observed. Results show that crack distribution of beams depends on corrosion degree. Corrosion degree less than 27% has a slight effect on the crack distribution. As corrosion progresses, the number of cracks decreases and the distribution of cracks becomes irregular. The relative parameters are listed in Table 5.1.

The experimental data obtained from Li and Yuan [164] are employed to validate the proposed model. Nine partially PC beams, including four pre-tensioned concrete

beams and five post-tensioned concrete beams, were manufactured. The dimensions of pre-tensioned and post-tensioned concrete beams were 150 mm × 200 mm × 2600 mm and 150 mm × 200 mm × 2000 mm, respectively. PC beams were prestressed with a 12.7 mm diameter seven-wire steel strand. The initial prestress of strand in pre-tensioned and post-tensioned concrete beams were 1158 MPa and 1185 MPa, respectively. Four reinforcement bars were used as hanger bars at the corners of beams. The stirrups had a 6 mm diameter and a 100 mm spacing. The average compressive strengths of pre-tensioned and post-tensioned concrete were 33.0 MPa and 35.2 MPa, respectively. The sodium chloride with a 3% mass fraction of cement was used in the concrete to catalyze the corrosion process. A four-point bending test was performed to evaluate the flexural capacity. During the loading test, the average crack spacing was measured. The relative parameters are given in Table 5.1.

Zeng et al. [165] presented a four-point bending test to evaluate flexural behaviors of corroded post-tensioned partially PC beams. Nine PC beams had a rectangular cross-section of 150 mm × 300 mm, and 2600 mm in length. PC beams were reinforced with a seven-wire steel strand. The diameter, yield strength and ultimate strength of strand were 15.2 mm, 1750 MPa and 1950 MPa, respectively. The initial prestress in each beam was different. Two deformed bars with the diameter of 16 mm (or 22 mm) were arranged at the bottom of beam, and two hanger bars with a 12 mm diameter were used at the top of beam. The shear reinforcement was provided by double-leg stirrups of plain bar with a diameter of 8 mm. The strand was corroded by the electrochemically accelerated method, and the current density was 200 uA/cm<sup>2</sup>. The average crack spacing was measured during the loading test. Experimental results show that the average crack spacing of specimens increases with increasing corrosion loss. The relative parameters are given in Table 5.1.

The proposed model is employed to predict the experimental results. The relevant parameters used in the model are selected as follows. The compatibility coefficient is expressed as  $\delta = 0.8099\rho^2 - 1.2771\rho + 1$  [127]. The rust expansion ratio  $n$  varies from 2 to 4 [162], and is taken as 3. The friction coefficient between corroded strand

and concrete is given as  $k_c = 0.37 - 0.26(x - x_{cr})$  [3],  $x$  is the corrosion depth of strand,  $x_{cr}$  is the critical corrosion depth of cover cracking. The coefficient of adhesion stress is expressed as  $f_{coh} = 2 - 10(x - x_{cr})$  [89]. The shape factor constant  $C_r$  is taken as 0.8 [89].

**Table 5.1. Comparison between experimental and theoretical results**

References	No.	$\rho(\%)$	$f'_c(\text{MPa})$	$M_e(\text{kN}\cdot\text{m})$	$M_{ut}(\text{kN}\cdot\text{m})$	$M_{ct}(\text{kN}\cdot\text{m})$	$M_{ut}/M_e$	$M_{ct}/M_e$
Zhang et al. [127]	B1	0	31.8	37.8	35.2	35.2	0.93	0.93
	CB1	73.65	31.8	13.5	16.8	14.2	1.24	1.05
	CB2	46.01	31.8	21.0	25.6	23.3	1.22	1.11
	CB3	61.67	31.8	15.9	21.8	19.6	1.37	1.23
	CB4	84.74	31.8	12.3	14.1	11.6	1.15	0.94
	CB5	12.06	31.8	33.0	34.1	31.4	1.03	0.95
	CB6	19.47	31.8	31.5	33.3	29.7	1.06	0.94
Li and Yuan [164]	CB7	26.96	31.8	28.8	30.8	27.8	1.07	0.97
	PRB1	1.73	33.0	27.7	29.8	26.5	1.08	0.96
	PRB2	2.19	33.0	27.5	28.4	26.2	1.03	0.95
	PRB3	2.24	33.0	25.1	28.3	26.2	1.13	1.04
	PRB4	2.87	33.0	25.0	28.3	26.1	1.13	1.04
	POB0	0	35.2	28.9	27.4	27.4	0.95	0.95
	POB1	0.94	35.2	25.8	30.1	27.2	1.17	1.05
	POB2	1.51	35.2	25.3	29.3	27.1	1.16	1.07
Zeng et al. [165]	POB3	1.98	35.2	26.3	29.2	27.0	1.11	1.03
	POB4	1.12	35.2	25.8	29.3	27.1	1.14	1.05
	L1	0	44.0	91.1	82.3	82.3	0.90	0.90
	L2	8.7	44.0	86.7	83.9	79.7	0.97	0.92
	L3	13.6	44.0	78.0	80.4	76.2	1.03	0.98
	L4	100	44.0	47.0	49.8	45.2	1.06	0.96
	L5	20.3	44.0	55.3	61.9	58.7	1.12	1.06
	L6	5.8	44.0	110.7	96.0	92.9	0.87	0.84
	L7	0	44.0	84.6	82.3	82.3	0.97	0.97
L8	26.0	44.0	48.3	57.1	52.5	1.18	1.09	
L9	1.7	44.0	75.8	85.7	81.5	1.13	1.08	
Average error							12%	7%

Note:  $M_e$  is the experimental moment;  $M_{ut}$  is the theoretical moment un-considering the effect of flexural cracks;  $M_{ct}$  is the theoretical moment considering the effect of flexural cracks.

Table 5.1 gives the theoretical values and experimental results. Comparing with the data in Table 5.1, it is found that the prediction values correlate well with the experimental results. The average errors of theoretical values un-considering and considering the effect of flexural cracks,  $M_{ut}$  and  $M_{ct}$ , respectively, are 12% and 7%. The prediction error may be ascribed to some simplifications of the analytical model and the variability of material properties. Another reason for the error is the measurement uncertainty of experimental data. Considering the complexity of corrosion process, the prediction error can be accepted. In general, it is evident that the proposed model can give an accurate prediction for the flexural capacity of corroded PC beams. Considering the effect of flexural cracks can improve the precision of the prediction model.

Bond strength is an important factor for the prediction of flexural capacity of corroded PC beams. The experimental parameters from Zhang et al. [127] are applied to investigate the corrosion-induced bond degradation. Bond strengths under different corrosion losses are shown in Fig. 5.6. Normalized bond strength in Fig. 5.6 is defined as the ratio of bond stress of corroded strand to that of un-corroded strand. As Fig. 6 shows, the slight corrosion less than 7.3% can increase the bond stress, and the further corrosion will lead to the bond degradation. When the corrosion loss is larger than 42.0%, the bond strength is almost totally lost.

To further investigate the effect of strand corrosion on the flexural capacity of PC beams, the experimental parameters from Zhang et al. [127] are also used to investigate the flexural capacity deterioration. For the prediction of flexural capacity of corroded PC beams, the bond strength of corroded strand is calculated as follow. For the safety reserve reasons, slightly corroded strand is considered to have the similar bond stress with the un-corroded strand until the corrosion loss exceeds 7.3%. As corrosion progresses, the bond degradation model proposed by the present study is employed to predict the bond strength of corroded strand.

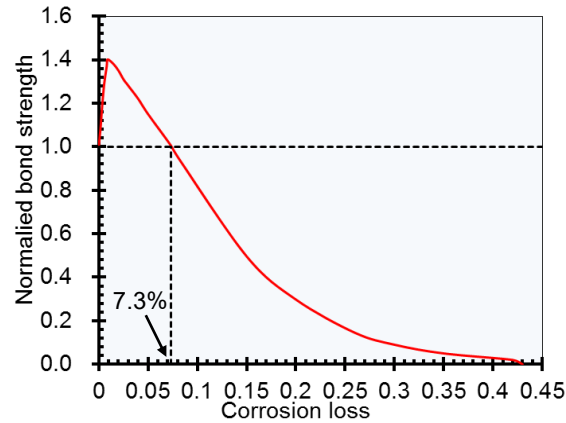


**Fig. 5.6. Bond strengths under different corrosion losses**

The flexural capacities under different corrosion losses are shown in Fig. 5.7. The normalized flexural capacity in Fig. 5.7 is defined as the ratio of flexural capacity of corroded PC beams to that of un-corroded PC beams. To further clarify the effect of flexural cracks on the flexural capacity, the prediction values considering and un-considering the effect of flexural cracks are also presented.

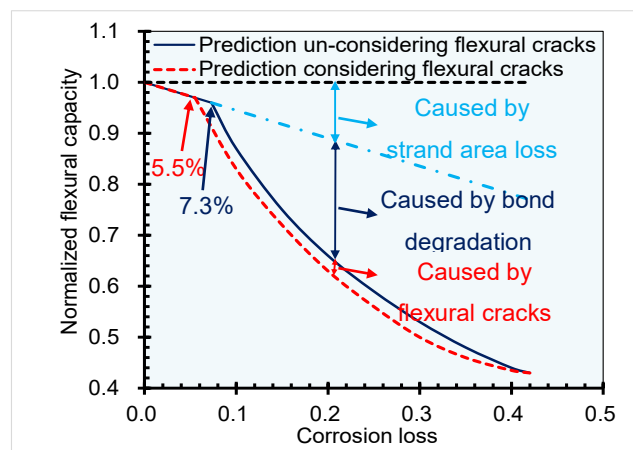


**Fig. 5.7. Flexural capacities under different corrosion losses**

As Fig. 5.7 shows, the flexural capacity deterioration depends on corrosion degree, and can be divided into two stages: the slight decrement and significant decrement. Strand corrosion less than the critical value can lead to a slight decrement of flexural capacity. The critical values considering and un-considering the effect of flexural cracks are 5.5% and 7.3%, respectively. In this stage, corrosion reduces the strand cross-section, but would not degrade the bond strength. The flexural capacity deterioration in this stage is mainly induced by the cross-section reduction of corroded strand. As corrosion progresses, the flexural capacity exhibits a significant deterioration. The further corrosion can reduce the strand cross-section and degrade the bond strength,

which leads to a significant deterioration of flexural capacity.

The flexural capacity deterioration caused by strand area loss, bond degradation and flexural cracks is also clarified in Fig. 5.7. Neglecting the effect of flexural cracks would overestimate the flexural capacity of corroded PC beams. The bond degradation, as compared with the strand area loss and flexural cracks, can lead to a remarkable deterioration of flexural capacity. This effect would become more noticeable as corrosion degree increases.

## 5.6 Conclusions

An analytical model, incorporating the effects of strand cross-section reduction, material deterioration, concrete cracking and bond degradation, is proposed to predict the flexural capacity of corroded PC beams. The effect of flexural cracks is also included in the model. The experimental results collected from the previous researches are employed to validate the proposed model. The following conclusions can be drawn:

- The proposed model can provide an accurate prediction for the flexural capacity of corroded PC beams. Considering the effect of flexural cracks can improve the precision of flexural capacity prediction.
- Corrosion-induced bond degradation, as compared with the strand area loss and flexural cracks, can lead to a remarkable deterioration of flexural capacity. This effect would become more noticeable as corrosion degree increases.
- Flexural capacity deterioration depends on corrosion degree. Strand corrosion less than 5.5% can lead to a slight decrement of flexural capacity. As corrosion progresses, the flexural capacity would exhibit a significant deterioration.

# Chapter 6 Conclusions and Perspectives

## 6.1 Conclusions

A summary of this study on the prestress and flexural capacity loss of pre-tensioned concrete structures due to corrosion cracks, and the conclusions are given below.

### **(1) Relationship of corrosive crack width and filling proportion of corrosion products**

The effect of stirrups on corrosion-induced cracking has been investigated based on the accelerated corrosion test. The corrosion morphology of strand is observed and the filling of strand corrosion products is investigated. The effects of stirrups on the filling of corrosion products and concrete cracking are also clarified. The filling extent of corrosion products varies with crack propagation. The rust filling extent increases with crack propagating until a critical width. Beyond the critical width, the rust filling extent keeps stable. The critical crack width decreases by 20% using stirrups. An empirical model for crack width is developed, incorporating the filling proportion of corrosion products and twisting shape of strand. The proposed model is verified by experimental results. Results demonstrate that the prediction of corrosion-induced crack is sensitive to the rust filling extent. The prediction model should rationally incorporate the filling effect of corrosion products.

### **(2) Effect of prestress on corrosion-induced cracking**

Strand corrosion-induced concrete cracking under various prestress is investigated experimentally and analytically. Experimental data on the critical time of cover cracking, crack width and corrosion loss obtained from the accelerated corrosion test are presented and discussed. The expansion ratio of strand corrosion products is estimated based on the infrared spectroscopy and thermal gravimetry. An analytical model, incorporating the coupled effects of prestress and strand corrosion, is proposed to predict the global process of concrete cracking from initiation to propagation. Strand

rust-expansion ratio and the residual stiffness of cracked concrete are also included in the model. Results show that prestress can accelerate the corrosion-induced cracking process. By varying prestress from 0 to 75% of strand tensile strength, the critical time of cover cracking decreases by 22% and the crack propagation rate increases by 9%. The proposed model is accurate in predicting corrosion-induced crack width in prestressed concrete beams.

### **(3) Prestress loss prediction in pre-tensioned concrete structures with corrosive cracking**

Strand corrosion-induced cracking can lead to prestress loss. A novel model is proposed to predict the corrosion-induced prestress loss in pre-tensioned concrete beams. The coupling effects of concrete cracking and bond deterioration are incorporated into the model. The effective prestress in eight corroded pre-tensioned concrete beams under various stress levels is explored by the four-point flexural test. The experimental results are employed to verify the proposed model. Prestress loss in corroded pre-tensioned concrete beams depends on corrosion level. Corrosion-induced concrete cracking would not degrade bond strength and effective prestress when the corrosion level is less than 6.6%. As corrosion further progresses, bond strength and effective prestress reduce monotonically, and then decrease to zero when the corrosion level reaches 34.0%.

### **(4) Flexural capacity prediction of corroded PC beams incorporating bond degradation**

An analytical model, incorporating the effects of strand cross-section reduction, material deterioration, concrete cracking and bond degradation, is developed to predict the flexural capacity of corroded prestressed concrete beams. Additionally, the effects of flexural cracks is also included in the model. An equivalent bond stress concept is introduced to consider the effect of flexural cracks, which is further implemented into the flexural capacity prediction of corroded PC beams. The proposed model is validated by the experimental results collected from the previous studies. The flexural capacity deterioration of prestressed concrete beams depends on corrosion degree. Strand

corrosion less than 5.5% can lead to a slight decrement of flexural capacity. As corrosion progresses, the flexural capacity would exhibit a significant deterioration.

## **6.2 Perspectives**

The electrochemical method was used to accelerate the strand corrosion in this study. Corrosion in the natural conditions is a relatively long process. Concrete cracking, prestress loss and bearing capacity degradation of PC structures caused by accelerated corrosion may be different from that in the natural conditions. Future work should be undertaken to investigate the mechanical behaviors of corroded PC structures in the natural conditions.

Future work in the strand corrosion should focus on the more accurate nondestructive measurement. A nondestructive method for observing the accumulated rust thickness at strand-concrete interface in the specimens at any stage of corrosion would be very valuable.

How to evaluate the prestress loss of corroded PC structures with local strand corrosion is still a problem. Further study should focus on developing methods for prestress loss prediction of locally corroded PC structures.

Finally, the test data from the corroded prestressed concrete beams often accompany with the uncertainty. The reliability analysis should be introduced to consider the uncertainty of test data, which needs to be studied further.

## References

- [1] Dang CN, Murray CD, Floyd RW, Micah Hale W, Martí-Vargas JR. Analysis of bond stress distribution for prestressing strand by Standard Test for Strand Bond. *Engineering Structures*. 2014, 72: 152-9.
- [2] Wang L, Zhang X, Zhang J, Ma Y, Xiang Y, Liu Y. Effect of insufficient grouting and strand corrosion on flexural behavior of PC beams. *Construction and Building Materials*. 2014, 53: 213-24.
- [3] Coronelli D. Corrosion cracking and bond strength modeling for corroded bars in reinforced concrete. *ACI Structural Journal*. 2002, 99(3): 267-276.
- [4] Iqbal S, Ali A, Holschemacher K, Bier TA, Shah AA. Strengthening of RC beams using steel fiber reinforced high strength lightweight self-compacting concrete (SHLSCC) and their strength predictions. *Materials & Design*. 2016, 100: 37-46.
- [5] Harries KA. Structural testing of prestressed concrete girders from the lake view drive bridge. *Journal of Bridge Engineering*. 2009, 14(2): 78-92.
- [6] Schupack M. Suarez MG. Some recent corrosion embrittlement failures of prestressing systems in the united states. *PCI Journal*. 1982, 38-55.
- [7] Darmawan MS, Stewart MG. Spatial time-dependent reliability analysis of corroding pretensioned prestressed concrete bridge girders. *Structural Safety*. 2007, 29(1): 16-31.
- [8] Jiang T, Kong Q, Zhong P, Wang L, Dai L, Qian F, et al. Monitoring of corrosion-induced degradation in prestressed concrete structure using embedded piezoceramic-based transducers. *IEEE Sensors Journal*. 2017, 17(18): 5823-30.
- [9] Enright MP, Frangopol DM. Probabilistic analysis of resistance degradation of reinforced concrete bridge beams under corrosion. *Engineering Structures*. 1998, 20(11): 960-71.
- [10] Wang X, Gao X, Liu X. Shear behaviour of RC beams with corrosion damaged partial length. *Materials & Structures*. 2012, 45(3): 351-79.
- [11] Francois R, Khan I, Dang VH. Impact of corrosion on mechanical properties of steel embedded in; 27-year-old corroded reinforced concrete beams. *Materials & Structures*. 2013, 46(6): 899-910.
- [12] Gardoni P, Pillai RG, Hueste MBD, Reinschmidt K, Trejo D. Probabilistic capacity models for

corroding posttensioning strands calibrated using laboratory results. *Journal of Engineering Mechanics*. 2009, 135: 906-16.

[13] Pillai RG, Gardoni P, Trejo D, Hueste M, Reinschmidt K. Probabilistic models for the tensile strength of corroding strands in posttensioned segmental concrete bridges. *Journal of Materials in Civil Engineering*. 2010, 22(10): 967-77.

[14] Pillai RG, Hueste MD, Gardoni P, Trejo D, Reinschmidt KF. Time-variant service reliability of post-tensioned, segmental, concrete bridges exposed to corrosive environments. *Engineering Structures*. 2010, 32(9): 2596-605.

[15] Deng Y, Morcous G, Ma ZJ. Strand bond stress–slip relationship for prestressed concrete members at prestress release. *Materials & Structures*. 2016, 49(3): 889-903.

[16] Casas JR, Crespo-Minguillon C. Probabilistic response of prestressed concrete bridges to fatigue. *Engineering Structures*. 1998, 20(11): 940-47.

[17] Walter P. Corrosion of Prestressing Steels and Its Mitigation. *PCI Journal*. 1992, 37(5): 34-55.

[18] Proverbio E, Longo P. Failure mechanisms of high strength steels in bicarbonate solutions under anodic polarization. *Corrosion Science*. 2003, 45(9): 2017-30.

[19] Cherry BW, Price SM. Pitting, crevice and stress corrosion cracking studies of cold drawn eutectoid steels. *Corrosion Science*. 1980, 20(11): 1163-83.

[20] Vélez W, Matta F, Ziehl P. Electrochemical characterization of early corrosion in prestressed concrete exposed to salt water. *Materials & Structures*. 2015, 49(1): 1-14.

[21] Kovač J, Leban M, Legat A. Detection of SCC on prestressing steel wire by the simultaneous use of electrochemical noise and acoustic emission measurements. *Electrochimica Acta*. 2007, 52(27): 7607-16.

[22] Vehovar L, Kuhar V, Vehovar A. Hydrogen-assisted stress-corrosion of prestressing wires in a motorway viaduct. *Engineering Failure Analysis*. 2001, 5(1): 21-27.

[23] Li F, Yuan Y, Li CQ. Corrosion propagation of prestressing steel strands in concrete subject to chloride attack. *Construction & Building Materials*. 2011, 25(10): 3878-85.

[24] Toribio J, Ovejero E. Microstructure-based modeling of hydrogen assisted cracking in pearlitic steels. *Materials Science & Engineering A*. 2001, 319(12): 540-43.

[25] Toribio J, Kharin V. Effect of residual stress-strain profiles on hydrogen-induced fracture of prestressing steel wires. *Materials Science*. 2006, 42(2): 263-71.

- [26] Valiente A, Guerrero MP, Iordachescu M. New testing method for assessing the cracking sensibility of stressed tendon rods in aggressive environments. *Engineering Failure Analysis*. 2016, 68: 244-53.
- [27] Toribio J, Lancha AM. Effect of cold drawing on susceptibility to hydrogen embrittlement of prestressing steel. *Materials & Structures*. 1993, 26(1): 30-37.
- [28] Vu NA, Castel A, François R. Effect of stress corrosion cracking on stress–strain response of steel wires used in prestressed concrete beams. *Corrosion Science*. 2009, 51(6): 1453-59.
- [29] Naito C, Sause R, Hodgson I, Pessiki S, Macioce T. Forensic examination of a non-composite adjacent precast prestressed concrete box beam bridge. *Journal of Bridge Engineering*. 2010, 15(4): 408-18.
- [30] Li H, Lan CM, Ju Y, Li DS. Experimental and numerical study of the fatigue properties of corroded parallel wire cables. *Journal of Bridge Engineering*. 2012, 17(2): 211-20.
- [31] Amin Jamali UA, Bryan Adey, Bernhard Elsener. Modeling of corrosion-induced concrete cover cracking: A critical analysis. *Construction and Building Materials*. 2013, 42: 225-37.
- [32] Du X, Jin L. Meso-scale numerical investigation on cracking of cover concrete induced by corrosion of reinforcing steel. *Engineering Failure Analysis*. 2014, 39(4): 21-33.
- [33] Zhao Y, Yu J, Hu B, Jin W. Crack shape and rust distribution in corrosion-induced cracking concrete. *Corrosion Science*. 2012, 55(none): 385-93.
- [34] Zhao Y, Wu Y, Jin W. Distribution of millscale on corroded steel bars and penetration of steel corrosion products in concrete. *Corrosion Science*. 2013, 66(1): 160-8.
- [35] Zhao Y, Yu J, Wu Y, Jin W. Critical thickness of rust layer at inner and out surface cracking of concrete cover in reinforced concrete structures. *Corrosion Science*. 2012, 59(6): 316-23.
- [36] Coronelli D, Hanjari KZ, Lundgren K, Rossi E. Severely corroded reinforced concrete with cover cracking: Part 1. Crack initiation and propagation. *Modelling of Corroding Concrete Structures*. 2011, 10(5): 195-205.
- [37] Michel A, Pease BJ, Geiker MR, Stang H, Olesen JF. Monitoring reinforcement corrosion and corrosion-induced cracking using non-destructive x-ray attenuation measurements. *Cement & Concrete Research*. 2011, 41(11): 1085-94.
- [38] Bhargava K, Ghosh AK, Mori Y, Ramanujam S. Analytical model for time to cover cracking in RC structures due to rebar corrosion. *Nuclear Engineering & Design*. 2006, 236(11): 1123-39.

- [39] Bhargava K, Ghosh AK, Mori Y, Ramanujam S. Model for cover cracking due to rebar corrosion in RC structures. *Engineering Structures*. 2006, 28(8): 1093-109.
- [40] Chernin L, Val DV. Prediction of corrosion-induced cover cracking in reinforced concrete structures. *Construction & Building Materials*. 2011, 25(4): 1854-69.
- [41] Malumbela G, Alexander M, Moyo P. Model for cover cracking of RC beams due to partial surface steel corrosion. *Construction & Building Materials*. 2011, 25(2): 987-91.
- [42] Reale T, O'Connor A. A review and comparative analysis of corrosion-induced time to first crack models. *Construction & Building Materials*. 2012, 36(4): 475-83.
- [43] Šavija B, Luković M, Pacheco J, Schlangen E. Cracking of the concrete cover due to reinforcement corrosion: A two-dimensional lattice model study. *Construction & Building Materials*. 2013, 44(44): 626-38.
- [44] Guzmán S, Gálvez JC, Sancho JM. Modelling of corrosion-induced cover cracking in reinforced concrete by an embedded cohesive crack finite element. *Engineering Fracture Mechanics*. 2012, 93: 92-107.
- [45] Du X, Jin L, Ma G. A meso-scale analysis method for the simulation of nonlinear damage and failure behavior of reinforced concrete members. *International Journal of Damage Mechanics*. 2013, 22(6): 878-904.
- [46] Balafas I, Burgoyne CJ. Environmental effects on cover cracking due to corrosion. *Cement & Concrete Research*. 2010, 40(9): 1429-40.
- [47] Zhao Y, Hu B, Yu J, Jin W. Non-uniform distribution of rust layer around steel bar in concrete. *Corrosion Science*. 2011, 53(12): 4300-8.
- [48] Nepal J, Chen HP, Alani AM. Analytical modelling of bond strength degradation due to reinforcement corrosion. *Key Engineering Materials*. 2013, 569: 1060-67.
- [49] Fang C, Lundgren K, Plos M, Gylltoft K. Bond behaviour of corroded reinforcing steel bars in concrete. *Cement & Concrete Research*. 2006, 36(10): 1931-38.
- [50] Fang C, Lundgren K, Chen L, Zhu C. Corrosion influence on bond in reinforced concrete. *Cement & Concrete Research*. 2004, 34(11): 2159-67.
- [51] Zhou H, Lu J, Xu X, Dong B, Xing F. Effects of stirrup corrosion on bond–slip performance of reinforcing steel in concrete: An experimental study. *Construction & Building Materials*. 2015, 93: 257-66.

- [52] Almusallam AA, Al-Gahtani AS, Aziz AR, Rasheeduzzafar. Effect of reinforcement corrosion on bond strength. *Construction & Building Materials*. 1996, 10(2): 123-29.
- [53] Yalciner H, Eren O, Sensoy S. An experimental study on the bond strength between reinforcement bars and concrete as a function of concrete cover, strength and corrosion level. *Cement & Concrete Research*. 2012, 42(5): 643-55.
- [54] Law DW, Tang D, Molyneaux TKC, Gravina R. Impact of crack width on bond: confined and unconfined rebar. *Materials & Structures*. 2011, 44(7): 1287-96.
- [55] Al-Hammoud R, Soudki K, Topper TH. Bond analysis of corroded reinforced concrete beams under monotonic and fatigue loads. *Cement & Concrete Composites*. 2010, 32(3): 194-203.
- [56] Choi YS, Yi ST, Kim MY, Jung WY, Yang EI. Effect of corrosion method of the reinforcing bar on bond characteristics in reinforced concrete specimens. *Construction & Building Materials*. 2014, 54(3): 180-89.
- [57] Zhao Y, Lin H, Wu K, Jin W. Bond behaviour of normal/recycled concrete and corroded steel bars. *Construction & Building Materials*. 2013, 48(11): 348-59.
- [58] Wang X, Liu X. Bond strength modeling for corroded reinforcements. *Construction & Building Materials*. 2006, 20(3): 177-86.
- [59] Coccia S, Imperatore S, Rinaldi Z. Influence of corrosion on the bond strength of steel rebars in concrete. *Materials & Structures*. 2016, 49(1-2): 537-51.
- [60] Lee HS, Kage T, Noguchi T, Tomosawa F. An experimental study on the retrofitting effects of reinforced concrete columns damaged by rebar corrosion strengthened with carbon fiber sheets. *Cement & Concrete Research*. 2003, 33(4): 563-70.
- [61] Berto L, Simioni P, Saetta A. Numerical modelling of bond behaviour in RC structures affected by reinforcement corrosion. *Engineering Structures*. 2008, 30(5): 1375-85.
- [62] Lundgren K. Effect of corrosion on the bond between steel and concrete: an overview. *Magazine of Concrete Research*. 2007, 59(6): 447-61.
- [63] Grassl P, Davies T. Lattice modelling of corrosion induced cracking and bond in reinforced concrete. *Cement & Concrete Composites*. 2011, 33(9): 918-24.
- [64] Abosrra L, Ashour AF, Youseffi M. Corrosion of steel reinforcement in concrete of different compressive strengths. *Construction & Building Materials*. 2011, 25(10): 3915-25.
- [65] Joyce E. Effect of corrosion products on bond strength and flexural behaviour of reinforced

- concrete slabs. *Journal of the South African Institution of Civil Engineering*. 2014, 56(2): 19-28.
- [66] Lan C, Kim JH, Yi ST. Bond strength prediction for reinforced concrete members with highly corroded reinforcing bars. *Cement & Concrete Composites*. 2008, 30(7): 603-11.
- [67] Wu YZ, Lv HL, Zhou SC, Fang ZN. Degradation model of bond performance between deteriorated concrete and corroded deformed steel bars. *Construction & Building Materials*. 2016, 119: 89-95.
- [68] Bhargava K, Ghosh AK, Mori Y, Ramanujam S. Corrosion-induced bond strength degradation in reinforced concrete—Analytical and empirical models. *Nuclear Engineering & Design*. 2007, 237(11): 1140-57.
- [69] Morcous G, Hatami A, Maguire M, Hanna K, Tadros MK. Mechanical and bond properties of 18-mm-(0.7-in.-) diameter prestressing strands. *Journal of Materials in Civil Engineering*. 2012, 24(6): 735-44.
- [70] Wang L, Zhang X, Zhang J, Yi J, Liu Y. Simplified Model for Corrosion-induced bond degradation between steel strand and concrete. *Journal of Materials in Civil Engineering*. 2017, 29(4): 04016257.
- [71] Caro LA, Marti-Vargas JR, Serna P. Prestress losses evaluation in prestressed concrete prismatic specimens. *Engineering Structures*. 2013, 48: 704-15.
- [72] Asamoto S, Kato K, Maki T. Effect of creep induction at an early age on subsequent prestress loss and structural response of prestressed concrete beam. *Construction & Building Materials*. 2014, 70(1): 158-64.
- [73] Youakim S, Hida AG, Karbhari V. Prediction of long-term prestress losses. *PCI Journal*. 2007, 52 (2): 116-30.
- [74] Kottari AK, Shing PB. Estimation of long-term prestress losses in post-tensioned girders. *ACI Structural Journal*. 2013, 111(5): 1091-100.
- [75] Barr PJ, Kukay BM, Halling MW. Comparison of prestress losses for a prestress concrete bridge made with high-performance concrete. *Journal of Bridge Engineering*. 2008, 13(5): 468-75.
- [76] Cavell DG, Waldron P. A residual strength model for deteriorating post-tensioned concrete bridges. *Computers and Structures*. 2001, 79: 361-73.
- [77] Castel A, Coronelli D, Vu NA, François R. Structural response of corroded, unbonded posttensioned beams. *Journal of Structural Engineering*. 2011, 137(7): 761-71.

- [78] Rodriguez J, Ortega LM, Casal J. Load carrying capacity of concrete structures with corroded reinforcement. *Construction & Building Materials*. 1997, 11(4): 239-48.
- [79] Castel A, François R, Arliguie G. Mechanical behaviour of corroded reinforced concrete beams–Part 1: Experimental study of corroded beams. *Materials & Structures*. 2000, 33(9): 539-44.
- [80] Castel A, François R, Arliguie G. Mechanical behaviour of corroded reinforced concrete beams–Part 2: Bond and notch effects. *Materials & Structures*. 2000, 33(9): 545-51.
- [81] Coronelli D, Castel A, Vu NA. Corroded post-tensioned beams with bonded tendons and wire failure. *Engineering Structures*. 2009, 31(8): 1687-97.
- [82] Rinaldi Z, Imperatore S, Valente C. Experimental evaluation of the flexural behavior of corroded P/C beams. *Construction and Building Materials*. 2010, 24(11): 2267-78.
- [83] Antonio B, Tullio M, Francesco B, Lignola GP, Prota A. Modeling of concrete cracking due to corrosion process of reinforcement bars. *Cement and Concrete Research*. 2015, 71: 78-92.
- [84] Hebé G, Eva GA, Francesco BB, Garcés P, Zornoza E. Corrosion behavior of steel reinforcement in concrete with recycled aggregates, Fly Ash and Spent Cracking Catalyst. *Materials*. 2014, 7(4): 3176-97.
- [85] Liu T, Weyers RW. Modeling the dynamic corrosion process in chloride contaminated concrete structures. *Cement & Concrete Research*. 1998, 28(3): 365–79.
- [86] Balafas I, Burgoyne CJ. Modeling the structural effects of rust in concrete cover. *Journal of Engineering Mechanics*. 2011, 137(3): 175-85.
- [87] Torres-Acosta Andrés A. Concrete cracking by localized steel corrosion-geometric effects. *ACI Materials Journal*. 2004, 101(6): 501- 7.
- [88] Lin H, Zhao Y. Effects of confinements on the bond strength between concrete and corroded steel bars. *Construction and Building Materials*. 2016, 118: 127-38.
- [89] Chen H-P, Nepal J. Analytical model for residual bond strength of corroded reinforcement in concrete structures. *Journal of Engineering Mechanics*. 2016, 142(2): 04015079.
- [90] Solgaard AS, Michel A, Geiker M, Stang H. Concrete cover cracking due to uniform reinforcement corrosion. *Materials and Structures*. 2013, 46(11): 1781-99.
- [91] Zhao Y, Jin W. Modeling the amount of steel corrosion at the cracking of concrete cover. *Advance in Structural Engineering*. 2006, 9: 687-96.
- [92] Lu C, Jin W, Liu R. Reinforcement corrosion-induced cover cracking and its time prediction

- for reinforced concrete structures. *Corrosion Science*. 2011, 53(4): 1337-47.
- [93] Branko Š, Mladena L, Hosseini SAS, Pacheco J, Schlangen E. Corrosion induced cover cracking studied by X-ray computed tomography, nanoindentation, and energy dispersive X-ray spectrometry (EDS). *Materials and Structures*. 2014, 8(7): 2043-62.
- [94] Val, D V, Chernin L, Stewart M G., Experimental and numerical investigation of corrosion-induced cover cracking in reinforced concrete structures. *Journal of Structural Engineering*. 2009, 35(4): 376-85.
- [95] Jaffer SJ, Hansson CM. Chloride-induced corrosion products of steel in cracked-concrete subjected to different loading conditions. *Cement and Concrete Research*. 2009, 39(2): 116-25.
- [96] Torres-Acosta AA, Navarro-Gutierrez S, Terán-Guillén J. Residual flexure capacity of corroded reinforced concrete beams. *Engineering Structures*. 2007, 29(6): 1145-52.
- [97] Li CQ, Yang ST. Prediction of concrete crack width under combined reinforcement corrosion and applied load. *Journal of Engineering Mechanics*. 2011, 137(11): 722-31.
- [98] Khan I, Francois R, Castel A. Prediction of reinforcement corrosion using corrosion induced cracks width in corroded reinforced concrete beams. *Cement and Concrete Research*. 2014, 56: 84-96.
- [99] Dai L, Wang L, Zhang J, Zhang X. A global model for corrosion-induced cracking in prestressed concrete structures. *Engineering Failure Analysis*. 2016, 62: 263-75.
- [100] Darmawan MS, Stewart MG. Effect of pitting corrosion on capacity of prestressing wires. *Magazine of Concrete Research*,. 2007, 59(2): 131-9.
- [101] Higgins C, Farrow WC. Tests of reinforced concrete beams with corrosion damaged stirrups. *ACI Structural Journal*. 2006, 103(1): 133-41.
- [102] Zhang R, Castel A, François R. Concrete cover cracking with reinforcement corrosion of RC beam during chloride-induced corrosion process. *Cement and Concrete Research*. 2010, 40(3): 415-25.
- [103] Standard for test methods of long-term performance and durability of ordinary concrete, GB-T50082–2009. Beijing, China: Ministry of Housing and Urban-Rural Development of the PR China; 2009.
- [104] Fu AQ, Cheng YF. Effects of alternating current on corrosion of a coated pipeline steel in a chloride-containing carbonate/bicarbonate solution. *Corrosion Science*. 2010, 52(2): 612-9.

- [105] Papadakis VG. Effect of supplementary cementing materials on concrete resistance against carbonation and chloride ingress. *Cement and Concrete Research*. 2000, 30(2): 291-9.
- [106] Scott A, Alexander MG. Effect of supplementary cementitious materials (binder type) on the pore solution chemistry and the corrosion of steel in alkaline environments. *Cement and Concrete Research*. 2016, 89: 45-55.
- [107] Nossoni G, Harichandran RS. Electrochemical-mechanistic model for concrete cover cracking due to corrosion initiated by chloride diffusion. *Journal of Materials in Civil Engineering*. 2014, 26(6): 04014001.
- [108] Bhargava K, Ghosh AK, Mori Y. Modeling of time to corrosion-induced cover cracking in reinforced concrete structures. *Journal of Building Structures*. 2005, 35(11): 2203-18.
- [109] EI Maaddawy T, Soudki K. A model for prediction of time from corrosion initiation. *Cement and Concrete Composition*. 2007, 29(3): 168-75.
- [110] Jamali A, Angst U, Adey B, Elsener B. Modeling of corrosion-induced concrete cover cracking: A critical analysis. *Construction and Building Materials*. 2013, 42: 225-37.
- [111] Kassir MK, Ghosn M. Chloride-induced corrosion of reinforced concrete bridge decks. *Cement & Concrete Research*. 2002, 32(1): 139-43.
- [112] Zhang W, Liu X, Gu X. Fatigue behavior of corroded prestressed concrete beams. *Construction and Building Materials*. 2016, 106: 198-208.
- [113] Frangopol DM, Dong Y, Sabatino S. Bridge life-cycle performance and cost: analysis, prediction, optimisation and decision-making. *Structure & Infrastructure Engineering*. 2017, 13(10): 1-19.
- [114] Cavaco ES, Neves LAC, Casas JR. On the robustness to corrosion in the life cycle assessment of an existing reinforced concrete bridge. *Structure & Infrastructure Engineering*. 2017, 14(2): 137-150.
- [115] Dang CN, Murray CD, Floyd RW, Hale WM, Martí-Vargas JR. Analysis of bond stress distribution for prestressing strand by Standard Test for Strand Bond. *Engineering Structures*. 2014, 72: 152-9.
- [116] Coronelli D, Castel A, Vu NA, François R. Corroded post-tensioned beams with bonded tendons and wire failure. *Steel Construction*. 2009, 31(8): 1687-97.
- [117] Jamali A, Angst U, Adey B, Elsener B. Modeling of corrosion-induced concrete cover

- cracking: A critical analysis. *Construction & Building Materials*. 2013, 42(5): 225-37.
- [118] Zhao Y, Ren H, Dai H, Jin W. Composition and expansion coefficient of rust based on X-ray diffraction and thermal analysis. *Corrosion Science*. 2011, 53(5): 1646-1658.
- [119] Cabrera JG. Deterioration of concrete due to reinforcement steel corrosion. *Cement & Concrete Composites*. 1996, 18(1): 47-59.
- [120] Jin Z, Xia Z, Zhao T, Li Y. Interaction between compressive load and corrosive-ion attack on reinforced concrete with accelerated potentiostatic corrosion. *Construction & Building Materials*. 2016, 113: 805-14.
- [121] González JA, Andrade C, Alonso C, Feliu S. Comparison of rates of general corrosion and maximum pitting penetration on concrete embedded steel reinforcement. *Cement & Concrete Research*. 1995, 25(2): 257-64.
- [122] Biondini F, Vergani M. Deteriorating beam finite element for nonlinear analysis of concrete structures under corrosion. *Structure & Infrastructure Engineering*. 2015, 11(4): 519-32.
- [123] Chernin L, Val DV, Volokh KY. Analytical modelling of concrete cover cracking caused by corrosion of reinforcement. *Materials & Structures*. 2010, 43(4): 543-56.
- [124] Bertolini L. Steel corrosion and service life of reinforced concrete structures. *Structure & Infrastructure Engineering*. 2008, 4(2): 123-37.
- [125] Maaddawy TE, Khaled S. A model for prediction of time from corrosion initiation to corrosion cracking. *Cement & Concrete Composites*. 2007, 29(3): 168-75.
- [126] Val DV, Chernin L., Stewart MG. Experimental and numerical investigation of corrosion-induced cover cracking in reinforced concrete structures. *Journal of Structural Engineering*. 2009, 135: 376-85.
- [127] Zhang XH, Wang L, Zhang JR, Ma YF, Liu YM. Flexural behavior of bonded post-tensioned concrete beams under strand corrosion. *Nuclear Engineering and Design*. 2017, 313: 414-24.
- [128] G1-03 A. Standard practice for preparing, cleaning, and evaluating corrosion test specimens. *American Standard Testing Materials (ASTM)*, West Conshohocken, PA. 2011.
- [129] Raman A, Kuban B, Razvan A. The application of infrared spectroscopy to the study of atmospheric rust systems - I. Standard spectra and illustrative applications to identify rust phases in natural atmospheric corrosion products. *Corrosion Science*. 1991, 32(12): 1295–306.
- [130] Jaffer SJ, Hansson CM. Chloride-induced corrosion products of steel in cracked-concrete

- subjected to different loading conditions. *Cement & Concrete Research*. 2009, 39(2): 116-25.
- [131] Yu L, François R, Dang VH, L'Hostis V, Gagné R. Distribution of corrosion and pitting factor of steel in corroded RC beams. *Construction & Building Materials*. 2015, 95: 384-92.
- [132] Zhang R, Castel A, François R. Concrete cover cracking with reinforcement corrosion of RC beam during chloride-induced corrosion process. *Cement and Concrete Research*. 2010, 40(3): 415-25.
- [133] Pantazopoulou SJ, Papoulia KD. Modeling cover-cracking due to reinforcement corrosion in structures. *Journal of Engineering Mechanics*. 2001, 127(4): 342-351.
- [134] Tasuji ME, Slate FO, Nilson AH. Stress-strain response and fracture of concrete in biaxial loading. *Journal of Proceedings*. 1978, 75: 306-312.
- [135] Li CQ, Yang ST. Prediction of concrete crack width under combined reinforcement corrosion and applied load. *Journal of Engineering Mechanics*. 2011, 137(11): 722-731.
- [136] Li CQ, Melchers RE, Zhang J. Analytical model for corrosion-induced crack width in reinforced concrete structures. *ACI Structural Journal*. 2006, 103(4): 479-487.
- [137] Han W, Wu J, Cai, CS, Chen S. Characteristics and dynamic impact of overloaded extra heavy trucks on typical highway bridges. *Journal of Bridge Engineering*. 2015, 20(2): 0000666.
- [138] Dang CN, Floyd, RW, Prinz GS, Hale WM. Determination of bond stress distribution coefficient by maximum likelihood method. *Journal of Structural Engineering*. 2016, 142(5): 04016003.
- [139] Lim S, Akiyama M, Frangopol DM. Assessment of the structural performance of corrosion-affected RC members based on experimental study and probabilistic modeling. *Engineering Structures*. 2016, 127: 189-205.
- [140] Zhang W, Ye Z, Gu X, Liu, X, Li S. Assessment of fatigue life for corroded reinforced concrete beams under uniaxial bending. *Journal of Structural Engineering*. 2017, 143(7): 04017048.
- [141] Zhang W, Yuan H. Corrosion fatigue effects on life estimation of deteriorated bridges under vehicle impacts. *Engineering Structures*. 2014, 71(7): 128-36.
- [142] Biondini F, Frangopo DM. Life-cycle performance of deteriorating structural systems under uncertainty: review. *Journal of Structural Engineering*. 2016, 142(9): 4016001.
- [143] Osborn GP, Barr PJ, Petty DA, Halling MW, Brackus TR. Residual prestress forces and shear capacity of salvaged prestressed concrete bridge girders. *Journal of Bridge Engineering*. 2012, 17(2):

302-9.

[144] Ward DB, Dang CN, Floyd RW, Hale WM. Prestress losses of double-tee girders cast with lightweight self-consolidating concrete. *Journal of Building Engineering*. 2016, 7: 133-142.

[145] AASHTO W, DC. AASHTO-LRFD bridge design specifications. AASHTO. 2010.

[146] CEB-FIP. Comité Euro-International du Béton–Fédération Internationale de la Précontrainte (CEB-FIP). 2010.

[147] PCI. Precast/Prestressed Concrete Institute (PCI) Industry Handbook Committee. PCI design handbook-Precast/prestressed concrete. 2010, 7th Ed., Chicago.

[148] Han SJ, Lee DH, Cho S-H, Ka S-B, Kim KS. Estimation of transfer lengths in precast pretensioned concrete members based on a modified thick-walled cylinder model. *Structural Concrete*. 2016, 17(1): 52-62.

[149] Wang L, Zhang X, Zhang J, Yi J, Liu Y. Simplified model for corrosion-induced bond degradation between steel strand and concrete. *Journal of Materials in Civil Engineering*. 2016, 29(4): 04016257.

[150] El-Tawil S, Ogunc C, Okeil A, Shahawy M. Static and fatigue analyses of RC beams strengthened with CFRP laminates. *Journal of Composites for Construction*. 2001, 5(4): 258-67.

[151] Vu NA, Castel A, François R. Response of post-tensioned concrete beams with unbonded tendons including serviceability and ultimate state. *Steel Construction*. 2010, 32(2): 556-69.

[152] Collins MP, Mitchell D. *Prestressed concrete structure*, Prentice Hall, NJ. 1991.

[153] Caro LA, Martí-Vargas JR, Serna P. Prestress losses evaluation in prestressed concrete prismatic specimens. *Engineering Structures*. 2013, 48: 704-15.

[154] Han WS, Wu J, Cai CS, Chen SR. Characteristics and dynamic impact of overloaded extra heavy trucks on typical highway bridges. *Journal of Bridge Engineering*. 2015, 20(2): 05014011.

[155] Yang DH, Yi TH, Li HN. Coupled fatigue-corrosion failure analysis and performance assessment of rc bridge deck slabs. *Journal of Bridge Engineering*. 2017, 22(10): 04017077.

[156] Yang DH, Yi TH, Li HN. A performance-based design method for chloride-induced cover cracking of RC structures. *Computer and Concrete*. 2017, 20(5): 573-82.

[157] Coronelli D, Castel A, Vu NA, François R. Corroded post-tensioned beams with bonded tendons and wire failure. *Engineering Structures*. 2009, 31(8): 1687-97.

[158] Li F, Luo X, Wang K, Ji Y. Pitting damage characteristics on prestressing steel strands by

combined action of fatigue load and chloride corrosion. *Journal of Bridge Engineering*. 2017, 22(7): 04017023.

[159] Rinaldi Z, Imperatore S, Valente C. Experimental evaluation of the flexural behavior of corroded P/C beams. *Construction & Building Materials*. 2010, 24(11): 2267-78.

[160] Wang L, Zhang X, Zhang J, Dai L, Liu Y. Failure analysis of corroded PC beams under flexural load considering bond degradation. *Engineering Failure Analysis*. 2017, 73: 11-24.

[161] Chen HP, Nepal J. Stochastic modelling and lifecycle performance assessment of bond strength of corroded reinforcement in concrete. *Structural Engineering and Mechanics*. 2015, 54(2): 319-36.

[162] Zhao Y, Yu J, Jin W. Damage analysis and cracking model of reinforced concrete structures with rebar corrosion. *Corrosion Science*. 2011, 53(10): 3388-97.

[163] Han SJ, Lee DH, Kim KS, Seo S-Y, Moon J, Monteiro PJM. Degradation of flexural strength in reinforced concrete members caused by steel corrosion. *Construction and Building Materials*. 2014, 54: 572-83.

[164] Li Fumin, Yuan Y. Experimental study on bending property of prestressed concrete beams with corroded steel strands. *Journal of Building Structures*. 2010, 31(2): 78-84. (In Chinese)

[165] Zeng YH, Huang QH, Gu XL, Zhang WP. Experimental Study on Bending Behavior of Corroded Post-Tensioned Concrete Beams. *Earth and Space 2010: Engineering, Science, Construction and Operations in Challenging Environments*, 2010.

## Acknowledgments

I would like to express my deep appreciation to my advisors, Prof. Potier-Ferry Michel, University of Lorraine, and MCF-HDR. Hanbing Bian, University of Lille, for the encouragements, guidance, patience, and support they provided me throughout my PhD studies in France.

I am extremely grateful to Prof. Jianren Zhang and Prof. Lei Wang, my advisors in China, who gave me the opportunity to work on this research project at Changsha University of Science and Technology.

Also, special thanks to the distinguished faculty members who served on my committee: Prof. Balayssac Jean-Paul, Prof. Buyle-Bodin François, Prof. Burlion Nicolas, and MCF. Chen Wen for their supports and useful suggestions.

I would like to thank the sponsors of this research project: the State Key Development Program for Basic Research of China (Grant No. 2015CB057705), and the National Natural Science Foundation of China (Grant No. 51678069).

Thanks are also due to the former graduate students, Yafei Ma, Xuhui Zhang and Ju Yi, for their work and contributions on this research project. I would like to recognize my colleagues, especially ZhengTian Yang, and WenQing Cheng, for their helps and friendliness.

Finally, I am grateful to my wife, parents and brothers for their constant support and continuous encouragement. Their belief in me and their pride in my accomplishments were the motivation and reward for all the hard work I did.

# Publications and Projects

## Publications

- [1] **Dai Lizhao**, Bian Hanbing, Wang Lei, Potier-Ferry Michel, Zhang Jianren. Prestress loss diagnostics in pre-tensioned concrete structures with corrosive cracking. *Journal of Structural Engineering*. 2019. doi: 10.1061/(ASCE)ST.1943-541X.0002554.
- [2] **Dai Lizhao**, Wang Lei, Bian Hanbing, Zhang Jianren, Zhang Xuhui, Ma Yafei. Flexural capacity prediction of corroded prestressed concrete beams incorporating bond degradation. *Journal of Aerospace Engineering*, 2019, 32(4): 04019027.
- [3] **Dai Lizhao**, Wang Lei, Deng Ming, Wu Binghui, Floyd Royce W., Zhang Jianren. Strengthening a 20-year-old post-tensioned concrete box beam with double-layer prestressed steel wire ropes. *Journal of Bridge Engineering*, 2018, 23(11): 05018009.
- [4] **Dai Lizhao**, Wang Lei, Zhang Jianren, Zhang Xuhui. A global model for corrosion-induced cracking in prestressed concrete structures. *Engineering Failure Analysis*, 2016, 62: 263-275.
- [5] Wang Lei, **Dai Lizhao**, Bian Hanbing, Ma Yafei, Zhang Jianren. Concrete cracking prediction under combined prestress and strand corrosion. *Structure and Infrastructure Engineering*, 2019, 15(3):285-295.
- [6] Wang Lei, **Dai Lizhao**, Zhang Xuhui, Zhang Jianren. Concrete cracking prediction including the filling proportion of strand corrosion products. *Materials*, 2017, 10(6): 1-20.
- [7] Wang Lei, Zhang Xuhui, Zhang Jianren, **Dai Lizhao**, Liu Yongming. Failure analysis of corroded PC beams under flexural load considering bond degradation. *Engineering Failure Analysis*, 2017, 73: 11-24
- [8] Jiang Tianyong, Kong Qingzhao, Peng Zhong, Wang Lei, **Dai Lizhao**, Feng Qian, Huo Linsheng, Song Gangbing. Monitoring of corrosion damage in prestressed concrete structure using embedded piezoceramic transducers. *IEEE Sensors Journal*, 2017, 17(18): 5823-5830.
- [9] Wang Lei, **Dai Lizhao**, Ma Yafei, He Xianfeng. Filling of strand corrosion products in cracked concrete based on accelerating corrosion method. *IABSE Symposium Report, IABSE Symposium Vancouver*, 2017: 373-380.
- [10] Wang Lei, **Dai Lizhao**, Ma Yafei, Zhang Jianren. Effect of strand corrosion on corrosion-

induced cracking of PC structures. IABSE Challenges in Design and Construction of an Innovative and Sustainable Built Environment, Stockholm, 2016: 1640-1648.

- [11] Wang Lei, **Dai Lizhao**, Ma Yafei, Zhang Xuhui, Zhang Jianren. Corrosion effect on compatibility between prestressing strand and concrete. IABSE Conference-structural Engineering Providing Solutions to Global Challenges, Geneva, 2015: 559-565.

## **Projects**

- [1] Hunan Provincial Academic Degree Committee. Experimental and theoretical research of corrosion-induced cracking of prestressed concrete structures, 2015.04-2016.04, PI.
- [2] Open Fund of Hunan Province University Key Laboratory of Bridge Engineering. Interface behavior between strand and concrete during corrosion-induced cracking process, 2015.11-2017.06, PI.
- [3] National Program on Key Basic Research Project of China (973 Program). Basic theories research on safety design and assessment of long-span bridges, 2015.01-2019.08, research assistant.
- [4] National Natural Science Fund of China (NSFC). Interface behavior between prestressed strand and concrete and flexural strength of beams considering corrosion, 2017.01 -2020.12, research assistant.